Proceedings of the ASY-EOS 2012 International Workshop on Nuclear Symmetry Energy and Reaction Mechanisms

4-7 September 2012

Siracusa, Sicily, Italy

Edited by E. De Filippo, A. Pagano, P. Russotto, G. Verde

Contents

1 Editor's introduction

The ASY-EOS-2012 workshop is the third edition of a series of topical conferences organized in Sicily by the Istituto Nazionale di Fisica Nucleare, Sezione di Catania and the Laboratori Nazionali del Sud (LNS) and University of Catania. The main aim of the ASY-EOS topical conferences consists of strengthening the link of scientific communities involved in the study of nuclear reactions and their implications on exotic nuclear systems and states of asymmetric nuclear matter. In addition to the investigation of the symmetry energy in nuclear physics, this edition of the ASY-EOS-2012 meeting has extended its focus towards the relevance on nuclear reaction mechanisms at the future radioactive beam facilities.

As in the previous editions, special attention was devoted to the valorization of Sicilian cultural resources and the dissemination of scientific and technologic research. This edition of the ASY-EOS conference took place in the historic town of Siracusa, famous for its ancient Greek history. Siracusa was home of the great scientist Archimedes (287-212 B.C.) to which a special conference session was dedicated in the "Paolo Orsi" archeological museum. Siracusa is one of the UNESCO World Heritage Sites. The event was sponsored by the Provincia Regionale of Siracusa.

INTERNATIONAL ADVISORY COMMITEE

Z. BASRAK Ruder Boskovic Institute, Zagreb, Croatia
A. CHBIHI GANIL, Caen, France
M. CHARTIER University of Liverpool, Liverpool, U.K.
M. COLONNA INFN-LNS, Catania, Italy
Y. LEIFELS GSI, Darmstadt, Germany
J. LUKASIK IFJ-PAN, Krakow, Poland
A. PAGANO INFN-Catania, Italy
P. RUSSOTTO INFN-Catania, Italy
H. SAKURAI Riken, Japan
W. TRAUTMANN GSI, Darmstadt, Germany
M.B. TSANG NSCL MSU, East Lansing, USA
G. VERDE INFN-Catania, Italy
S. YENNELLO Texas A&M, College Station, USA

LOCAL ORGANIZING COMMITEE

C. AGODI INFN-LNS, Catania, Italy
G. CARDELLA INFN-Catania, Italy
G. LANZALONE “Kore” University, Enna & INFN-LNS, Catania, Italy
E. DE FILIPPO INFN-Catania, Italy
L. FRANCALANZA University of Catania & INFN-LNS, Catania, Italy
S. PIRRONE INFN-Catania, Italy
G. POLITI University of Catania & INFN-Catania, Italy
F. RIZZO University of Catania & INFN-LNS, Catania, Italy
P. RUSSOTTO INFN-Catania, Italy
G. VERDE INFN-Catania, Italy

SECRETARY AND PRESS OFFICE

A.L. MAGRI’ INFN-Catania, Italy
S. REITO INFN-Catania, Italy

Energy deposition in heavy-ion reactions at intermediate energies

Z. Basrak[1], *Ph. Eudes*[2], *M. Zorić*[1,2] *and F. Sébille*[2]
[1]*Ruđer Bošković Institute, P.O.Box 180, HR-10 002 Zagreb, Croatia*
[2]*SUBATECH, EMN-IN2P3/CNRS-Université de Nantes,*
P.O.Box 20722, F-44 307 Nantes, France

Abstract

Semiclassical transport simulation of heavy-ion reactions between about the Fermi energy and 100*A* MeV reveals that independently of reaction entrance channel parameters (system size, asymmetry and energy) the maximal excitation energy put into a nuclear system is a constant fraction of the system available energy.

It is commonly admitted that in central heavy-ion reactions (HIR) the fraction of system available energy which is converted into the heat and dissipated during the reaction monotonically decreases with the increase of incident energy $E_{\rm in}$. In HIR projectile energy per nucleon $E_{\rm in}$ and reaction geometry determine the dominant reaction mechanism. In central HIR for $E_{\rm in}$ from about the Fermi energy $E_{\rm F}$ the elementary nucleon-nucleon (NN) collisions starts to overcome the mean-field contribution. Consequently, the course of a HIR is "decided" in the very first instances of a collision [1,2]. In central, the most violent collisions the largest fraction of the entrance channel energy is converted into internal degrees of freedom. Thus, the central collisions are of our greatest interest.

We have shown theoretically that an intermediate energy HIR follows a two-stage scenario, a prompt first compact-stage and a second after-breakup one [2]. The emission pattern of central collisions is characterized by a copious and prompt dynamical emission occurring during the compact and prior-to-scission reaction phase [2–4]. This is the main system-cooling component and the amount of deposited energy into the compact system linearly increases with the projectile energy [5]. These results witness the above conclusion that global characteristics of HIR exit channel are determined in the first prompt reaction stage underlying the interest in studying the first instances of nuclear collisions.

In this work we theoretically examine how much of the system energy may be temporarily stocked into the reaction system in the form of excitation energy as a

function of $E_{\rm in}$, system size $A_{\rm sys} = A_P + A_T$ (A_P and A_T are projectile and target number of nucleons, respectively) and system mass asymmetry. Four mass symmetric and four mass asymmetric central reactions were studied at several energies. Simulation was carried with the Landau-Vlasov (LV) semiclassical transport model with momentum-dependent Gogny force [6]. The LV model is especially appropriate for describing the early stages of HIR when the system is hot and compressed.

The observable studied is the thermal component (heat), with compression the main intrinsic-energy deposition component of the early-reaction-stage energy transformation. Heat is stocked into the compact system predominantly by NN collisions which occurs in the overlap zone. In the most of cases under study the time is too short for the full relaxation of the pressure tensor and establishment of a global equilibrium in momentum space. Therefore, it is more correct to name this component the excitation energy $E_{\rm x}$. Detailed definition of the transformation of the (system) available energy $E^{\rm c.m.}_{\rm avail} = E_{\rm c.m.}/A$ into intrinsic and collective degrees of freedom may be found elsewhere [5, 7, 8].

As an example of the time evolution of excitation energy per nucleon the inset of Fig. 1 shows $E_{\rm x}/A$ for the Au+Au reaction at six energies studied. Within a laps of time of merely 40–75 fm/c after the contact of colliding nuclei occurring at 0 fm/c the excitation energy per nucleon $E_{\rm x}/A$ reaches a maximum. The regular and nearly symmetric rise and decrease of $E_{\rm x}/A$ with the reaction time is a common behavior for all reactions studied. The observed regularity suggests that maxima of $E_{\rm x}/A$ are proportional to the total energy deposited during HIR.

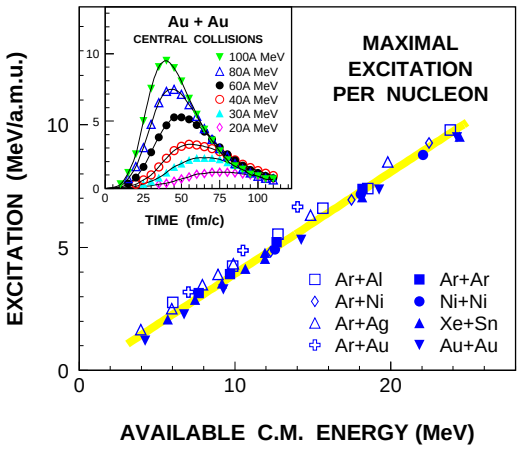

Figure 1: Simulation results of the thermal excitation energy per nucleon $E_{\rm x}/A$ for central collisions. Excitation maxima $(E_{\rm x}/A)_{\rm max}$ as a function of the system available energy $E^{\rm c.m.}_{\rm avail}$ for the mass asymmetric (open symbols) and the mass symmetric (filled symbols) systems studied. The thick grey line is due to the best linear fit to all data points.

We are examining the maximal energy that may be dissipated in HIR. Thus, we take the maxima of $E_{\rm x}/A$ which we denote by $(E_{\rm x}/A)_{\rm max}$. Figure 1 depicts how these maxima depends on $E^{\rm c.m.}_{\rm avail}$ for all studied HIR. All data points lie very close to the fit line. One is facing a peculiar universal linear rise which is independent of

A_{sys} and mass asymmetry in the full and a rather large span of E_{in} covered in this study.

A universal linear dependence of $(E_x/A)_{max}$ on $E^{c.m.}_{avail}$ as well as its nearly exact crossing of the origin in Fig. 1 has an important and remarkable consequence: Expressing the value of maximal excitation in percentage of the system available energy one obtains that the relative fraction of $(E_x/A)_{max}$ in $E^{c.m.}_{avail}$ has an almost constant value for all but symmetric systems at $E_{in} < E_F$ as can be seen in Fig. 2a). From Fig. 2a) one infers that share of E_x/A in $E^{c.m.}_{avail}$ weekly depends on either reaction system or E_{in} and amounts 0.39 ± 0.03 of $E^{c.m.}_{avail}$. In other words, during the early energy transformation in HIR the maximal excitation energy that may be deposited in the system is a constant which amounts about 40 % of the system available energy. Let us underline that this constancy of the maximum-of-excitation-energy share in available energy is evidenced in the fairly broad range of E_{in} (quotient of the highest and the lowest $E^{c.m.}_{avail}$ covered in the simulation is ~ 9) and it is nearly independent of system size (studied is the range of $60 \lesssim A_{sys} \lesssim 400$ nucleons) and mass asymmetry ($A_P : A_T$ is varied between 1:1 and 1:5).

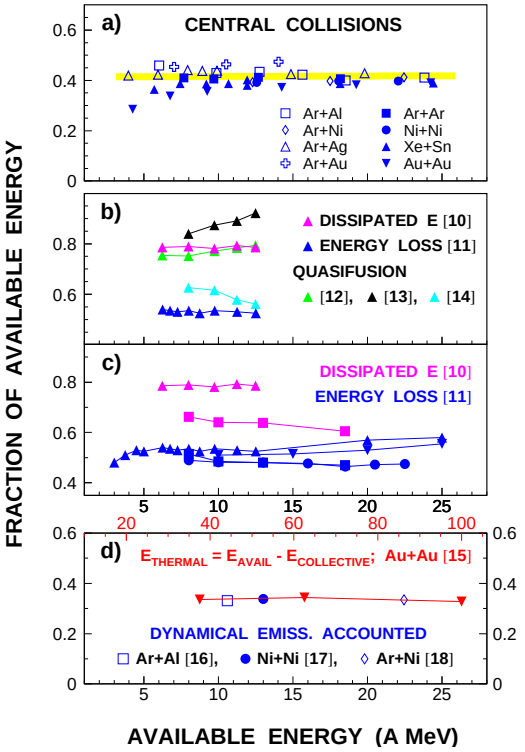

Figure 2: Ratio of the excitation energy per nucleon and the corresponding $E^{c.m.}_{avail}$ as a function of this same available energy $E^{c.m.}_{avail}$. *Panel a)*: Simulation results of Fig. 1. *Panel b)*: Five different analysis of the Xe+Sn reaction for $25A \leq E_{in} \leq 50A$ MeV. *Panel c)*: Ratio values reported in the analyses based on the pure kinematical considerations. *Panel d)*: Ratio values reported in analyses which thoroughly accounted for the pre-equilibrium emission component as well as the results on the total thermal energy reported above $100A$ MeV and for which the abscissae labels above the panel frame are relative to.

An important question is whether the existing central HIR experimental data

support our simulation results and in particular whether E_x linearly depends on E_{in}. Most of the energy put into the system during the early reaction phase is released by the emission of particles and light and intermediate mass fragments owing to the thermal excitation component E_x. At the instant at which the maximum $(E_x/A)_{max}$ is reached a negligible emission occurs and at energies of our interest it amounts at most 3–5 % of the total system mass [5]. Thus, conjunction of the $(E_x/A)_{max}$ with the total (kinetic) energy released in HIR seems to be a natural assumption. One must bear in mind, however, that one should limit the comparison simulation–experiment to general trend of experimental data, i.e. to the degree of linearity of (E_x/A) as a function of $E^{c.m.}_{avail}$ without seeking to reproduce the simulation absolute value because experimental data reflects an integral of the full reaction history.

Experimental non single-E_{in}-energy data on E_x/A and total energy dissipated in central HIR published in periodics during the last two decades ranges from Ar+Al to Au+Au [9–15]. Data points belonging to the same system and the same analysis mostly display close-to-linear dependence on $E^{c.m.}_{avail}$. Unlike the simulation result on $(E_x/A)_{max}$ the experimental data points span a large domain of the E_x/A vs. $E^{c.m.}_{avail}$ plane: The extracted excitations per nucleon lie between one third and almost the full accessible system energy $E^{c.m.}_{avail}$. One may speculate that the different approaches used in extracting from experiments the pertinent information on the global energy deposition in HIR might be at the origin of these much more scattered results. Indeed, data analyzed on a same footing seems to fall into much narrower zones of the $E^{c.m.}_{avail}$ vs. E_x/A plane.

Linear dependence of E_x/A on $E^{c.m.}_{avail}$ is not sufficient to obtain a constancy of its fraction in available energy: The line passing through data points should also pass close to the origin of the $E^{c.m.}_{avail}$ vs. E_x/A plane. As an example in Fig. 2b) are shown results for the Xe+Sn system which have been extensively studied by the INDRA collaboration. Displayed are five analyses of apparently the same data set for $25A \leq E_{in} \leq 50A$ MeV [10–14]. Each analysis has used its own approach in selecting data by centrality and its own philosophy in extracting the total excitation E_x and the primary source mass A. Reported E_x/A differ substantially among them: The absolute value at the same E_{in} differs up to 80 %. Moreover, some of presumed single-source (quasifusion) analyses display a rising fraction of E_x/A in $E^{c.m.}_{avail}$ as E_{in} increases [12, 13], other falling fraction as E_{in} increases [14], whereas the most probable dissipated energy [10] and the total energy loss [11] displays a weak if any dependence on E_{in}.

Dissipated energy and total energy loss are the analyses inspired by the kinematical arguments and do not require presumption on the dominant reaction mechanism. Their drawback is in their applicability to the mass-symmetric systems only. Figure 2c) displays results for all systems studied by these two approaches in a fairly broad range of E_{in}. The total energy loss within the error bars gives the

same constant value for all four systems studied [11]. The results of Figure 2c) are rather weekly depending on $E_{\rm in}$ and may be considered constant. Another example of cases with the constant fraction of $E_{\rm x}/A$ in $E^{\rm c.m.}_{\rm avail}$ is shown in Fig. 2d). Displayed are three single-energy studies that carefully accounted for the copious midrapidity emission [16–18] which occurs during the compact and prior-to-scission reaction phase discussed above as well as the only $E_{\rm x}/A$ result reported so far above 100A MeV [15]. Within blast model extracted is the total thermal energy for the Au+Au reaction from 150A to 400A MeV [15]. These Au+Au data have recently been revised [19] but a strict linearity of the studied ratio as a function of $E_{\rm in}$ did not change so that the value of our fraction should merely be slightly increased.

In conclusion, a semiclassical transport model study of the early reaction phase of central heavy-ion collisions at intermediate energies has been carried out for a variety of system masses, mass asymmetries, and energies below 100A MeV. It has been found that the maxima of the excitation energy $E_{\rm x}$ deposited at this early reaction stage into the reaction system represents a constant fraction of about 40 % of the total center-of-mass available energy of the system $E^{\rm c.m.}_{\rm avail}$. In heavy-ion experiments extracted total dissipated energy per nucleon and total energy loss deduced on kinematical arguments display a similar constancy of their share in the system available energy. A similar result may be found in total excitation energy extracted from experimental observations under condition that the pre-equilibrium emission is properly accounted for. This indicates that the stopping power of nuclear matter is significant even below the threshold of nucleon excitation and that it does not change appreciably over a wide range of incident energies, a result corroborated experimentally [20].

References

[1] A. Bonasera, *et al.*, *Eur. Phys. J.* A **30** (2006) 47.

[2] Ph. Eudes, Z. Basrak and F. Sébille, *Phys. Rev.* C **56** (1997) 2003.

[3] F. Haddad, *et al.*, *Phys. Rev.* C **60** (1999) 031603.

[4] Z. Basrak and Ph. Eudes, *Eur. Phys. J.* A **9** (2000) 207; Ph. Eudes, Z. Basrak and F. Sébille, *Proc. 36th Int. Winter Meeting on Nucl. Phys. (Bormio)* ed. Iori I (University of Milan Press, Milan, 1998), p. 277.

[5] I. Novosel, *et al.*, *Phys. Lett.* B **625** (2005) 26.

[6] F. Sébille, *et al.*, *Nucl. Phys.* A **501** (1989) 137.

[7] P. Abgrall, *et al.*, *Phys. Rev.* C **49** (1994) 1040.

[8] V. de la Mota, *et al.*, *Phys. Rev.* C **46** (1992) 677.

[9] J. Péter, *et al.*, *Nucl. Phys.* A **593** (1995) 95; Sun Rulin, *et al.*, *Phys. Rev. Lett.* **84** (2000) 43; E. Vient, *et al.*, *Nucl. Phys.* A **571** (1994) 588; N. Bellaize, *et al.*, *Nucl. Phys.* A **709** (2002) 367; J.C. Steckmeyer, *et al.*, *Phys. Rev. Lett.* **76** (1996) 4895; J. Wang, *et al.*, *Phys. Rev.* C **72** (2005) 024603; J. Wang, *et al.*, *Phys. Rev.* C **71** (2005) 054608; M. D'Agostino, *et al.*, *Nucl. Phys.* A **724** (2003) 455.

[10] V. Métivier, *et al.*, *Nucl. Phys.* A **672** (2000) 357.

[11] G. Lehaut, *Ph.D. Thesis* (Université de Caen, Caen, France, 2009).

[12] B. Borderie, *et al.*, *Nucl. Phys.* A **734** (2004) 495.

[13] N. Le Neindre, *et al.*, *Nucl. Phys.* A **795** (2007) 47.

[14] E. Bonnet, *et al.*, *Phys. Rev. Lett.* **105** (2010) 142701.

[15] W. Reisdorf, *et al.*, *Nucl. Phys.* A *612* (1997) 493.

[16] G. Lanzanò, *et al.*, *Nucl. Phys.* A *683* (2001) 566.

[17] D. Thériault, *et al.*, *Phys. Rev.* C *71* (2005) 014610.

[18] D. Doré, *et al.*, *Phys. Lett.* B *491* (2000) 15.

[19] W. Reisdorf, *et al.*, *Nucl. Phys.* A *848* (2010) 366.

[20] G. Lehaut, *et al.*, *Phys. Rev. Lett.* **104** (2010) 232701.

The SuperB Project

Giovanni Batignani
INFN, sezione di Pisa, Italy

Tensor Interaction and its effect on Spin-orbit Splitting of Shell Model States

Rupayan Bhattacharya
Department of Physics, University of Calcutta

Abstract

After inclusion of tensor interaction in Skyrme Hartree Fock theory SKP set of parameters have been used to calculate the splitting of single particle shell model states of ^{208}Pb where there is abundant experimental data. For proton states, nuclei ^{207}Tl and ^{209}Bi have been considered for comparison whereas for neutron states nuclei ^{207}Pb and ^{209}Pb were considered. The level splittings of spin-orbit partners are reproduced quite admirably thus vindicating the importance of inclusion of tensor interaction. Neutron skin has also been calculated which may shed light on nuclear symmetry energy.

The genesis of magic numbers is known to be due to a strong spin-orbit interaction in nuclei [1-3]. However, the evolution of single particle energy levels with increasing N or Z forming islands of stability does not follow a simple geometrical rule. With the advent of new experimental facilities like radioactive ion beams it has been observed that new areas of magicity have developed [4-8] while conventional shell gaps have weakened thus necessitating a relook in the mean field type of nuclear structure calculations.

Conventional mean-field calculations [9-15] mainly deal with bulk properties of nuclei, viz., binding energy, rigidity modulus, charge density radius etc. From the point of view of nuclear theory, ^{208}Pb, the doubly magic nucleus, is one of the anchor points in the parameterizations of effective interactions for mean-field calculations. Moreover, there are several experimental results available for lead isotopes [16-20] which provide important information about single particle shell model states near the Fermi surface and systematic data of isotope shifts. Effect of tensor interaction in mean-field type calculations on the evolution of shell structure has recently drawn a lot of interest [21-26] due to its simplistic approach and wide applicability. In this paper we have incorporated the tensor interaction in Skyrme-Hartree-Fock theory to investigate the effect of tensor interaction on the splitting of spin-orbit partners of shell model states near the Fermi surface of ^{208}Pb. We have also calculated the neutron skin of ^{208}Pb given by $S = \langle R_n^2 \rangle - \langle R_p^2 \rangle$, which has a bearing on the evaluation of the symmetry energy for the isotope.

The spin-orbit potential in Skyrme Hartree-Fock theory with the inclusion of tensor component is given by

$$V^{q}_{s.o.} = \frac{W_0}{2r}\left(2\frac{d\rho_q}{dr} + \frac{d\rho_{q'}}{dr}\right) + \left(\alpha\frac{J_q}{r} + \beta\frac{J_{q'}}{r}\right) \tag{1}$$

where $J_{q(q')}(r)$ is the proton or neutron spin-orbit density defined as

$$J_{q(q')}(r) = \frac{1}{4\pi r^3}\sum_i v_i^2(2j+1)\left[j_i(j_i+1) - l_i(l_i+1) - \frac{3}{4}\right]R_i^2(r) \tag{2}$$

The tensor interaction is given by

$$\begin{aligned} V_T = \frac{T}{2}\Big\{&\left[(\sigma_1.k')(\sigma_2.k') - \frac{1}{3}(\sigma_1.\sigma_2)k'^2\right]\delta(r_1 - r_2) + \\ &\delta(r_1 - r_2)\left[(\sigma_1.k)(\sigma_2.k) - \frac{1}{3}(\sigma_1.\sigma_2)k^2\right]\Big\} + \\ &U\{(\sigma_1.k')\delta(r_1 - r_2)(\sigma_1.k) - \frac{1}{3}(\sigma_1.\sigma_2)\times[k'.\delta(r_1 - r_2)k]\} \end{aligned} \tag{3}$$

The coupling constants T and U denote the strength of the triplet-even and triplet-odd tensor interactions respectively.

In Eq.(1) $\alpha = \alpha_c + \alpha_T$ and $\beta = \beta_c + \beta_T$. The central exchange contributions are written in terms of the usual Skyrme parameters as

$$\alpha_c = \frac{1}{8}(t_1 - t_2) - \frac{1}{8}(t_1x_1 + t_2x_2) \tag{4}$$

$$\beta_c = -\frac{1}{8}(t_1x_1 + t_2x_2) \tag{5}$$

The tensor contributions are expressed as

$$\alpha_T = \frac{5}{12}U, \qquad \beta_T = \frac{5}{24}(T+U) \tag{6}$$

In our calculation we have recast α as

$$\alpha = \alpha_c(1 + \alpha_T/\alpha_c) = S_f\alpha_c$$

where S_f is the scale factor $= 1 + \alpha_T/\alpha_c$. Similarly for β we get

$$\beta = S'_f\beta_c, \text{ where } S'_f = (1 + \beta_T/\beta_c).$$

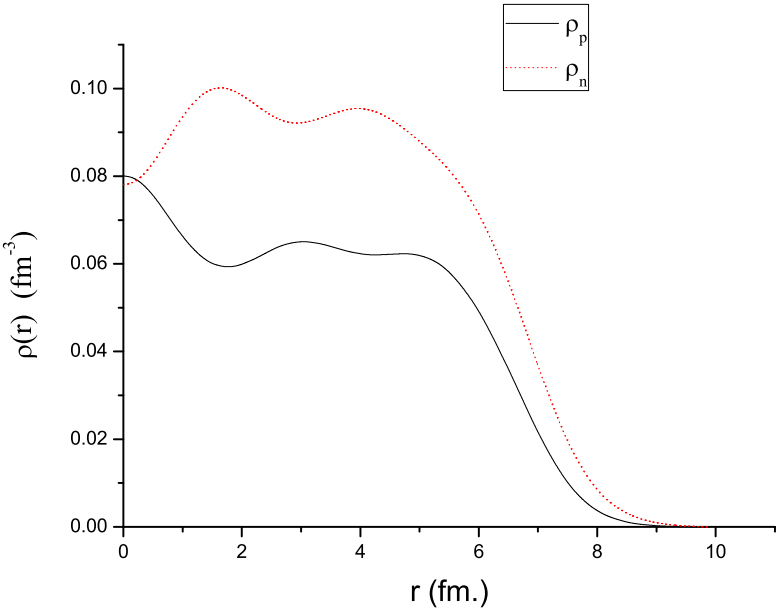

Figure 1: Charge and neutron distribution of ^{208}Pb

We have used SKP set of parameters to calculate the splitting of single particle shell model states of ^{208}Pb. The reasons behind the use of SKP set are: i) it takes the J^2 terms from the central force into account which is necessary for inclusion of the tensor force, ii) it reproduces the ground state properties and the single particle structure of ^{208}Pb quite nicely. From the inclusion of tensor interaction in the Skyrme energy density functional one expects that it will affect the spin-orbit splitting by altering the strength of the spin-orbit field in spin-unsaturated nuclei as expressed in Eq. (1). However, one must remember that the spin-orbit potential is readjusted through each pair of scale factors which are connected to the tensor coupling terms.

The success of the SKP parameters led us to use this set to evaluate the effect of inclusion of tensor forces in finding out the evolution of single particle states in different areas of nuclear chart. The optimal parameters of tensor interaction α_T and β_T were found for SKP forces by optimizing the reproduction of observed splitting of spin-orbit partners of single particle states around ^{208}Pb. In a two parameter search we have found the scale factors $f = -2.4$ and $f' = -1.6$ produces the best result. Because of the fact that the formation of shells depends crucially on the

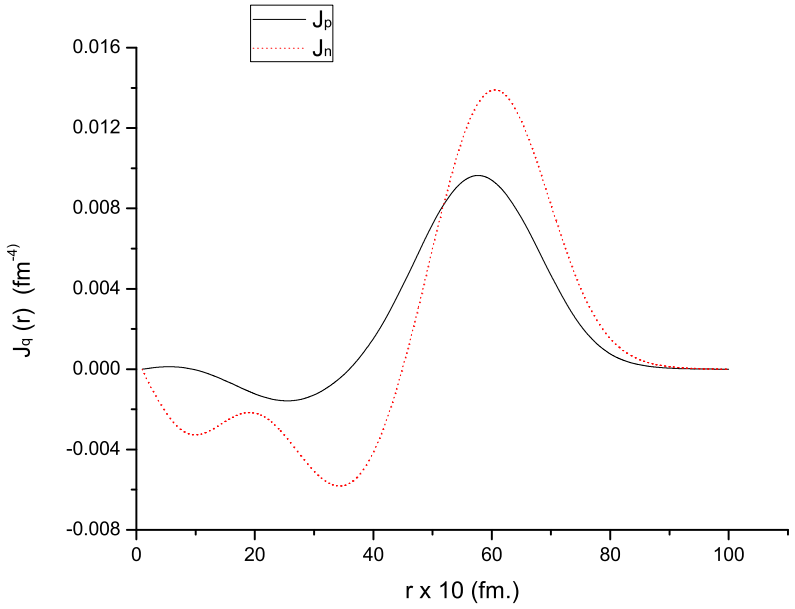

Figure 2: Spin-density distributions of ^{208}Pb

spin-orbit splitting of the single particle states we have chosen the scale factors such that it creates the shell gap in the right place. At the same time, locations of the individual states have not been compromised. In our calculation the value of α came out to be -80.18 and the value of β is 78.14.

In Table I we present our calculated single particle spectrum for ^{208}Pb for different parameter sets SKM, Z_σ, Sly4, SKX and SKP. Single particle behaviour of these states has been well established from detailed spectroscopic measurements. It is quite apparent from the table that SKP produces the best single particle (-hole) spectrum both for proton as well as neutron states of ^{208} Pb. Out of eighteen states studied only in the cases of proton $1g_{9/2}$ state and neutron $1h_{9/2}$ and $1i_{11/2}$ states we find some discrepancies of the order of 1 MeV, otherwise there is a very good agreement.

In Table II the calculated splitting of the spin-orbit partners of proton and neutron single particle states around ^{208}Pb have been presented along with their experimental values. For proton states nuclei ^{207}Tl and ^{209}Bi have been considered for comparison whereas for neutron states nuclei ^{207}Pb and ^{209}Pb were considered. The level splittings are reproduced quite admirably by SKP parameter set with

Table 1: Single particle levels in ^{208}Pb

nlj	-E_{nlj} (MeV)					
	SKM	Z_σ	Sly4	SKX	SKP	EXPT
Proton						
$1g_{9/2}$	16.12	17.50	16.44	16.15	15.18	16.03
$1g_{7/2}$	12.32	13.34	14.67	11.36	11.43	11.51
$2d_{5/2}$	10.16	10.88	11.25	9.64	10.33	10.23
$2d_{3/2}$	8.28	8.87	7.07	7.54	8.80	8.38
$3s_{1/2}$	7.56	8.04	9.01	7.04	8.11	8.03
$1h_{11/2}$	8.42	9.58	8.11	9.95	8.72	9.37
$1h_{9/2}$	2.95	3.62	5.54	3.07	3.52	3.60
$2f_{7/2}$	1.81	2.13	2.32	2.47	3.21	2.91
Neutron						
$1h_{11/2}$	17.27	18.09	16.32	16.52	15.03	14.50
$1h_{9/2}$	11.73	12.09	14.09	9.46	9.84	11.28
$2f_{7/2}$	11.50	11.68	11.21	9.98	10.50	10.38
$2f_{5/2}$	8.53	8.40	9.81	6.67	8.11	7.95
$3p_{3/2}$	8.56	8.63	8.65	7.10	8.21	8.27
$3p_{1/2}$	7.40	7.33	8.10	5.81	7.32	7.38
$1i_{13/2}$	9.42	9.55	7.06	10.37	8.51	9.38
$1i_{11/2}$	2.07	1.83	3.82	1.02	1.84	3.15
$2g_{9/2}$	3.35	2.92	1.64	3.19	3.71	3.74
$2g_{7/2}$	0.27	1.03	0.04	0.95	0.71	1.45

the inclusion of tensor interaction thus vindicating the importance of inclusion of tensor interaction.

In Table III the calculated root mean square proton and neutron radii for ^{208}Pb is presented along with their experimental counterparts for comparison. Though for charge radius we have obtained a very good fit, for neutron the calculated rms radius is slightly smaller than the experimental value. As a result we have obtained a smaller skin thickness S.

In fig. 1 we have presented the charge and neutron distribution of ^{208}Pb. In contrast to a peak in the charge distribution near the centre, the neutron distribution shows a dip. In fig. 2 spin-density $J_q(r)$ for both neutron and proton cases have been presented. As ^{208}Pb is spin-unsaturated in neutron and proton systems tensor interaction has an important role to play.

In this paper we have shown that inclusion of tensor interaction in the Skyrme

Table 2: Splitting of spin-orbit doublets

Protons	Energy in MeV					
	Sly5	Sly4	SKM*	SIII	SKP-T	EXP
Δ1h	6.43	6.22	5.94	5.20	4.64	5.56
Δ2d	1.95	1.89	2.37	1.63	1.55	1.33
Δ2f	2.69	2.61	2.57	2.32	2.17	1.93
Δ3p	1.05	1.02	0.97	0.87	0.79	0.84
Neutrons						
Δ1h	5.83	5.59	5.55	4.73	5.32	5.10
Δ1i	7.65	7.25	7.26	6.39	6.93	6.46
Δ2f	2.05	1.96	2.93	2.67	2.27	2.03
Δ2g	3.68	3.57	3.58	3.30	2.83	2.51
Δ3p	1.17	1.13	1.13	1.02	0.84	0.90
Δ3d	1.72	1.67	1.60	1.47	1.31	0.97

Table 3: R.M.S. Proton and Neutron Radius of ^{208}Pb

R_c (Th.) (fm)	R_c (Expt.) (fm)	R_n (Th.) (fm)	R_n (Expt.) (fm)	R_n - R_p (Th.) (fm)	R_n-R_p (Expt.) (fm) ref. [27]
5.497	5.501	5.554	5.653	0.11	0.195±0.057

Hartree Fock theory the shell gap at $Z = 82$ and $N = 126$ is better reproduced than the conventional mean-field type calculation.

References

[1] M.G. Meyer, Phys. Rev. 74, 235 (1948)

[2] O. Haxel, J.H.D. Jensen and H.E. Suess, Phys. Rev. 75, 1766 (1949)

[3] M. G. Meyer, Phys. Rev. 75, 1969 (1949)

[4] M. Beiner et al, Nucl. Phys. A238, 29 (1975)

[5] J. Dobaczewski et al, Phys. Rev. Lett. 72, 981 (1994)

[6] A. Ozawa et al, Phys. Rev. Lett., 84, 5493 (2000)

[7] M. Stanoiu et al Phys. Rev. C 69, 034312 (2004)

[8] M. Belleguic et al Nucl. Phys. A 682, 136c (2001)

[9] H. Flocard et al, Nucl. Phys. A 231, 176 (1974)

[10] J. Friedrich and P.-G. Reinhard, Phys. Rev. C 33, 335 (1986)

[11] S. Aberg, H. Flocard and W. Nazarewicz, Ann. Rev. Nucl. Part. Sc 40, 439 (1990)

[12] J.P. Blaizot et al, Nucl. Phys. A 591, 435 (1995)

[13] J. Dobaczewski et al, Phys. Rev. C 53, 2809 (1996)

[14] E. Chabanat et al, Nucl. Phys. A 635, 231 (1998)

[15] M. Bender etal, Rev. Mod. Phys. 75, 121 (2003)

[16] M.J. Martin, Nucl. Data Sheets 63, 723 (1991)

[17] M.J. Martin, Nucl. Data Sheets 70, 315 (1993)

[18] M. Anselment et al, Nucl. Phys. A 451, 471 (1986)

[19] G.D. Sprouse et al, Phys. Rev. Lett. 63, 1463 (1989)

[20] G. Mairle and P. Grabmyr, Euro. Phys. Jour. **A 9**, 313 (2000)

[21] T. Otsuka et al, Acta Phys. Pol. B 36, 1213 (2005)

[22] T. Otsuka et al, Phys. Rev. Lett. 95, 232502 (2006)

[23] B.A. Brown et al, Phys. Rev. C 74, 061303(R), (2006)

[24] T. Otsuka et al, Phys. Rev. Lett. 97, 162501 (2006)

[25] G. Colo, H. Sagawa, S. Fracasso and P.F. Bortignon Phys. Lett. B 646, 227 (2007)

[26] D. M. Brink and Fl. Stancu, Phys. Rev. C 75, 064311 (2007)

[27] X. Roca-Maza et al Phys. Rev. Lett. 106, 252501 (2011)

Probing the symmetry energy and in medium cross-section via heavy ion collisions

Zbigniew Chajecki
NSCL, Michigan State University, East Lansing, MI, USA

Constraints on the density dependence of symmetry energy from elliptic flow data

M.D. Cozma
IFIN-HH, Reactorului 30, 077125 Măgurele-Bucharest, Romania

Abstract

An isospin dependent version of the QMD transport model is used to study the impact of the isovector part of the equation of state of nuclear matter on elliptic flow observables. The model dependence of neutron-proton elliptic flow difference is studied for AuAu collisions at an incident energy of 400 MeV per nucleon. It is found that the sensitivity to microscopical nucleon-nucleon cross-sections, compressibility modulus of nuclear matter and width of nucleon wave function are moderate compared to the dependence on the stiffness of the isospin asymmetric part of the equation of state. Comparison with published experimental FOPI-LAND data can be used to set an upper limit to the softness of symmetry energy.

Introduction

One of the remaining open questions in nuclear physics is the equation of state (EoS) of isospin asymmetric nuclear matter (asy-EoS), *i.e*. the density dependence of the symmetry energy (SE). Its precise knowledge is mandatory for a proper understanding of nuclear structure of rare isotopes, dynamics and products of heavy-ion collisions, and most importantly for astrophysical processes such as neutron star cooling and supernovae explosions [1, 2]. Intermediate energy nuclear reactions involving radioactive beams have allowed, by studying the thickness of neutron skins, deformation, binding energies and isospin diffusion to constrain the density dependence of SE at densities below saturation (ρ_0) [3, 4]. Existing theoretical models describing its density dependence generally agree with each other in this density regime, but their predictions start to diverge well before regions with densities $\rho \geq 2\rho_0$ are reached [2].

Several observables that can be measured in heavy-ion reactions have been determined to bear information on the behavior of the SE above ρ_0: the neutron/proton ratio of squeezed out nucleons [5], light cluster emission [6], π^-/π^+ multiplicity ratio in central collisions [7, 8], double neutron to proton ratios of nucleon emission from isospin-asymmetric but mass-symmetric reactions [9], elliptic

flow ratios [10] and others. The FOPI experimental data for the π^-/π^+ ratio [11] have been used to set constraints on the suprasaturation density behavior of SE by various authors with contradicting results: Xiao *et al*. [7] made use of the IBUU transport model supplemented by the isovector momentum dependent Gogny inspired parametrization of SE [12] to point toward a soft asy-EoS, while the study of Feng *et al*. [8], which employed IQMD and a power-law parametrization of the symmetry energy $S(\rho) = S_0\,(\rho/\rho_0)^\gamma$, favors a stiff SE. The study of elliptic flow ratios (npEFR) of Ref. [10] favors, by making use of the power-law parametrization of SE, an asy-EoS dependence on density above saturation point close to a linear one: γ=0.9±0.4.

Elliptic flows of protons and neutrons cannot be used separately to constrain the isovector part of the equation of state above saturation point due to their sizable dependence on the values of transport model parameters, that are either inaccurately determined or do not represent measurable quantities, like in-medium nucleon-nucleon (NN) cross-sections, compressibility modulus of nuclear matter and width of nucleon wave function [13]. In this proceeding the case of neutron-proton elliptic flow difference (npEFD) is presented by studying in detail its model dependence and from a comparison with published experimental FOPI-LAND data [14] an upper limit on the softness of SE is inferred. The current status of constraining the asy-EoS from elliptic flow data can be found in Ref. [15].

Elliptic flow difference

The azimuthal distribution of protons (or neutrons) resulted in heavy-ion collisions can be approximately described by $dN/d\phi = (N/(2\pi)\,[\,1 + a_1 \cos\phi + a_2 \cos 2\phi\,]$. The elliptic flow parameter a_2 can by extracted from simulated or experimental data by computing the following average over the respective particle specie in the final state: $a_2 = (1/N) \sum_{i=1,N} ({p_x^i}^2 - {p_y^i}^2)/{p_T^i}^2$. The neutron-proton elliptic flow difference can readily be obtained: $a_2^{n-p} = a_2^n - a_2^p$. The results presented in this Section are restricted to Au+Au collisions at an incident energy of 400 MeV per nucleon. Simulations have been performed using an isospin depedent QMD transport model, all its relevant details for the present study can be found in Ref. [13].

We begin by demonstrating the sensitivity of npEFD to the stiffness of asyEoS, presented in the left panel of Fig. 1. The stiffness of SE is varied between an extreme soft (x=2) and extreme stiff (x=-2) scenario. Furthermore the compressibility modulus is varied from a soft (K=210 MeV) to a stiff (K=380 MeV) value. The most reliable extraction of this model parameter (K) has been made possible by studying the multiplicity ratio of K^+ production in heavy (Au+Au) over light (C+C) nuclei at incident energies close to 1 AGeV favoring a soft EoS, but harder

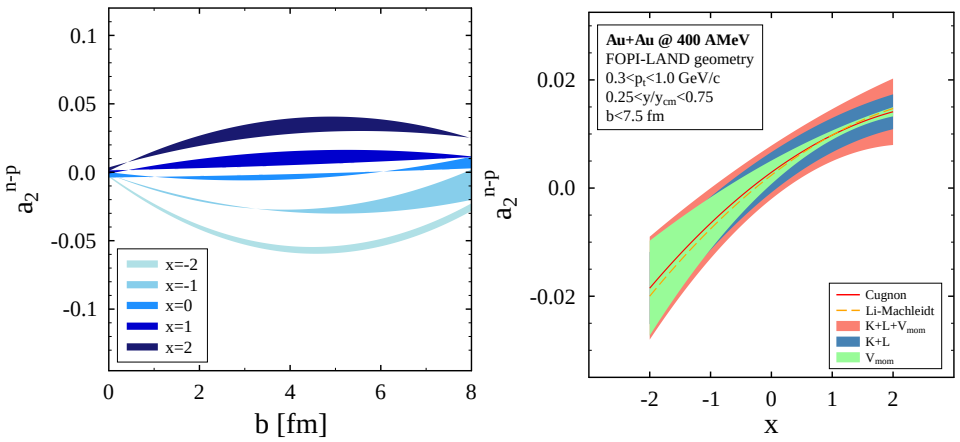

Figure 1: *(Left)* Dependence of the npEFD on the stiffness of asy-EoS The width of each band represents the sensitivity to the change of the stiffness of the isoscalar part of the EoS from a soft (K=210 MeV) to a stiff (K=380 Me) one. *(Right)* Summed up sensitivity of impact parameter integrated npEFD due to variations of the values of compressibility modulus, width of nucleon wave function and optical potential.

scenarios are not excluded since studying sidewards flow (FOPI collaboration data) points towards soft or hard EoS of state depending on system size. Secondly, elliptic flows of protons and neutrons taken separately are strongly dependent of the precise value of K [13]. The clear separation of the results corresponding to different values of x is a clear indication of the feasibility of using npEFD in the attempt to constrain the supranormal density dependence of SE. The presented results have been obtained by applying kinematical cuts specific to the FOPI experiment [16], the case of the FOPI-LAND data is not as favorable.

The study is extended, in the right panel of Fig. 1, by considering additional model dependence due to various parametrization of the nucleon-nucleon cross-sections, value of the nucleon wave-packet width and parametrization of the optical potential. For the first we employ two different vacuum parametrizations: Cugnon and Li-Machleidt and several scenarios for the density and asymmetry dependence of second (details in Ref. [13]). The width of the nucleon wave function is usually set in literature to $2L^2$=4 fm^2 for light systems, while for heavy systems an increase to the value $2L^2$=8 fm^2 is found necessary in order to generate nuclei with stable static properties (*e.g.* rms) and consequently is varied within these limits. For the nucleon optical potential we switch between the Gogny inspired (monopole) and the Hartnack-Aichelin (customarily employed by QMD transport models) parametrizations which differ mostly in their higher energy part, the for-

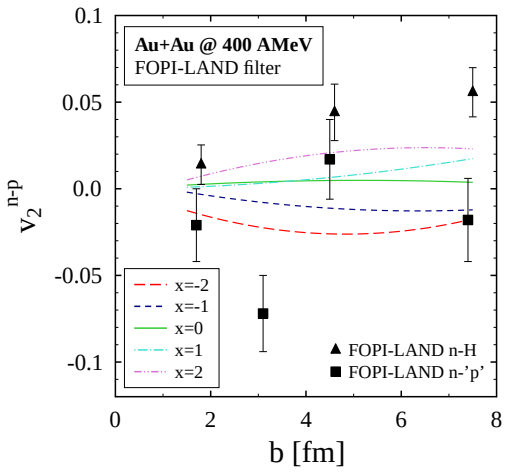

Figure 2: Comparison of the theoretical estimates for npEFD with the experimental FOPI-LAND values for neutron-proton and neutron-hydrongen EFD [14].

mer being attractive while the latter repulsive. Additionally we present results for FOPI-LAND kinematics, of special interest since both proton and neutron elliptic flow parameters have been measured. It is concluded that model dependence, while important, does not obstruct irreparably the sensitivity of npEFD to the stiffness of asy-EoS. A study, with similar conclusions, can be performed for neutron-proton elliptic flow ratios (npEFR)(proposed in Ref. [10]) and together with npEFD a constraint on the stiffness of SE can be extracted with a proper understanding of the impact of model dependence on the final result [17].

In Fig. 2 a comparison of theoretical values for npEFD with published experimental results [14] for npEFD and nHEFD (H-hydrogen) is presented. Due to insufficient calorimeter resolution the extraction of pure proton spectra has not been straightforward and as a result the impact parameter dependence of npEFD is not smooth making an extraction of the stiffness of the asyEoS not trustworthy. nHEFD does not suffer from a similar problem. Together with the known fact that heavier isobars present stronger elliptic flow we can use nHEFD to extract an upper limit to the softness of the asyEoS. An exclusion of the super-soft scenarios thus emerges from a comparison of model and experimental data.

To conclude, we have studied the sensitivity of npEFD to different model parameters like microscopic NN cross-sections, compressibility modulus of nuclear matter, optical potential and width of nucleon functions as compared to the sensitivity to the stiffness of the asy-EoS. We have found that summed together (in

quadrature) the indetermination of npEFR due to inaccurately known model parameters amounts to about 40% of the splitting of the same observable between the super-stiff and super-soft asy-EoS scenarios. A comparison with published npEFD experimental data is problematic due to their scattered impact parameter dependence, while a comparison with nHEFD data suggests that super-soft scenarios for asy-EoS can be excluded. A better understanding of model dependence of theoretical estimates together with higher accuracy data expected to be delivered by the ASY-EOS collaboration [18] will make possible the extraction of tight constraints on the stiffness of asy-EoS using elliptic flow observables.

Acknowledgments

M.D.C. would like to thank the organizers of the ASYEOS-2012 workshop for their great job, W. Trautmann for extensive discussions on the topic and the Romanian Ministry of Education and Research for financial support (PN09370103 grant).

References

[1] V. Baran V, *et al.* 2005 *Phys. Rep.* **410** 335.

[2] B.A. Li, K.W. Chen and C.M. Ko 2008 *Phys. Rep.* **464** 113.

[3] B.A. Li, C.M. Ko and W. Bauer 1998 *Int. J. Mod. Phys.* E **7** 147.

[4] L.W. Chen, C.M. Ko and B.A. Li 2005 *Phys. Rev. Lett.* **94** 032701.

[5] G.C. Yong, B.A. Li and L.W. Chen 2007 *Phys. Lett.* B **650** 344.

[6] L.W. Chen, C.M. Ko and B.A. Li 2003 *Phys. Rev.* C **68** 017601.

[7] Z. Xiao, *et al.* 2009 *Phys. Rev. Lett.* **102** 062502.

[8] Z.Q. Feng and G.M. Jin 2010 *Phys. Lett.* B **683** 140.

[9] Q. Li, Z. Li and H. Stöcker 2006 *Phys. Rev.* C **73** 051602.

[10] P. Russotto, *et al.* 2011 *Phys. Lett.* B **697** 471.

[11] Reisdorf W*et al.* [FOPI Collaboration] 2007 *Nucl. Phys.* A **781** 459.

[12] C.B. Das, *et al.* 2003 *Phys. Rev.* C **67** 034611.

[13] M.D. Cozma 2011 *Phys. Lett.* B **700** 139.

[14] D. Lambrecht *et al.* [FOPI-LAND Coll.] 1994 *Z. Phys.* A **350** 115.

[15] W. Trautmann and H. Wolter, 2012 *Int. J. Mod. Phys.* E **21** 1230003.

[16] A. Andronic *et al.* 2001 *Nucl. Phys.* A **679** 765.

[17] M.D. Cozma *et al.*, in preparation.

[18] P. Russotto *et al.* [ASY-EOS Collaboration] arXiv:1209.5961 [nucl-ex].

Probing the symmetry energy at low density using observables from neck fragmentation mechanism

E. De Filippo[1], *F. Amorini*[2], *L. Auditore*[3], *V. Baran*[4], *I. Berceanu*[5], *G. Cardella*[1], *M. Colonna*[2], *L. Francalanza*[6,2], *E. Geraci*[6], 1, *S. Giani*[2], *L. Grassi*[2], *A. Grzeszczuk*[7], *P. Guazzoni*[8], *J. Han*[2], *E. La Guidara*[1], *G. Lanzalone*[9,2], *I. Lombardo*[10], *C. Maiolino*[2], *T. Minniti*[3], *A. Pagano*[1], *E.V. Pagano*[6,2], *M. Papa*[1], *E. Piasecki*[11,12], *S. Pirrone*[1], *G. Politi*[6,1], *A. Pop*[5], *F. Porto*[6,2], *F. Rizzo*[6,2], *P. Russotto*[1], *S. Santoro*[3], *A. Trifirò*[3], *M. Trimarchi*[3], *G. Verde*[1], *M. Vigilante*[10], *J. Wilczyński*[12] *and L. Zetta*[8]

[1] *INFN sezione di Catania, Italy*
[2] *INFN, Laboratori Nazionali del Sud, Catania, Italy*
[3] *INFN, Gr. Coll. Messina and Dip. di Fisica, Univ. di Messina, Italy*
[4] *Physics Faculty, University of Bucharest, Romania*
[5] *Nat. Inst. of Physics and Nucl. Engineering, Bucharest, Romania*
[6] *Dip. di Fisica e Astronomia, Univ. di Catania, Catania, Italy*
[7] *Institute of Physics, University of Silesia, Katowice, Poland*
[8] *INFN, Sez. Milano and Dip. di Fisica, Univ. di Milano, Italy*
[9] *"Kore" Università, Enna, Italy*
[10] *INFN, Sez. Napoli and Dip. di Fisica, Univ. di Napoli, Italy*
[11] *Heavy Ion Laboratory, University of Warsaw, Warsaw, Poland*
[12] *National Centre for Nuclear Research, Otwock-Świerk, Poland*

Abstract

We present new data from the ^{64}Ni + ^{124}Sn (neutron rich) and ^{58}Ni + ^{112}Sn (neutron poor) studied in direct kinematics and compared with the same reaction in reverse kinematics at the beam incident energy (35 *A* MeV). The ensamble of data of the two experiments collect a unique set of information on the midrapidity neck fragmentation mechanism in semi-peripheral dissipative collisions. By comparing data of the reverse kinematics experiment with a stochastic mean field (SMF) calculations we show that observable from neck fragmentation mechanism add valuable constraint on the symmetry energy term of the EOS. An indication is found for a linear behavior of

the symmetry potential. Perspectives and projects for the next future using stable and radiactive beams are also given.

Introduction and Results

The main goal of this contribution is to present new experimental data for the ^{64}Ni+^{124}Sn and ^{58}Ni+^{112}Sn reactions studied in direct kinematics with the CHIMERA detector at the same beam incident energy (35 *A* MeV) of the previously studied experiment in reverse kinematics [1, 2]. We show that the Intermediate Mass Fragments (IMF, 3≤Z≤20) midrapidity emission presents many experimental properties (like the N/Z isospin asymmetry enhancement) that in transport models calculations are attributed to the formation, in the early stage of the reaction, of a low density region ("neck") connecting projectile-like and target-like fragments. These properties, correlated with the timescale evolution of the nuclear reactions, can be linked to the reaction dynamics. We have compared experimental data for the reverse kinematics experiment with a stochastic mean field calculation (SMF) in order to get a parametrization for the potential symmetry energy term of EOS. We selected almost complete events where the total charge is 45≤ Z_{TOT} ≤80 and the parallel momentum of the colliding system is at least 60% of the total one. Semipheripheral collisions were selected gating on the total charged particle multiplicity M≤7. We considered in the data analysis a subset of events where the total charge of the three biggest fragment Z(1)+Z(2)+Z(3) ≥ 45 and their momentum $p(1) + p(2) + p(3) \geq 0.6 p_{beam}$. The three biggest fragments of each event were sorted according to the decreasing value of their parallel velocity, following the method described in [2]. The three particles, labeled as PLF,IMF (3≤Z≤20) or TLF, depending upon their respective velocity were analyzed to check the correct attribution event by event; finally the fragment-fragment relative velocities $V_{REL}(PLF, IMF)$ and $V_{REL}(TLF, IMF)$ were calculated and are reported in Fig. 1.

The relative velocities are normalized to the one corresponding to the Coulomb repulsion as given by the Viola systematics. Fig. 1 shows the correlations between the two relative velocities: $r_1 = V_{REL}/V_{Viola}(PLF, IMF)$ and $r_2 = V_{REL}/V_{Viola}(TLF, IMF)$ for the IMFs charges Z = 4,6,10,14. We note that we can populate with similar efficiency both the regions along the r_1=1 axis (whose yield is dominated by sequential emission from PLF) and r_2=1 axis (whose yield is mainly due to sequential emission from TLF); values of r_1 and r_2 simultaneously larger than unity indicate a prompt ternary division (dynamical origin). We can observe that heavier fragments (as Z=14 in the figure) are originated mainly by the break-up or fission of the heavy partner, i.e. the target-like residue in our case and they lie along the r_2=1 axis, while light fragments are concentrated along the diagonal, indicating

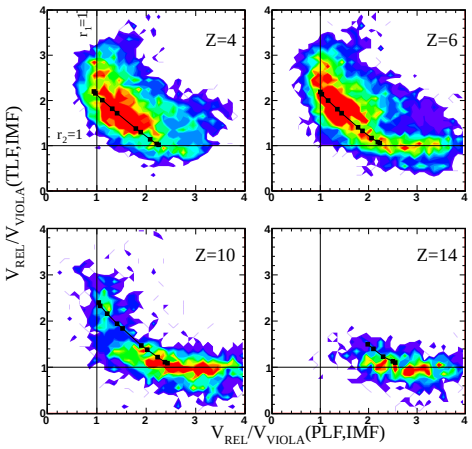

Figure 1: For the ^{64}Ni+^{124}Sn reaction, correlations between relative velocities V_{REL}/V_{Viola} of the three biggest fragments in the event for Z_{IMF}=4,6,10,14.

their prevailing dynamic origin. In Fig. 1 a timescale calibration was done, as in Ref. [1] using a three-body collinear Coulomb trajectory calculation. The inner points along the diagonal correspond to the shortest timescales (40-60 fm/c), with IMFs predominantly emitted from the dynamically expanding neck region formed at midrapidity, between the projectile-like and target-like primary fragments.

We have evaluated the angle θ_{PROX} to study the alignment properties of midvelocity fragments. As shown in the inset of Fig. 2d), if the IMF had its origin from a PLF break-up, θ_{PROX} is the angle between the (PLF-IMF center of mass)-TLF relative velocity axis, and the PLF-IMF break-up axis (relative velocity between PLF and IMF oriented from the light to the heavy fragment). This definition requires the explicit detection of a TLF and PLF fragments in the same event. cos(θ_{PROX})=1 indicates a complete alignment with the IMF emitted in the backward hemisphere respect to the PLF; cos(θ_{PROX}) $<$ 0 indicates the emission in the forward hemisphere respect to the PLF. Of course the IMF emission could be attributed also to a TLF break-up. As a first approximation, we have calculated cos(θ_{PROX}) requiring the condition $V_{REL}(PLF,IMF)/V_{Viola}$ <1.6. A more complete analysis in the direct kinematics experiment will give the possibility to extend and complete these results considering the contribution due to both the TLF and PLF break-up [3].

Fig. 2 shows the cos(θ_{PROX}) angular distribution for Z=4 and Z=8 IMFs for the two reactions under study in the direct kinematic reaction (a,b left panels) and in the reverse kinematic reaction (c,d right panels) respectively. The yields are normalized to the respective area. For a statistical emission the cos(θ_{PROX}) distribution is expected to show a forward-backward symmetry around cos(θ_{PROX}) = 0.

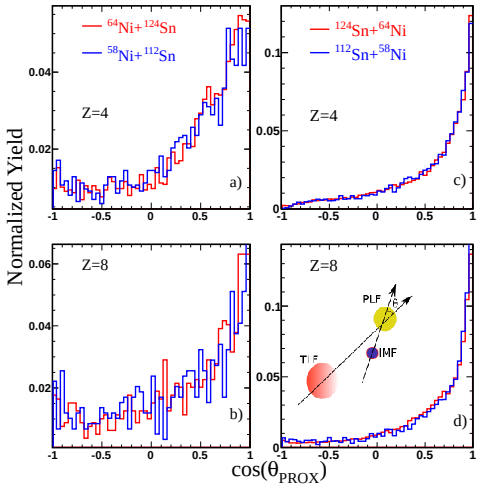

Figure 2: a),b) panels: $\cos(\theta_{PROX})$ angular distribution calculated for a PLF (Ni-like) break-up and production of Z=4 and Z=8 IMFs for the reactions $^{64}Ni + ^{124}Sn$ (red histogram) and ^{58}Ni+^{112}Sn (blue histogram); c), d) panels: same distributions for the for the reverse kinematic reactions ^{124}Sn+^{64}Ni (red histogram) and ^{112}Sn+^{58}Ni (blue histogram) for a PLF (Sn-like) break-up. The insert in Fig. 4d) gives a sketch of the θ_{PROX} definition.

We note that the distributions are peaked at $\cos(\theta_{PROX}) \approx 1$ indicating a strong anisotropy favoring the backward emission respect to the forward one in a strict aligned configuration along the TLF-PLF separation axis.

Fig. 3a) shows the $< N/Z >$ as a function of the IMFs atomic number Z for the reaction ^{124}Sn+^{64}Ni. Fragments statistically emitted in the PLF forward hemisphere have been selected by using the condition $\cos(\theta_{PROX}) < 0$. The relative points are shown as solid squares in Fig. 3a). Solid circles shows the $< N/Z >$ for dynamically emitted IMFs. Events for these particles are selected by imposing that $\cos(\theta_{PROX}) > 0.8$ (highest enhancement for backward emission) and selecting events near the diagonal in the $V_{REL}/V_{Viola}(PLF, IMF) - V_{REL}/V_{Viola}(TLF, IMF)$ relative velocities correlation plot. We note that the $< N/Z >$ ratio is systematically larger for dynamically emitted particles respect to the statistically emitted ones. In Fig. 3c) we have reported (solid circles), for the same reaction, the correlation between $\cos(\theta_{PROX})$ and $< N/Z >$ for all fragments with charges between $5 \leq Z \leq 8$. We observe an increase of the $< N/Z >$ at values of $\cos(\theta_{PROX})$ approaching to 1, corresponding to the highest degree of alignment. A similar result has been found recently, in a different data analysis contest, for the ^{124}Xe+^{124,112}Sn system [4].

The data, for the inverse kinematics neutron rich reaction ^{124}Sn+^{64}Ni, were compared with a transport theory using the stochastic mean field model (SMF)

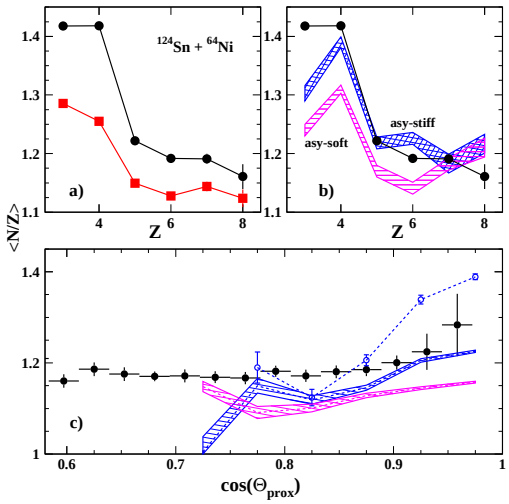

Figure 3: a) For the ^{124}Sn+^{64}Ni reaction, experimental $< N/Z >$ distribution of IMFs as a function of charge Z for dynamically emitted particles (solid circles) and statistically emitted particles (solid squares); b) solid circles: same experimental data of Fig. 5a) for dynamically emitted particles. Blue hatched area: SMF-GEMINI calculations for dynamically emitted particles and asy-stiff parametrization; magenta hatched area: asy-soft parametrization for dynamically emitted particles. c) solid circles: experimental $< N/Z >$ as a function of cos(θ_{PROX}) for charges $5 \leq Z \leq 8$; empty circles: SMF calculation for primary fragment (asy-stiff parametrization); SMF-GEMINI calculations are indicated by blue-hatched area (asy-stiff parametrization) and magenta hatched area (asy-soft) respectively.

based on Boltzmann-Norheim-Vlasov (BNV) equation [5]. The potential part of the symmetry energy is taken into account using two different parametrizations as a function of density named *asy-stiff* and *asy-soft*. The first one linearly increases with the density while the second one exhibits a weak variation around the saturation density ρ_0. The slope parameter of the symmetry energy is in the current calculation around 80 MeV for the asy-stiff and 25 MeV for the asy-soft choice. The statistical code GEMINI is used as a second step de-excitation phase applied to the SMF primary hot fragments. In Figs. 3b,c) the SMF + GEMINI calculations are plotted as hatched area histograms for dynamically emitted fragments. As can be observed in Fig. 3b) the asy-stiff parametrization (blue hatched area) produces more neutron rich fragments respect to the asy-soft choice and the difference persists after the GEMINI secondary-decay stage for Z<7. In Fig. 3c) SMF calculations for primary fragments and asy-stiff parametrization are also shown (empty circles symbol). The asy-stiff parametrization matches the experimental data fairly

well. This is confirmed in Fig. 3c) where the asy-stiff parametrization better reproduces the $< N/Z >$ enhancement observed for values of $\cos(\theta_{PROX}) > 0.9$.

All these aspects open new perspectives for reaction studies with exotic beams. Our first outlook is in fact the possibility to plan new experiments using a 30 *A* MeV ^{68}Ni beam recently produced at LNS [6]. As a second outlook, we have recently proposed to study the ^{124}Xe+^{64}Zn reaction as compared with ^{124}Sn+^{64}Ni system where only the N/Z changes for the two systems with the same masses. We hope this study will permit to disentangle mass from isospin asymmetry effects evidencing the effective role of symmetry energy in the dynamics of the reactions.

References

[1] De Filippo E et al. (2005) *Phys. Rev. C* **71** 044602

[2] De Filippo E et al. (2012) *Phys. Rev. C* **86** 014610

[3] S. Gianì: Master thesis (Catania University) 2012

[4] Hudan S et al. (2012) *Phys. Rev. C* **86** 021603(R)

[5] Chomaz P, Colonna M and Randrup J (2004) *Phys. Rep.* **389** 263

[6] Pagano A (2012) *Proceedings of the IWM2011, Int. Workshop on Multifragmentation and Related Topics*, Caen (France) 2-5 November 2011, EPJ Web of Conferences vol. 31, 00005

Kaon properties in cold or dense nuclear matter

Laura Fabbietti
Excellence Cluster Universe, TUM Munich, Germany

Abstract

Kaons properties have been extensively studied in the last 2 decades employing heavy ion collisions and p-Nucleus collisions. Kinematic and global variables are employed to extract information about the average Kaon-Nucleus potential under different temperature and density of the system. In this talk the data measured by the HADES collaboration in Ar+KCl, p+p and p+Nb reactions will be presented together with the future perspectives.

An investigation into quasifree scattering of neutron-rich carbon and nitrogen nuclei around N=14

P. Díaz Fernández for the R3B collaboration
Dept. of Particle Physics, Universidade de Santiago de Compostela, 15782 Santiago de Compostela, Spain

Abstract

The well established shell structure of stable nuclei is observed to evolve towards the dripline. New magic numbers are found to emerge around N=14 and N=16, with traditional ones such as N=20 eroding. Experimental evidence of this evolution is already available for the oxygen isotopic chain, however very little information is known for the case of lower charges. Neutron-rich carbon and nitrogen isotopes are very important to understand the persistence of the N=14 and the N=16 shell-closures in lighter nuclei. Quasi-free scattering reactions that knock-out valence and deeply bound protons in (p,2p) and neutrons in (p,pn), are a powerful tool to study simultaneously the proton and neutron single-particle properties of the nuclei in the psd shell.

The quasi-free scattering was used for many decades to study the single-partile properties of the nuclei [1], is a tecnique that differs from the knock-out because the excitation energy is bigger and it is possible to study deeply bound states. The experiment was performed at GSI (Darmstadt) using the R3B-LAND setup. Secondary cocktail beams were produced by fragmentation of a ^{40}Ar primary beam on a thick berylium target, the ions of interest were selected at the Fragment Separator and transported to the experimental cave. The incoming beam was identified (Fig.1) measuring the time-of-flight with two plastic scintillators and the energy loss with a Position Sentive silicon Pin diode. Targets of CH_2 (922 mg/cm^2) and C (935 mg/cm^2) were used to study the quasi-free scatering reactions.

Surrounding the target there was a 4π spherical calorimerer made of NaI (Tl) crystals (~20 cm long) used for detection of gamma rays, protons and neutrons (energies, angular distributions and multiplicities) and 8 Silicon Strip Detectors, four of them setting up a box around the target and dedicated to angular measurements. The rest are located in the beam axis in pairs, before and after the target. They are used to track incoming beam and fragments and also for charge identification. A large acceptance dipole is used for particle deflection. Depending on their E, A and

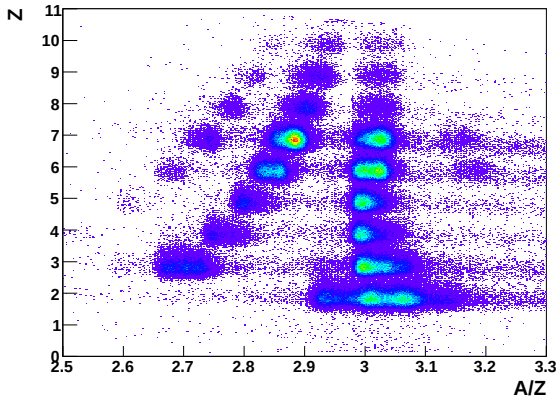

Figure 1: Incoming identification plot for A/Z equal 3.

Z the outgoing fragments experience different bendings. There are three detection branches: one for heavy-fragments, one for protons and another for neutrons. The heavy-ion branch consist of two scintillating fiber detectors for particle tracking in the horizontal direction and a time-of-flight plastic wall for time-of-flight and energy loss measurements. The mass of the outgoing particles needs to be calculated using a dedicated tracking subroutine [1], reconstructing the trajectories through the magnetic field for the outgoing fragments and protons from the laboratory positions of the detectors, the charge of the fragment being tracked and the magnet current. Fig.2 shows an example of the recontructed mass

This complex experimental setup provides all the ingredients to study the reactions of interest. The detection of gamma rays emitted in flight is analyzed using an addback algorithm. The program looks for the crystal with the maximum energy deposited in one event and add-up the energy of the first neighbours, this is called cluster. Once a cluster is built this energy is Doppler corrected and the energies of the crystals involved in a cluster are set to zero and the process starts again, until all the energies above a certain threshold have been used. All the results are for the ^{22}O because exist a lot of information available in order to test our analysis. Results for the ^{22}O gamma rays in good agreement with previous results ([2], [3]) are shown in Fig.3.

The quasi-free scattering reactions([1], [4], [5]) have a very well defined angular signatures of the recoil neutrons and protons given by the kinematics of the

[1]Developed by Ralf Plag for the R3B collaboration.
Information about the detectors and the tracking programme http://www-linux.gsi.de/ rplag/land02/index.php?page=tracking2

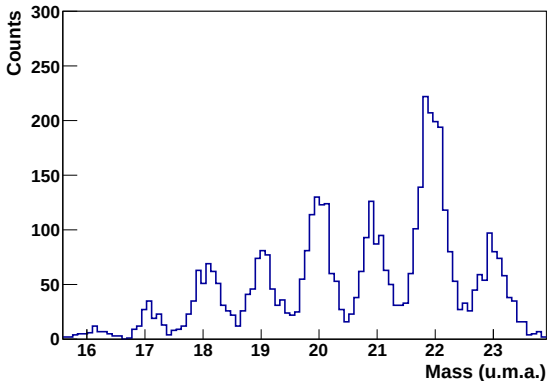

Figure 2: The mass spectrum for reacted events using Crystal Ball sum trigger for the CH_2 target.

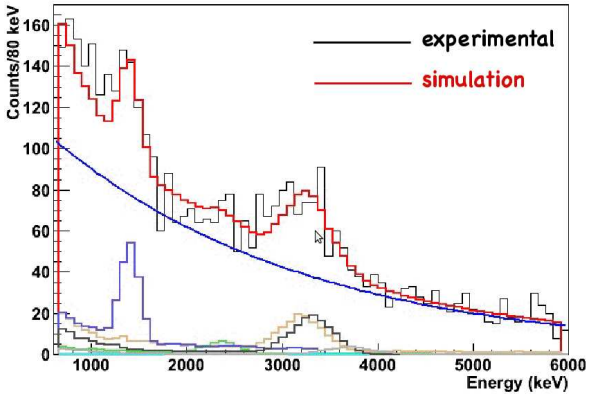

Figure 3: Gamma energy obtained after addback, experimental (black) and simulation (red) spectra.

reaction. The proton and the neutron are expected to be emitted back-to-back in azimuthal angle and the opening angle of both particles will be at ~90^o. The calorimeter is also used to identify the quasi-free scattering events in the data with a specific electronic read-out. In Fig.4 we show an example of the mentioned angular distributions corresponding to the recoil neutron and proton after the quasi-free scattering reaction.

With all the exprimental information mentioned above it is possible to evaluate the momentum distributions of the fragments. When a nucleon is removed from a shell via quasi-free, the momentum of the residual nucleus contains the information

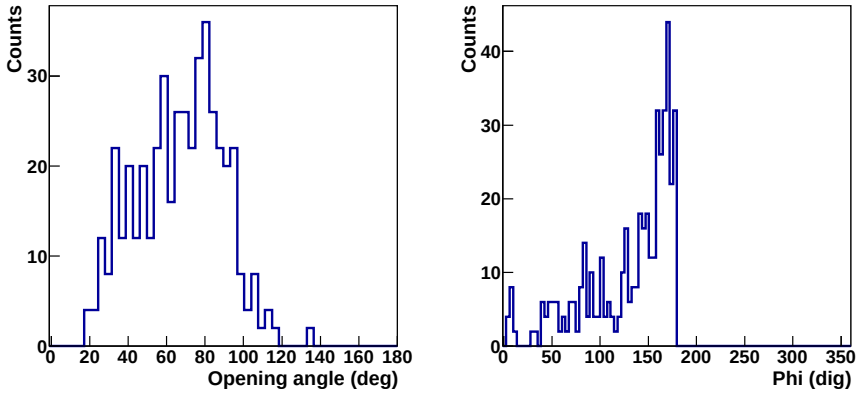

Figure 4: Left: opening angle distributions of the recoil neutron and proton coming from a quasi-free scattering reaction in a CH_2 target. Right: difference between the azimuthal angles of the recoil neutron and proton coming from a quasi-free scattering reaction in a CH_2 target.

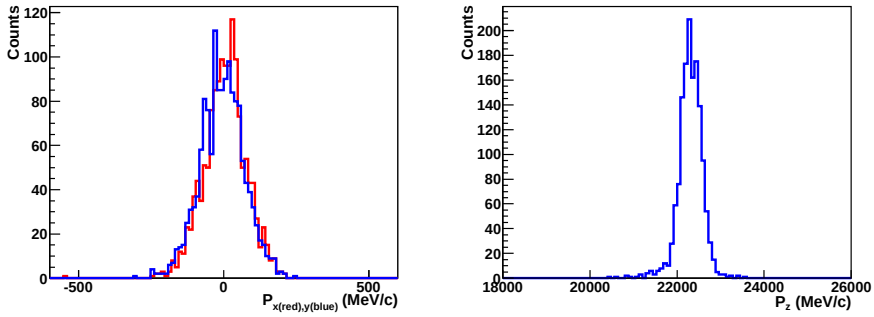

Figure 5: Left: Transversal momentum distributions in X and Y direction of the ^{22}O. Right: Longitudinal momentum distribution of the ^{22}O.

about the angular momentum of the ejected nucleon [1]. Fig.5 shows the different momentum projections for ^{22}O. The width[2] of the X and Y components is ~71 Mev/c and the width for the longitudinal component is ~230 MeV/c.

The analysis of this experiment is still ongoing and the interpretation of the data is not finish yet. Preliminary results of ^{23}(p,pn)^{22}O, together with another preliminary results for other channels, have been presented in the ASYEOS-2012

[2]In this case width means sigma.

workshop. In this summary a complete tracking of the fragments before and after the reaction, the gamma rays spectra and the momentum distributions for the ^{22}O have been shown and briefly disscused.

Acknowledgments

Special thanks to the directors of my work Héctor Álvarez Pol and Dolores Cortina Gil, the members of my group at the University of Santiago de Compostela and the members of the R3B collaboration.

References

[1] G. Jacob and T. A. J. Maris, Quasi-Free Scattering and Nuclear Structure.Reviews of Modern Physics, **38**, 121-142 (1966).

[2] D.Cortina et al., Shell Structure of the Near-DripLine Nucleus ^{23}O, Physical Review Letters, **93**(6)(2004).

[3] M. Staniou et al., N=14 and N=16 shell gaps in neutron-rich oxygen isotopes, Physical Review C, **69**(3), 1-10 (2004).

[4] F. Wamers, Quasi-Free-Scattering and One-Proton-Removal Reactions with the Proton-Dripline Nucleus ^{17}Ne at Relativistic Beam Energies. PhD thesis,TU-Darmstadt (2011).

[5] J. Taylor, Proton Induced Quasi-free Scattering with Inverse Kinematics. PhD thesis, Liverpool (2011)

The NEUland detector of the R3B collaboration

Igor Gasparic
TU Darmstadt/IRB Zagreb, Darmstadt, Germany

Rare Kaon Signals from Au+Au Collisions at HADES

K. Gill[7], G. Agakishiev[6], C. Behnke[7], D. Belver[16], A. Belyaev[6], J.C. Berger-Chen[8], A. Blanco[1], C. Blume[7], M. Böhmer[9], P. Cabanelas[16], S. Chernenko[6], C. Dritsa[10], A. Dybczak[2], E. Epple[8], L. Fabbietti[8], O. Fateev[6], P. Fonte[1,a], J. Friese[9], I. Fröhlich[7], T. Galatyuk[4,b], J. A. Garzón[16], M. Golubeva[11], D. González-Díaz[4], F. Guber[11], M. Gumberidze[14], S. Harabasz[4], T. Hennino[14], R. Holzmann[3], P. Huck[9], C. HÄšhne[10], A. Ierusalimov[6], A. Ivashkin[11], M. Jurkovic[9], B. Kämpfer[5,c], T. Karavicheva[11], I. Koenig[3], W. Koenig[3], B. W. Kolb[3], G. Korcyl[2], G. Kornakov[16], R. Kotte[5], A. Krása[15], E. Krebs[7], F. Krizek[15], H. Kuc[2,14], A. Kugler[15], A. Kurepin[11], A. Kurilkin[6], P. Kurilkin[6], V. Ladygin[6], R. Lalik[8], S. Lang[3], K. Lapidus[8], A. Lebedev[12], M. Lorenz[7], L. Lopes[1], L. Maier[9], A. Mangiarotti[1], J. Markert[7], V. Metag[10], J. Michel[7], C. Müntz[7], R. Münzer[8], L. Naumann[5], M. Palka[2], Y. Parpottas[13,d], V. Pechenov[3], O. Pechenova[7], J. Pietraszko[7], W. Przygoda[2], B. Ramstein[14], L. Rehnisch[7], A. Reshetin[11], A. Rustamov[7], A. Sadovsky[11], P. Salabura[2], T. Scheib[7], H. Schuldes[7], J. Siebenson[8], Yu.G. Sobolev[15], S. Spataro[e], H. Ströbele[7], J. Stroth[7,3], P Strzempek[2], C. Sturm[3], O. Svoboda[15], A. Tarantola[7], K. Teilab[7], P. Tlusty[15], M. Traxler[3], H. Tsertos[13], T. Vasiliev[6], V. Wagner[15], M. Weber[9], C. Wendisch[5,c], J. Wüstenfeld[5], S. Yurevich[3], Y. Zanevsky[6]

(HADES collaboration)

[1]LIP-Laboratório de Instrumentação e Física Experimental de Partículas , 3004-516 Coimbra, Portugal

[2]Smoluchowski Institute of Physics, Jagiellonian University of Cracow, 30-059 Kraków, Poland

[3]GSI Helmholtzzentrum für Schwerionenforschung GmbH, 64291 Darmstadt, Germany

[4]Technische Universität Darmstadt, 64289 Darmstadt, Germany

[5]Institut für Strahlenphysik, Helmholtz-Zentrum Dresden-Rossendorf, 01314 Dresden, Germany

[6]Joint Institute of Nuclear Research, 141980 Dubna, Russia

[7]Institut für Kernphysik, Goethe-Universität, 60438 Frankfurt, Germany

[8]Excellence Cluster 'Origin and Structure of the Universe' , 85748 Garching, Germany

[9]Physik Department E12, Technische Universität München, 85748 Garching, Germany

[10]II.Physikalisches Institut, Justus Liebig Universität Giessen, 35392 Giessen, Germany

[11]Institute for Nuclear Research, Russian Academy of Science, 117312 Moscow, Russia

[12]Institute of Theoretical and Experimental Physics, 117218 Moscow, Russia

[13]Department of Physics, University of Cyprus, 1678 Nicosia, Cyprus

[14]Institut de Physique Nucléaire-Université Paris Sud, F-91406 Orsay Cedex, France

[15]Nuclear Physics Institute, Academy of Sciences of Czech Republic, 25068 Rez, Czech Republic

[16]LabCAF. Dpto. Física de Partículas, 15706 Santiago de Compostela, Spain

Abstract

The K^+/K^0 ratio in isospin asymmetric relativistic heavy-ion collisions has been suggested as a promising observable for symmetry energy effects. However, the high density behavior of the symmetry energy is at present largely unconstrained. Recently the HADES detector recorded 7 billion Au 1.23A GeV Au events with a mean data rate during the flat top of the extracted beam was 100 MBytes/s at an event rate of 10 kHz. In this contribution we present the current status of the Au+Au data analysis, focused on the identification of charged and neutral kaons.

Experimental setup and data taking

The HADES detector is installed at the Helmholtzzentrum für Schwerionenforschung (GSI) in Darmstadt, Germany. The most important physics aspects are the systematic measurements of the electron pairs produced in the dense phase of the heavy-ion collisions and the measurement of the strangeness production. The accelerator infrastructure at GSI provides HADES different beams like protons, ions and π. With bombarding energies of 1-2A GeV of heaviest ions, e.g. Au, HADES reaches nuclear densities of 2-3 times the normal nuclear matter density (ρ_0) and temperatures of about 100 MeV. In this density region, the difference in the symmetry energy term in the nuclear equation of state for different stiffness models becomes large [1]. The HADES experiment might be sensitive to the symmetry energy term, e.g. can measure the ratio of produced K^+/K^0 in an isospin asymmetric collision system. The ratio of the K^+/K^0 production yields is a promising observable to determine the stiffness of the symmetry energy term in the nuclear equation of state [2], [3], [4].

The HADES detector [5] consists of a Ring Imaging CHerenkov detector (RICH) and an electromagnetic Shower detector for lepton identification. Multi-wire drift chambers (MDC) with a magnetic field in between are used for tracking of charged particles and provide, in addition, information on the energy loss. The RPC (Resistive Plate Chamber) and TOF (Time of Flight) detectors are located at the end of the detector and provide time of flight information. For the Au+Au beam time, a major improvement of the spectrometer in terms of granularity and particle identification capability was achieved by replacing the old TOFino detector by the new shielded timing RPC time-of-flight detectors. Results with in beam measurements

show a RPC efficiency of 99 % and a time resolution of 73 ps [6], [7]. In addition, a new detector read-out and data-acquisition (DAQ) systems have been implemented which greatly improved data-taking rates [8]. Following this detector upgrade the Au+Au beam time took place in April 2012. A gold beam of up to 1.5×10^6 ions per second was incident on a segmented gold target [9]. The new DAQ system was running at event rates of more than 8 kHz. Within the 557 hours of beam on target, a total of $7.3 \cdot 10^9$ events with a total data volume of 140 TB were collected. This is, compared to the data volumes recorded in the previous beam times, an enormous gain of statistics.

Data analysis

For the results, presented in this report, the total statistic of the April 2012 measuring campaign is analysed.
The different particle species are clearly visible in a wide momentum range in the velocity distribution in the RPC detector, as shown in Fig. 1.

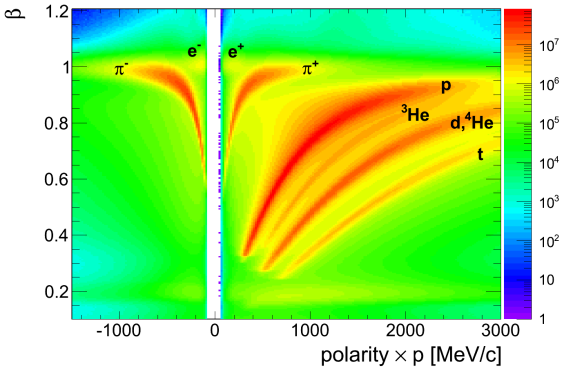

Figure 1: Velocity (β) as a function of the particle momentum (p) times polarity in the RPC detector

For particle identification, cuts on the quality of the track reconstruction are applied. In addition, cuts on the energy loss distribution and the velocity distribution were applied, using graphical cuts around the Bethe-Bloch curve and the velocity distribution. The resulting mass spectra for the charged pions in the region covered by the RPC detector are shown in Fig. 2. The peak of the K^+ and K^- can clearly be identified.

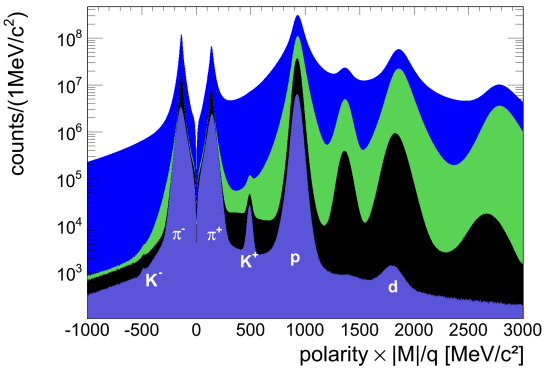

Figure 2: $M/|q|$ of the reconstructed particles in the RPC detector (upper blue curve), after the track quality (green curve), momentum (< 750 MeV/c) (black curve) and energy loss of particles in the multiwire drift chambers (lower blue curve) cuts applied

Neutral kaons were in the analysis reconstructed via the decay channel $K_s^0 \rightarrow \pi^+\pi^-$ ($branchingratio = 69.2\%$) . The decay particles π^+ and π^- were identified via the same method as described for the charged kaons, i.e. with cuts on energy loss, tracking quality and the momentum of the particle candidates. To identify pions originating from decayed neutral kaons, cuts on geometrical vertex parameters, e.g. the distance of the estimated secondary vertex of the two pions from the primary vertex, were applied. The resulting invariant mass spectrum after the decay topology cuts is shown in Fig. 3 for the real data and in Fig. 4 for the simulation. After all cuts applied, the peak of the K_s^0 is clearly visible at around 497.6 MeV/c^2.

Summary

The HADES experiment recorded about 7 billion Au+Au events at 1.23A GeV. The total data set was analyzed. We have shown, that K^+, K^- and K^0 are produced in Au+Au collisions at 1.23A GeV. At this energies strange particles are produced far below their NN production threshold. Using cuts on the track reconstruction quality, energy loss and velocity for the particle identification, the K^-, K^+ and K_s^0 could be reconstructed. In an upcoming analysis the efficiency and acceptance corrections will be done and the multiplicities of the kaons will be estimated. This allows to calculate the ratio of the K^+/K^0 production. The ratio of the K^+/K^0 production yields is a promising observable to determine the stiffness of the symmetry energy term in the nuclear equation of state.

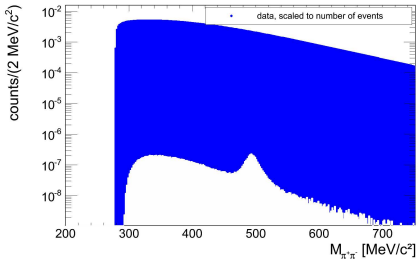

Figure 3: Invariant mass spectra of all combined π^+ and π^- pairs within the detector acceptance for data (dark blue) and after geometrical vertex cuts (white), scaled to the number of events

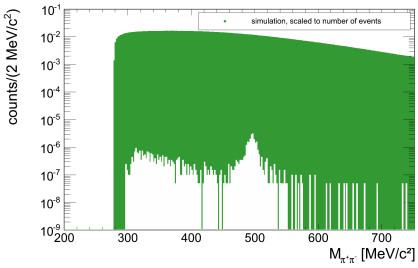

Figure 4: Invariant mass spectra of all combined π^+ and π^- pairs within the detector acceptance for simulation (dark green) and after geometrical vertex cuts (white), scaled to the number of events

Acknowledgments

Work supported by BMBF (06FY9100I and 06FY7114), HIC for FAIR, EMMI and GSI.

References

[1] Trautmann W., Wolter H.; Int.J.Mod.Phys. E21 (2012) 1230003.

[2] Di Toro M. et al; Int.J.Mod.Phys. E19 (2010) 856-868.

[3] Ferini G. Nuclear Phys A762 (2005) 147-166.

[4] Fuchs C. Prog.Part.Nucl.Phys. 56 (2006) 1-103.

[5] G. Agakishiev et al. (HADES Collaboration), Eur. Phys. J. A41 (2009) 243.

[6] H. Alvarez-Pol *et al.*, Nucl. Instr. Meth. A **535**, 277 (2004).

[7] A. Blanco *et al.*, Nucl. Instr. Meth. A **602** (2009).

[8] J. Michel *et al.*, Journal of Instr., JINST 6 C12056 (2011).

[9] B. Kindler *et al.*, Nucl. Instr. Meth. A **655** (2011).

Compressed baryonic matter: the CBM experiment at SIS100

Norbert Herrmann
University of Heidelberg, Heidelberg, Germany

Abstract

With the startup version of FAIR the study of compressed baryonic matter will be taken up again with modern detector technology. The physics case and the potential will be discussed comparing to previous measurements in the same energy range. Special emphasis will be put on the high rate capability of the experiment that enables the detection of rare probes to characterize the high density phase of the reaction.

New Opportunity for Nuclear Symmetry Energy Using LAMPS in Korea Rare Isotope Accelerator

Byungsik Hong
Korea University, Seoul 136-701, South Korea

Abstract

The new rare isotope accelerator RAON and the various user facilities will be built in Korea. For the nuclear physics experiments, the Korea broad acceptance recoil spectrometer and apparatus (KOBRA) and the large-acceptance multipurpose spectrometer (LAMPS) are being designed. In particular, LAMPS is dedicated to the study of the nuclear symmetry energy of dense matter with the large neutron-to-proton ratio (N/Z). This contribution gives an overview of RAON and the user facilities for nuclear physics with emphasis on LAMPS.

Rare Isotope Accelerator, RAON

The rare isotope science project (RISP) was launched in Korea in December, 2011. The RISP aims to design and construct the forefront rare isotope accelerator RAON and the various experimental facilities for basic sciences and applications.

RAON, schematically shown in Fig. 1, is characterized by the high-intensity rare isotope beams from the isotope separator on-line (ISOL) as well as the in-flight fragmentation (IF). The ISOL system provides rare isotopes from the direct fission of ^{238}U target induced by the intense (1 mA) proton beams at 70 MeV. It employes a superconducting LINAC for post acceleration of rare isotopes up to 18.5 MeV/u. The IF system also generates rare isotopes from the fragmentation of the high-current (8 pμA) ^{238}U beams at 200 MeV/u, using superconducting LINACs. The total powers of the ISOL and IF systems are 70 and 400 kW, respectively. The multiple modes will be simultaneously operated for maximum use of the facility. In addition, RAON will eventually combine the ISOL and IF techniques to provide more exotic neutron-rich isotopes for users. Several user facilities are being designed at RAON. Among them, KOBRA and LAMPS are the dedicated systems for nuclear physics.

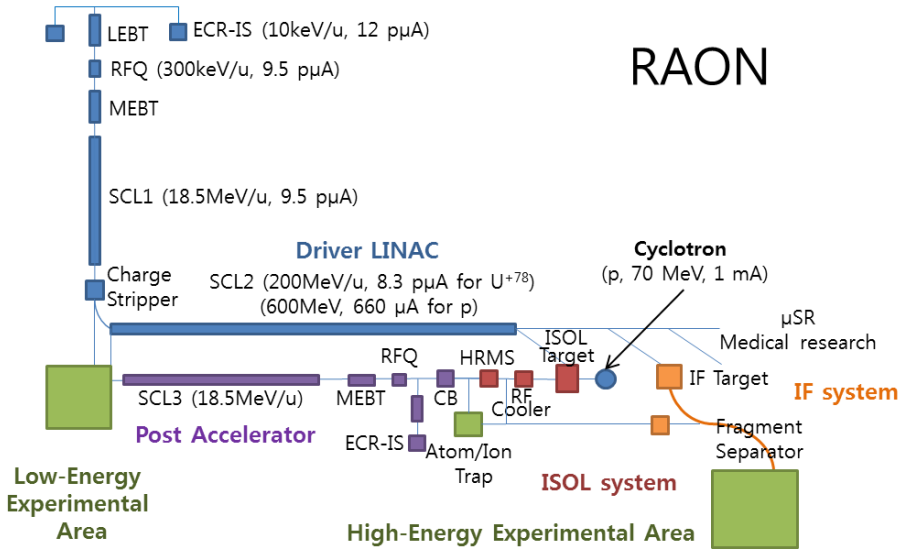

Figure 1: Schematic layout of RAON.

Recoil Spectrometer, KOBRA

KOBRA is dedicated to the nuclear structure and the nuclear astrophysics with low-energy beams up to 18.5 MeV/u. It is a double achromatic focusing system with the two Wien filters and many magnet components (Fig. 2). The mass resolution $\Delta M/M$ is less than 0.5%, the momentum resolution $\Delta p/p$ is about 0.05%, and the background reduction factor is smaller than 10^{-12}. The maximum magnetic rigidity is about 1.5 T·m and the angular acceptance is ±100 mrad at maximum. KOBRA will be a powerful device for the structure of exotic nuclei near the neutron and proton drip lines and various astrophysical processes (r-, s-, and rp-processes), using the cross sections, the transfer reactions, and the decay measurements.

Large-Acceptance Spectrometer, LAMPS

LAMPS is dedicated to the detailed study of the properties of nuclear matter from sub-saturation to supra-saturation densities. One of the primary goals is to investigate the nuclear equation of state (EoS) and the symmetry energy in a wide range of beam energy. For this the charged hadrons, nuclear fragments, and neutrons should be measured precisely in large phase space. Presently, the two different versions of LAMPS are conceived; one at the low-energy experimental area and another one

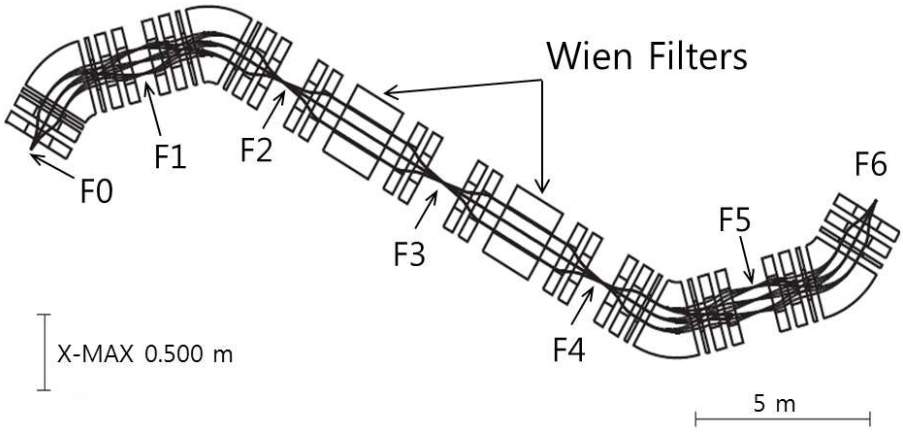

Figure 2: Schematic layout of KOBRA at RAON.

at the high-energy experimental area.

The low-energy setup of LAMPS consists of the gamma and Si detectors, covering almost 4π, and the neutron detector array in the forward region. It will measure gammas, the charged fragments, and neutrons for the pygmy dipole resonances (PDR), the ratios of mirror nuclei, and the various isospin diffusion phenomena at sub-saturation densities [1].

On the other hand, the high-energy setup of LAMPS, displayed schematically in Fig. 3, is a combination of the solenid and dipole spectrometers with the neutron detector array, among which the solenoid spectrometer and the neutron detector array are the most relevant to the study of the nuclear symmetry energy. LAMPS at the high-energy experimental area is suitable to investigate, for example, the following observables as functions of N/Z for the reaction system and beam energy:

- Particle ratios such as n/p, ^{3}H/^{3}He, ^{7}Li/^{7}Be, π^-/π^+, etc. [2, 3]
- Directed and elliptic flows of n, p, and heavier fragments [4]
- Isospin diffusion (or tracing) parameter [5–7]
- Isospin fractionation and isoscaling in nuclear multifragmentation [8]

The time-projection chamber (TPC) inside the solenoid magnet has a cylindrical shape, and is read out by the gas-electron multiplier (GEM) from both endcaps. It covers the pseudorapidity η from -0.7 to 1.6 with full azimuthal angle. The outer diameter and length of TPC are 0.5 and 1.2 m, respectively. At present, the GEM

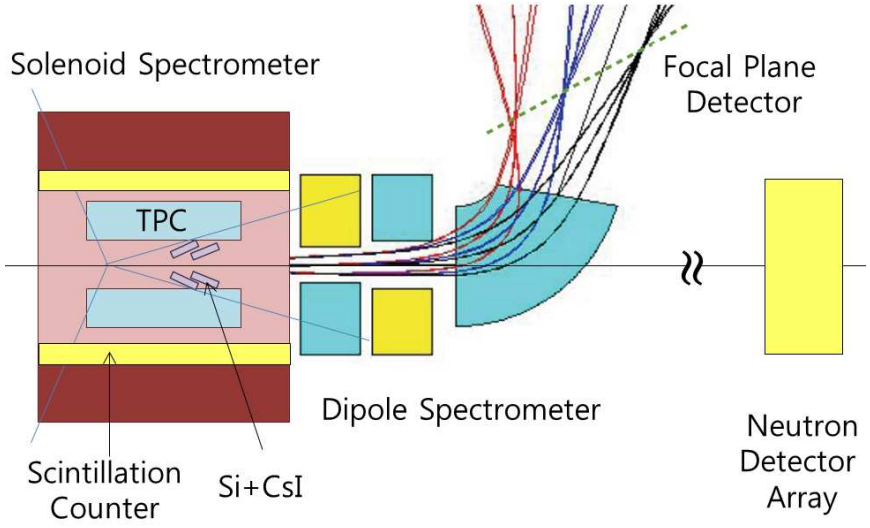

Figure 3: Schematic layout of LAMPS at the high-energy experimental area at RAON.

simulation using GARFIELD++ is underway to understand the detailed performace of TPC for different gas mixtures.

The Si-CsI detector covers the laboratory polar angle from 14° to 24°. Each module of the detector consists of three sillicon strip (or pixel) layers and one CsI crystal layer. The thicknesses of the three sillicon layers are 100, 400, and 400 μm, respectively, from the entrance window, and the thickness of the CsI crystal is 10 cm. In the back of each CsI, one more sillicon detector layer is added in order to veto the passing-through particles, which deteriorate the overall performance of the detector.

The neutron detector array consists of total ten layers along the beam direction, and each layer consists of total twenty scintillation bars. (An additional scintillation-bar layer is positioned upstream of the neutron detector array to veto the charged particles.) The longest side of each bar follows the horizontal and vertical directions, alternatively, for consecutive layers along the beam axis. The overall dimension of the detector is 2.0×2.0 m^2 perpendicular to the beam axis, and the depth is 1.0 m. The energy resolution from the time-of-flight information is estimated as about 2% at 50 MeV, and increases to about 3% at 200 MeV, assuming the time resolution of 1 ns. More detailed simulation for the performance of the neutron detector array, including the multihit capability, is now underway.

Conclusions

The new project for the design and construction of the rare isotope accelerator RAON and various user facilities has been launched in Korea. In this facility, the recoil spectrometer KOBRA and the large-acceptance multipurpose spectrometer LAMPS will be provided for nuclear physics. KOBRA is a double achromatic focusing system for the precision measurements of the nuclear structure and the nuclear astrophysics. LAMPS at the high-energy experimental area is a combination of the solenoid and dipole spectrometers with the neutron detector array at the forward region. Its primary goal is to study the nuclear symmetry energy of dense matter with large N/Z ratio. LAMPS provides a new opportunity for the nuclear symmetry energy and equation of state in the future. The RISP team aims to complete RAON and the user facilities in 2018.

Acknowledgments

The author acknowledges support from RISP, in particular, Profs. Sun Kee Kim and Yongkyun Kim. This work was supported by the Ministry of Education, Science and Technology through the National Research Foundation of Korea (NRF).

References

[1] B.A. Li, L.W. Chen and C.M. Ko, Phys. Rep. **464**, 113 (2008).

[2] W. Reisdorf, *et al.*, Nucl. Phys. A **781**, 459 (2007).

[3] M.A. Famiano, *et al.*, Phys. Rev. Lett. **97**, 052701 (2006).

[4] P. Russotto, *et al.*, Phys. Lett. B **697**, 471 (2011).

[5] F. Rami, *et al.*, Phys. Rev. Lett. **84**, 1120 (2000).

[6] B. Hong, *et al.*, Phys. Rev. C **66**, 034901 (2002).

[7] M.B. Tsang, *et al.*, Phys. Rev. Lett. **92**, 062701 (2004).

[8] T.X. Liu, *et al.*, Phys. Rev. C **76**, 034603 (2007).

Tracking saddle-to-scission dynamics using N/Z in projectile breakup reactions

S. Hudan for the FIRST collaboration
Department of Chemistry and Center for Exploration of Energy and Matter
2401 Milo B. Sampson Lane, Bloomington IN 47405, USA

Abstract

Fragments resulting from the binary splits of an excited projectile-like fragment (PLF*) formed in heavy-ion collision at an incident energy of 45-50 MeV/A are examined. A clear dependence of the light fragments ($4 \leq Z_L \leq 8$) isotopic composition on rotation angle is observed. This dependence corresponds to changes in the N/Z of the fragments persisting for times as longs as 2-3 zs. A strong target dependence is observed for systems corresponding to ^{64}Zn beam, indicating a dependence of the fragment composition to the target composition.

Talk's Summary

The nuclear symmetry energy, in particular its density dependence, impacts many phenomena from the properties on neutron stars to the existence of superheavy elements [1–3]. In this paper, we elect to study the binary breakup of an excited PLF* produced in peripheral collision of a projectile and target nuclei at intermediate energies. It has been shown that such system is relatively long lived [4] and therefore presents an unique opportunity to study N/Z equilibration.

In order to focus on binary decays, events were selected in which two fragments ($Z \geq 3$) were detected at forward angle [5]. These two fragments were distinguished from each other by their atomic number, with the larger (smaller) atomic fragment designated as Z_H (Z_L). To ensure that the PLF* comprised a large fraction of the original projectile, Z_H was required to represent at least $\approx$ 40 % of the projectile. In the first part, we will focus on data for the ^{124}Xe + ^{112}Sn and ^{124}Xe + ^{124}Sn systems at an incident energy of 49 MeV/A.

The angle between the direction of the two fragments center-of-mass velocity, $v_{c.m.}$, and their relative velocity, v_{REL}, is a good quantity to characterized the binary decay of the PLF* [4–6]. The corresponding angular distributions are characterized

by a large asymmetry with larger yield corresponding to the Z_L fragment emitted backward of the Z_H fragment. To assess the influence of the target on the observed angular distribution, the distribution for the ^{124}Sn target was area normalized to the one for the ^{112}Sn target for forward angles ($-1 \leq \cos(\alpha) \leq 0$). Given this normalization, the distributions, for a given Z_L , are very similar, indicating that the emission probability does not depend on the target. The same observations can be made for the ^{64}Zn + ^{27}Al, ^{64}Zn, and ^{209}Bi systems.

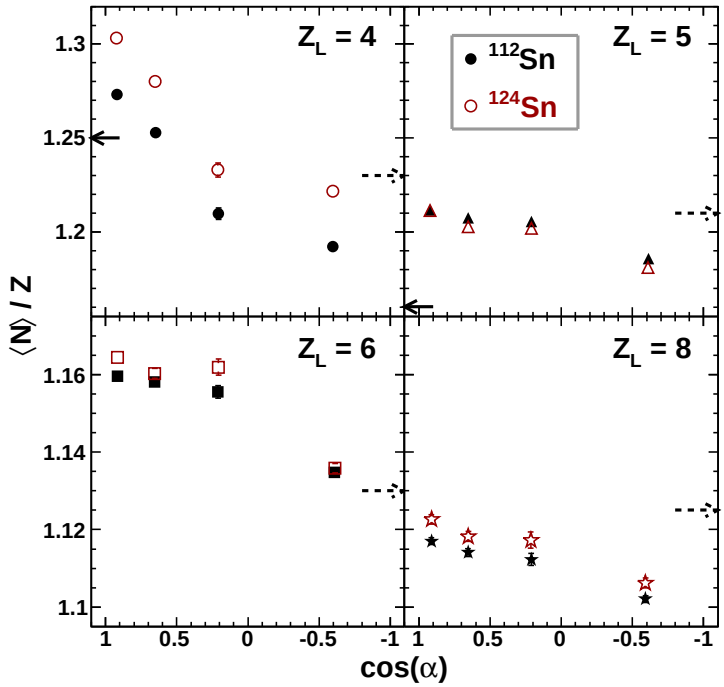

Figure 1: Isotopic composition for different Z_L fragments for the ^{124}Xe + ^{112}Sn and ^{124}Sn systems as a function of their decay angle. For each Z_L, the solid (dashed) arrow corresponds to β stability (data from [7]).

The isotopic composition of the Z_L fragments is examined in Fig. 1 as a function of the decay angle. The data for the ^{112}Sn target are shown as the closed symbols. An enhancement in $\langle N \rangle / Z$ is observed for fragments emitted at backward angles. While all fragments shown exhibit larger $\langle N \rangle / Z$ for the most aligned decay, the trend is the strongest for $Z_L = 4$ fragments. The observed $\langle N \rangle / Z$ for the ^{124}Sn target is shown as the open symbols in Fig. 1. The neutron content of the Z_L fragment, to the exception of $Z_L = 4$, does not seem to depend on the target composition. Although the target N/Z changes by 20 %, a small enhancement is observed

for Be fragments. One concludes that the neutron composition of the target does not strongly influence neither the yield nor the isotopic composition of the emitted Z_L fragment.

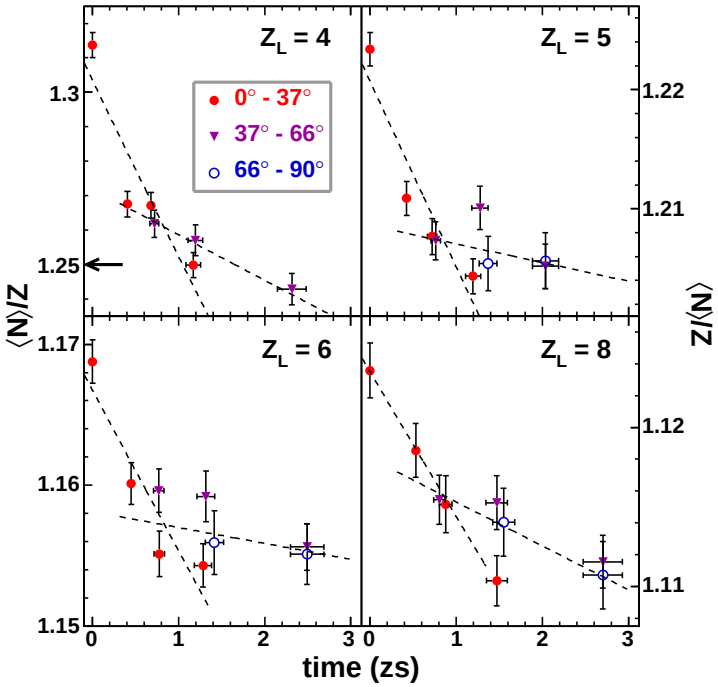

Figure 2: Dependence of the ⟨N⟩/Z on time for $4 \leq Z_L \leq 8$. The dashed lines correspond to linear fits.

Using the rotation angle as a clock [5], one can extract the time dependence of the fragment isotopic composition as shown in Fig. 2. The timescale is expressed in zeptoseconds (1zs = $1x10^{-21}$s) with the longest times extracted corresponding to a quarter rotation of the PLF*. For all fragments shown a change in ⟨N⟩/Z is observed for times as long as 3 zs (900 fm/c). This persistence of decreasing N/Z for such long times indicates that N/Z equilibration is a slow process. Closer examination of Fig. 2 shows that for the lighter fragments, the N/Z time dependence is characterized by two different timescales. While the most aligned decays correlate with a rapid decrease with time, decays with larger rotation angle correspond to a softer decrease of ⟨N⟩/Z with time. This trend is shown by the linear fits performed and represented by the dashed lines. The bimodal nature of the N/Z equilibration might be related to different initial configurations of the dinuclear system composed of the Z_H and Z_L fragments.

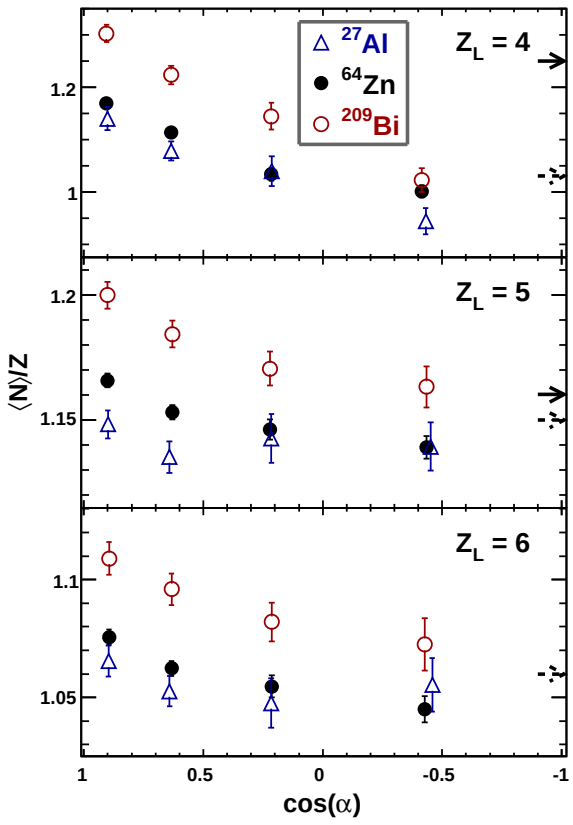

Figure 3: Average neutron to proton ratio for selected Z_L as a function of the decay angle for the ^{64}Zn + ^{27}Al, ^{64}Zn and ^{209}Bi systems. The ratio for the ^{64}Zn, ^{209}Bi, and ^{27}Al targets is represented by the closed circle, open circle and open triangle respectively. See Fig. 1 for the arrows.

To further characterized N/Z equilibration, the study was extended to the ^{64}Zn + ^{27}Al, ^{64}Zn and ^{209}Bi systems at an incident energy of 45 MeV/A. The isotopic composition of the Z_L fragment is shown in Fig. 3 as a function of the decay angle. The same overall trend observed in Fig. 1 for the bigger system is also observed for these lighter systems, with smaller decay angles characterized by larger $\langle N \rangle / Z$ of the Z_L fragment. For each Z_L shown, larger value of $\langle N \rangle / Z$ are observed for the ^{209}Bi target as compared to the lighter ^{27}Al and ^{64}Zn targets. The larger value observed for the Bi target might be attributed to the preferential pickup of neutrons by the PLF* from the Bi target.

Conclusions

We have shown in this contribution that a correlation exists between the isotopic composition of the fragment produced in the binary decay of a PLF* and its decay angle. The time dependence of the fragment isotopic composition shows that N/Z changes for times as long as 2-3 zs (600-900 fm/c). The long lifetime of the PLF* allows to access the timescale for N/Z equilibration. For the lighter systems studied we have also shown that the N/Z of the fragments depends on the neutron-richness of the target.

Acknowledgments

This work was supported by the U.S. Department of Energy under Grant Nos. DEFG02-88ER-40404 (IU) and DE-FG03-93ER40773 (TAMU). Support from the Robert A. Welch Foundation through Grant No. A-1266 is gratefully acknowledged. Collaboration members from Université Laval recognize the support of the Natural Sciences and Engineering Research Council of Canada.

References

[1] J. Lattimer and M. Prakash, Astrophys. J. **550**, 426 (2001).

[2] A. Steiner *et al.*, Phys. Rep. **411**, 325 (2005).

[3] P. Möller *et al.*, Phys. Rev. Lett. **108**, 052501 (2012).

[4] A. B. McIntosh *et al.*, Phys. Rev. C **81**, 034603 (2010).

[5] S. Hudan *et al.*, Phys. Rev. C **86**, 021603(R) (2012).

[6] B. Davin *et al.*, Phys. Rev. C **65**, 064614 (2002).

[7] C. Sfienti *et al.*, Phys. Rev. Lett. **102**, 152701 (2009).

SAMURAI-TPC: A Time Projection Chamber to Study the Nuclear Symmetry Energy at RIKEN-RIBF with Rare Isotope Beams

T. Isobe[A] *and A.B. McIntosh*[B] *for the SAMURAI-TPC collaboration*
[A]*RIKEN, Nishina Center, Saitama Japan*
[B]*Cyclotron Institute, Texas A&M University, TX United States*

Abstract

The density dependence of the nuclear symmetry energy, particularly at high density, is an important open question in nuclear physics. Constraints can be placed on the symmetry energy at supra-saturation density by studying flow and yield ratios for pions and light particles (A<5) produced in heavy ion collisions around E/A = 200 MeV. To measure charged pions and light charged particles produced in such reactions, a Time Projection Chamber is being constructed by the multi-national Symmetry Energy Project collaboration. The TPC will be installed in the SAMURAI dipole magnet at the RIKEN-RIBF facility in Japan for highly asymmetric heavy ion collision experiment.

Introduction

The nuclear equation of state (EoS) is a fundamental bulk property of nuclear matter and describes the relationships between the parameters of a nuclear system, such as energy and density. Understanding the nuclear EoS has been one of the major goals of nuclear physics.

Investigation of heavy-ion collision is one of the methods that can be used to study the nuclear EoS. An international collaboration, the Symmetry Energy Project, was formed in 2009 to study the nuclear EoS over a wide range of nuclear matter densities. The collaboration planned to install a time projection chamber (TPC) in the SAMURAI dipole magnet at the Radioactive Ion Beam Facility (RIBF). By using TPC, experimental observables, such as the flow and yield ratios of charged particles, particularly π^+ and π^- particles, produced in heavy-ion collisions will be measured. At RIBF energy of E/A = 200-300 MeV, a nuclear density of $\rho \sim 2\rho_0$ is expected to be achieved. Experiments using the TPC will allow us to impose constraints on the EoS isospin asymmetry term at high nuclear matter density [1].

Table 1: Specifications of SAMURAI-TPC

pad size	8 mm × 12 mm
number of pads	12096 (108 × 112)
drift length	~50 cm
chamber gas	P10 (Ar-90% + CH_4-10%)
magnetic field	0.5 T
pressure	~1 atm.
electric field for drift	120 V/cm

Designing of SAMURAI-TPC

Figure 1 shows an exploded view of the SAMURAI-TPC. The design is based on the EOS-TPC used at the BEVALAC accelerator [2]. Multi-wire drift chamber (MWDC)-type gas with a cathode-pad readout for the induced signals will be employed for obtaining good position resolution. The target will be located near the TPC entrance. Table 1 lists some specifications of the SAMURAI-TPC.

This detector is designed to measure ions ranging from pions to oxygen ions, corresponding to a wide range of stopping powers, and consequently, to a wide range of induced signals on the pads. A GET electronics modules [3] with more than 10k channels will be employed for the TPC readout. GET stands for Generic Electronics for TPCs. It is a readout electronics system developed by an international program for a reconfigurable medium sized system to cover nuclear physics requirements for systems up to 30 k channels. The input dynamic range of the readout is adjustable, 120 fC, 1 pC and 10pC, through slow control. A switched capacitor array (SCA)-type analog buffer is employed.

To determine spatial distortions, and in order to calibrate and monitor the TPC, a laser calibration system will be implemented. It is planed to use 16 laser beams for simulating straight particle tracks in the TPC volume. UV-laser beams can produce ionization in gaseous detectors via a two-photon ionization process. We plan to use a Nd-YAG frequency-quadrupled laser (λ = 266 nm) and to send the laser beams into the TPC field cage.

The design and construction of the TPC is being performed in the United States. After the completion of the TPC construction and testing of the TPC by using cosmic rays, the TPC is expected to be shipped to RIBF for first experiment at 2013.

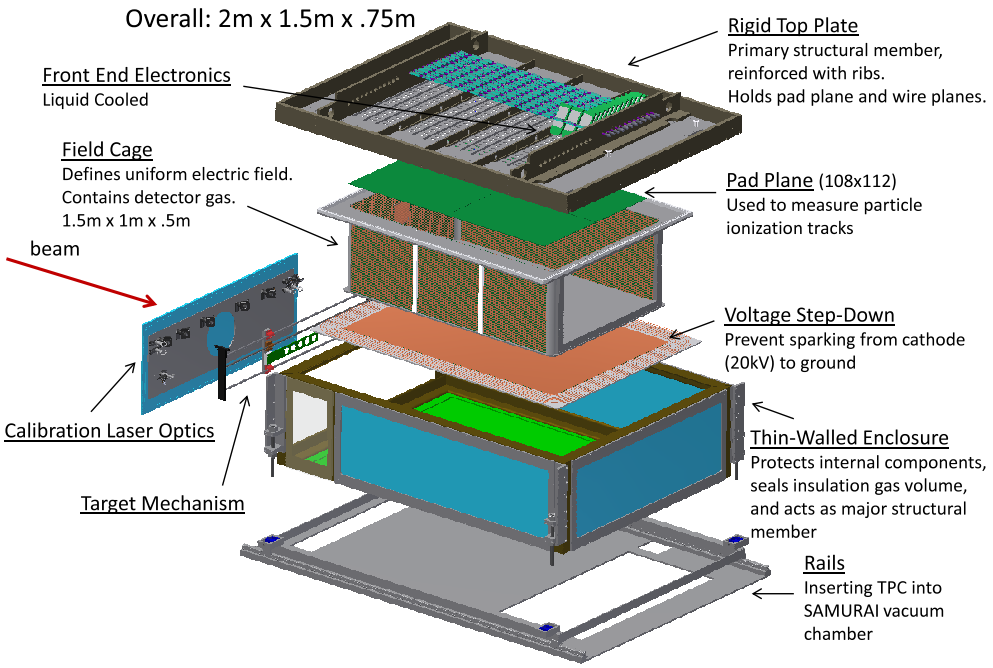

Figure 1: SAMURAI-TPC exploded view

Conclusions

For the experimental study of the density dependent nuclear symmetry energy, a Time Projection Chamber is being constructed by the multi-national Symmetry Energy Project collaboration, which is to measure charged pions and light charged particles produced in highly asymmetric heavy ion collisions. The TPC will be installed in the SAMURAI dipole magnet at the RIKEN-RIBF facility in Japan for the first experiment planned at 2014.

Acknowledgments

This project is funded by U.S.A. Department Of Energy, Science program and Japan MEXT, Science program of Grant-In-Aid for Scientific Research on Innovative Areas.
We acknowledge the support from Nishina Center (RIKEN), Cyclotron Institute (Texas A&M University) and National Superconducting Cyclotron Laboratory (NSCL, MSU).

References

[1] L. W. Chen et al.: Phys. Rev. Lett. **94**, 032701 (2005).

[2] G. Rai et al.: IEEE Trans. on Nucl. Sci. **37**, 56 (1990).

[3] E. Pollacco et al.: Physics Procedia **37**, 1799 (2012).

How does the sensitivity of the symmetry energy depend on the treatment of reaction dynamics?

Z. Kohley
NSCL, Michigan State University, E. Lansing, Michigan, 48824, USA

Abstract

Experimental measurements of the transverse flow of intermediate mass fragments (IMFs) from heavy-ion collisions were compared to multiple theoretical models to explore the sensitivity to the symmetry energy. The results show that the IMF flow appears to be a strong probe for the density dependence of the symmetry. However, the sensitivity of the symmetry energy to the experimental data varied between the different models. This suggests that the different treatments of the nuclear reaction dynamics in the models will effect the extracted information about the density dependence of the symmetry energy and requires constraints. The results discussed in the following summary are also presented in Ref. [1].

Talk's Summary

Heavy-ion collisions (HICs) offer experimentalist the unique opportunity to produce nuclear matter at densities, temperatures, pressures, and isospin concentrations away from stable ground state nuclei. Thus, measurements of the reaction products from HICs have developed into one of the primary tools for exploring the density dependence of the symmetry energy. Constraints on the symmetry energy from HICs are dependent on the ability of the theoretical models to accurately simulate the very complex collisions dynamics, fragmentation, and clustering.

Recent works by Rizzo *et al*. [2] and Colonna *et al*. [3] have demonstrated how the description of the nuclear dynamics in different models can change the multi-fragmentation process and, thus, effect the HIC observables used in constraining the symmetry energy. Similarly, Zhang *et al.* [4] and Coupland *et al.* [5] have explored how adjustments to the input physics of the transport calculations can affect the resulting HIC observables. In the following, we compare the Constrained Molecular Dynamics (CoMD) [6], Antisymmetrized Molecular Dynamics (AMD) [7], and Stochastic Mean Field (SMF) [8] models to recent measurements of the IMF transverse flow. Additional details about the conditions/inputs used for each simulation can be found in Ref. [1].

A variety of different studies aimed at extracting information about the symmetry energy have been completed using these simulations in similar configurations. Thus, it is important to directly compare how the sensitivity of the symmetry energy changes between the models. The nucleon-nucleon interaction or mean-field potential used in each model was chosen to produce an equation of state (EoS) with a soft compressibility, K, for symmetric nuclear matter between 200-230 MeV. Therefore, the symmetric part of the EoS was kept relatively constant between the models and the isospin-dependent part of the interaction could be varied.

The different forms of the density dependence of the symmetry energy used in each model can be characterized by their magnitude, slope, and curvature at the saturation density ($\rho_\circ = 0.16 fm^{-3}$), which are presented in Table 1. Additionally, the symmetry energy is plotted as a function of the reduced density for each parameterization in Fig. 1. In comparing the different forms of the symmetry energy, it is important to note that the IMF flows should probe density regions near and below $\rho_\circ$ [9].

Table 1: Symmetry energy (E_{sym}), slope (L), curvature (K) at normal nuclear density from the different forms of the density dependence of the symmetry energy used in the theoretical simulations.

Simulation	Form	$E_{sym}(\rho_\circ)$	L (MeV)	K_{sym} (MeV)
AMD	Stiff	30.5	65	-96
	Soft	30.5	21	-277
SMF	Stiff	33	95	-72
	Soft	33	19	-249
CoMD	Super-Stiff	30	105	93
	Stiff	30	78	-24
	Soft	30	51	-65

The observable chosen to compare the three models to was the transverse flow of intermediate fragments. In Ref. [9], the transverse flow, $\overline{\langle Px \rangle}$, of $Z = 3-7$ fragments was measured from the 35 MeV/u ^{64}Ni+^{64}Ni, ^{70}Zn+^{70}Zn, and ^{64}Zn+^{64}Zn systems. It was shown that the ratio of the transverse flow (R_{Flow}) was sensitive to the density dependence of the symmetry energy. R_{Flow} was calculated as

$$R_{Flow} = \frac{\overline{\langle Px \rangle / N}^{64Zn} - \overline{\langle Px \rangle / N}^{70Zn}}{\overline{\langle Px \rangle / N}^{64Ni} - \overline{\langle Px \rangle / N}^{70Zn}} \quad (1)$$

and defines the magnitude of the flow from the ^{64}Zn system in comparison to the ^{64}Ni and ^{70}Zn systems. The ratio should minimize any experimental biases and al-

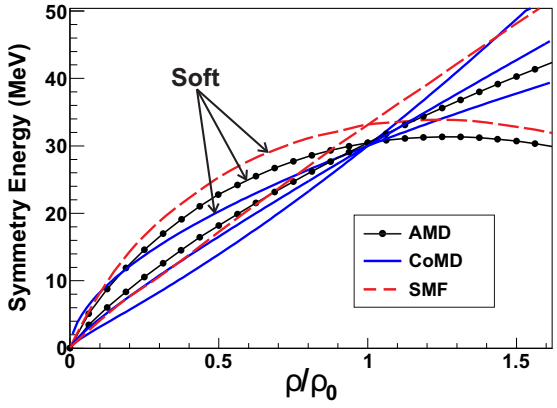

Figure 1: The different forms of the density dependence of the symmetry energy used in the AMD, CoMD, and SMF simulations. The soft density dependence is indicated for each calculation.

low for the relative differences in the flow to be compared between the experiment and theory. A value of R_{Flow} = 0.61±0.14 was calculated from the experimental IMF flows for the mid-peripheral reactions as discussed in Ref. [1]. This represents that the nucleon-averaged flow from ^{64}Zn system was below that of the ^{64}Ni system and above the ^{70}Zn system. The same procedure described above for calculating the R_{Flow} for the experiment was completed for the AMD, CoMD, and SMF models. The results from the simulations are compared with the experiment in Fig. 2.

The AMD model shows agreement for a slope of L = 65 MeV and demonstrates that a very soft form of the symmetry energy (L = 21 MeV) is unable to reproduce the experimental data. A consistent result is obtained with the CoMD model showing agreement with L = 51 and 78 MeV. The CoMD model also shows that a very stiff form of the symmetry energy (L = 105 MeV) produces a R_{Flow} value larger than the experimental constraints. The results from the SMF model, in agreement with the AMD and CoMD, demonstrate that neither a very soft (L = 19 MeV) or stiff (L = 95 MeV) form of the symmetry energy can reproduce the experimental IMF flow. A linear interpolation between the soft and stiff SMF results indicates that the best agreement with the experimental data would result from a slope of 62 MeV. Despite the differences in the theoretical models, the relative agreement in the form of the symmetry energy that reproduces the experimental data is surprising.

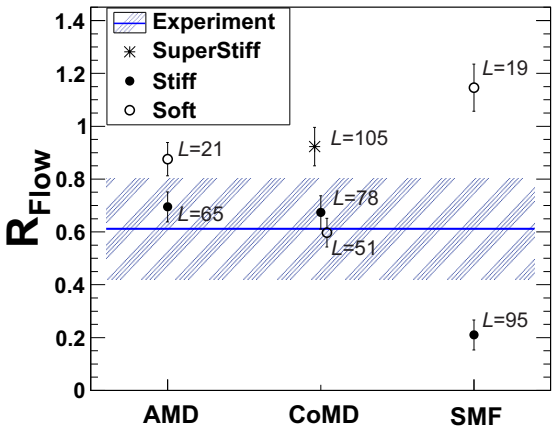

Figure 2: R_{Flow} value from the nucleon-averaged flow of the mid-peripheral reactions is shown for the different symmetry energy parameterizations of the AMD, CoMD and SMF models. The corresponding symmetry energy slope (L) is shown next to each calculation. The experimental value is represented by the solid blue line with the statistical uncertainty shown as the hashed blue area.

Conclusions

The AMD, CoMD, and SMF models were compared with the experimental data in order to examine how the treatment of the nuclear dynamics can affect the sensitivity of the simulation to the EoS. The results demonstrated that the relative differences in the IMF transverse flow is dependent on the isospin-dependent part of the mean-field or nucleon-nucleon interaction in each model. However, the sensitivity of the IMF flow to the form of the symmetry energy varied between the different simulations. Despite the differences in the models, better agreement with the experimental data was achieved with a form of the symmetry energy having a slope (L) in the range of ~50-80 MeV for each simulation, which is in good agreement with current constraints [10]. However, the significance of this agreement is outweighed by the differences in the overall sensitivity of the models to L. Overall, the results indicate that robust constraints on the density dependence of the symmetry energy will require consistent theoretical comparisons. Additionally, the use of multiple models, while time-consuming, should become an important aspect in trying to extract information on the form of the nEoS from heavy-ion collision observables.

Acknowledgments

This work was done in collaboration with the members of Sherry Yennello's research group at Texas A&M. Additionally, I would like to thank M. Colonna (INFN), A. Bonasera (TAMU), and R. Wada (TAMU) for help in running the different theoretical calculations.

References

[1] Z. Kohley *et al.,* Phys. Rev. C **85**, 064605 (2012).

[2] J. Rizzo, M. Colonna, and A. Ono, Phys. Rev. C **76**, 024611 (2007).

[3] M. Colonna, A. Ono, and J. Rizzo, Phys. Rev. C **82**, 054613 (2010).

[4] Y. Zhang *et al.,* Phys. Rev. C **85**, 024602 (2012).

[5] D. D. S. Coupland, W. G. Lynch, M. B. Tsang, P. Danielewicz, and Y. Zhang, Phys. Rev. C **84**, 054603 (2011).

[6] M. Papa, G. Giuliani, and A. Bonasera, J. Comput. Phys. **208**, 403 (2005).

[7] A. Ono and H. Horiuchi, Prog. Part. Nucl. Phys. **53**, 501 (2004).

[8] J. Rizzo, M. Colonna, M. Di Toro, and V. Greco, Nucl. Phys. **A732**, 202 (2004).

[9] Z. Kohley *et al.,* Phys. Rev. C **82**, 064601 (2010).

[10] M. B. Tsang *et al.,* Phys. Rev. Lett. **102**, 122701 (2009).

A New Approach to Detect Hypernuclei and Isotopes in the QMD Phase Space Distribution at Relativistic Energies

A. Le Fèvre[1], *J. Aichelin*[2], *Ch. Hartnack*[2], *Y. Leifels*[1]
([1]GSI Darmstadt, Germany; [2]Subatech Nantes, France)

Abstract

We developed an improved clusterisation algorithm which aims at predicting more realistically the yields of clusters in the framework of the Quantum Molecular Dynamics model. This new approach is able to predict isotope yields as well hypernucleus production at relativistic energies. To illustrate its predicting power, we confront this new method to experimental data from 100 A.MeV to 2 A.GeV, with a closed view on isotope yields and flows, and show the sensitivity on the parameters which govern the cluster formation.

Introduction

In heavy ion reactions at energies between 20 A.MeV and several GeV, many clusters are formed. This cluster formation presents a big challenge for transport models in which nucleons are the degrees of freedom which are propagated. In many approaches, the fragment formation is simply omitted, which invalidates the single particle observables as well, because the cluster formation depends on the phase space region and, therefore, single particle spectra are modified. Identifying clusters in a transport code which transports nucleons is all but simple. Quantum effects as well as range and strength of the different parts of the nuclear potential, like bulk, symmetry energy and pairing, in a complicated environment at finite temperature, influence the fragment yield.

Simulated Annealing Clusterisation Algorithm: The principles

If we want to identify fragments early, while the reaction is still going on, one has to use the momentum as well as the coordinate space informations. The idea how to do this has been introduced by Dorso et al. [1] and it has been further developped

into the Simulated Annealing Clusterisation Algorithm (SACA) [2]. This approach consists in the following steps: starting from the positions and momenta of the nucleons at a given time, nucleons are combined in all possible ways into fragments or single nucleons. Neglecting the interaction among nucleons in different clusters, but taking into account the interaction among the nucleons in the same fragment, this algorithm identifies that combination of fragments and free nucleons which has the highest binding energy. It has been shown that clusters obtained by that approach are the pre-fragments for the final state clusters. The reason for this is the fact that fragments are not a random collection of nucleons at the end, but an initial-final state correlation. The advantage of the SACA approach, as compared to other methods which rely only on proximity in coordinate space, like MST ("Minimum Spanning Tree") [3], is the possibility to identify fragments quite early during the heavy ion reaction. This has been demonstrated in [4], in which is also shown that MST gives only reliable results after 200-400 fm/c whereas SACA identifies the fragment already shortly after the high density phase of the heavy ion collision. This is crucial, because the fragment partitions can reflect the early dynamical conditions (Coulomb, density, flow details, strangeness...).

Improving the prediction of isotope production

Our goal is to improve the description of the fragment yields within the scope of the QMD transport code. In its initial version, SACA contains as ingredients only the potentials which are responsible for the average binding energy of the clusters: a volume component (Skyrme mean field) which dominates, and a correction for surface effects in the form of a Yukawa potential. This version has already shown its strong predictive power concerning the fragment yields within the scope of the BQMD transport model [9, 10].

If we want to extend our model to predict the absolute multiplicity of the isotope yields, we have to add new features to the SACA cluster identification like asymmetry energy, pairing and quantum effects. For the asymmetry energy, we use the parametrisation from IQMD [5] which we use in the present article as transport code for the transport of nucleons:

$$E_{asy} = E_0(\frac{<\rho_B>}{\rho_0})^{\gamma-1}\frac{\rho_n - \rho_p}{\rho_B}$$

where E_0=32 MeV, γ=1 ("stiff" asymmetry potential), and ρ_n, ρ_p, ρ_B, ρ_0 are, respectively, the neutron, proton, baryonic and saturation densities.

Another significant part of the binding energy of light isotopes are the shell and odd-even effects (pairing). In the conditions of high pressure and temperature where SACA is used to determine the pre-fragments, these structure effects are not well known. E. Khan et al. in [6] showed that there are some indications that they affect the primary fragments. The authors demonstrate that the pairing vanishes above a nuclear temperature $T_V \approx 0.5\Delta_{pairing}$ (pairing energy). At normal density the pairing energy tends to be negligible for heavy nuclei, with $\Delta_{pairing} = \frac{12}{\sqrt{A}}MeV$, whereas it is strong for light isotopes, like ^4He and ^3He with 12 MeV and 6.9 MeV, respectively. In SACA the primary fragments are usually produced quite cold, with $T < 1-2MeV$, and hence below T_V. The description of Khan et al. applies to the saturation density, ρ_0, but pairing effects have to vanish at high or low density which SACA clusters may reach. Therefore we use the computed pairing densities for each isotope which is created by SACA and apply a correction factor of the ρ_0 pairing energy, depending on the cluster density. In [7], within the Hartree-Fock-Bogolioubov method, Khan et al. have derived the following function for the pairing potential

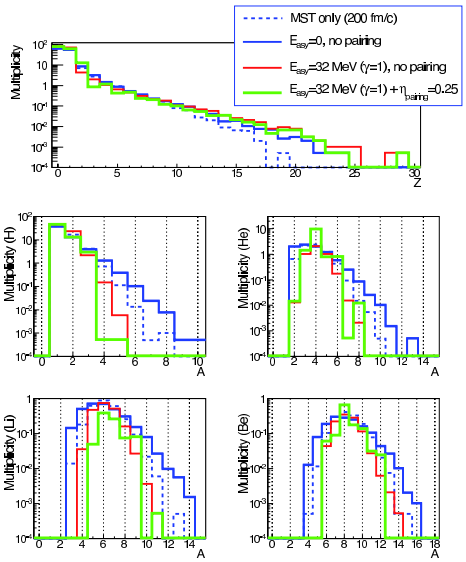

Figure 1: IQMD predictions for the central ($b < 0.2b_{max}$) collisions of $^{124}Xe + ^{112}Sn$ at 100 A.MeV incident energy. Dashed line for the MST (coalescence) algorithm alone (performed at the late time 200 fm/c), blue line for the initial SACA model, which has been implemented an asymmetry term (red) and additionnal pairing contribution (green). The top panel shows the mean multiplicity distribution of fragments as a function of their charge. The four others depict the yields of H, He, Be and Li isotopes.

$$V_{pairing} = V_0(1 - \eta\frac{\rho(r)}{\rho_0})\delta(\mathbf{r}_1 - \mathbf{r}_2)$$

where η provides the surface-to-volume character of the interaction (η=1 or 0 would mean pure surface or volume interaction, respectively). We have adopted this parametrisation to derive a correction factor $f_\eta(< \rho_B >)$ depending on the mean density of the fragment which is applied to the deviation of the binding energy with respect to the Bethe-Weizäcker formula (liquid drop model) without pairing term $\Delta B_{pairing}(N, Z, \rho_0)$. The "structure" contribution to the binding energy of a nucleus (N,Z) at baryonic density ρ_B would then become $\Delta B_{pairing}(N, Z, \rho_B) =$

$\Delta B_{pairing}(N,Z,\rho_0)\, f_\eta(<\rho_B>)$. Isotopes which are not stable at all in nature, are discarded in SACA by assigning to them a very repulsive $\Delta B_{pairing}$. Fig. 1 shows the influence of the asymmetry energy and of the pairing energy of the isotope yield in the reaction $^{124}Xe + ^{112}Sn$ at 100 A.MeV which has been measured by the INDRA ref. [8]. We display here the results for central collisions ($b < 0.2 b_{max}$). We have obtained the best agreement with the INDRA data of ref. [8] for the light isotope yields using $\eta = 0.25$. This figure illustrates as well how the various ingredients influence the fragments yield obtained in SACA, assuming an early clusterisation at t=60 fm/c where pre-fragments are already stabilised in size. We see that the charge distributions are not strongly modified by the ingredients, whereas details of the isotopic yield are strongly influenced: the asymmetry energy tends to narrow the distributions towards the valley of stability, and the pairing component tends to restore the natural abundances.

How the dynamical patterns of isotopes are affected

The way the fragments are formed has an important side effect on the dynamical features, as shown in fig. 2. There, we see that the ratios of the transversal and of the longitudinal width of the momentum distributions for those isotopes whose binding energy is strongly modified (tritons, ^3He, ^4He) is strongly influenced by the new ingredients of SACA, which do not affect at all neutrons and protons. Any study of the flow of light fragments should take care of that aspect.

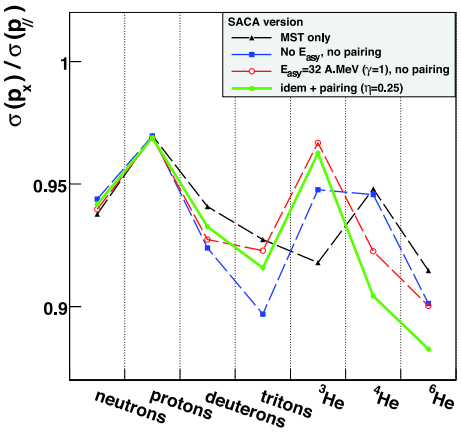

Figure 2: The ratio of the width of the transversal and of the longitudinal momentum distribution (with respect to the reaction plane) for various light isotopes for the same parametrisations of the potential as used in fig. 1.

Excitation energy and density of the primary fragments

The pre-fragments, called also "primary" fragments, created in SACA, are often produced non relaxed in shape and density. Going back to their ground state shape and density creates an excitation energy, whose dependence on the fragments size and on the incident energy of the projectile is depicted in fig. 3. Here, the excitation energy is calculated as the

difference between the binding energy of the fragment obtained by SACA and the experimentally measured value, and we include in SACA the asymmetry and "pairing" contributions. We note that at low bombarding energy (100 A.MeV), for $Z > 1$, where a large fraction of the fragments is formed from participant matter, the primary fragments have on the average 2 A.MeV excitation energy. This value is close to the 3 A.MeV of S. Hudan et al. in [11] that have been derived experimentally for central Xe+Sn at the somehow lower (50 A.MeV) incident energy. This excitation energy is sufficiently large to cause a significant contribution of the secondary decay of the pre-fragments to the yield of small clusters. On the contrary, at relativistic energies, heavier fragments are produced from spectator matter and are therefore much colder on the average. The contribution from secondary decay is getting negligible, except for He and Li. Another interesting feature of the primary

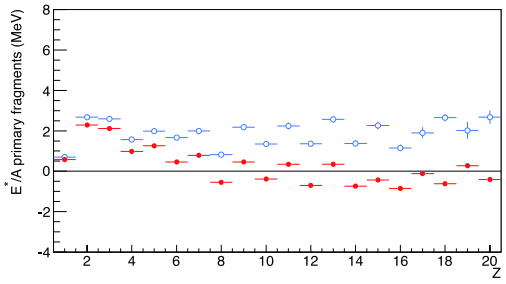

Figure 3: Mean excitation energy of fragments as a function of their charge as predicted by IQMD+SACA (with all binding energy ingredients) for central ($b < 0.2b_{max}$) collisions of $^{124}Xe+^{112}Sn$ at 100 A.MeV (open blue symbols) and $^{197}Au+^{197}Au$ at 600 A.MeV (full red symbols) incident energy.

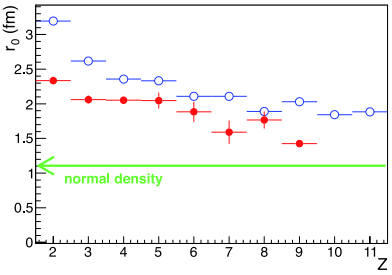

Figure 4: The same as fig. 3 for the mean radius of primary fragments.

clusters in SACA is their internal density. Fig. 4 shows its dependence on the fragments size and on the incident energy. Although the medium is close to ρ_0 at this early stage of the collisions (60 and 40 fm/c for 100 and 600 A.MeV bombarding energy, respectively), the clusters are produced very dilute, around $\rho = \rho_0/6$. This is explained by the fact that the dense clusters are disfavoured, because they would contain nucleons which are flowing against each other. In this case the nucleons have a too high relative momenta to form a cluster. Therefore only the low density behaviour of the potentials, which are contributing to the binding energy, is important for the fragment formation.

About the apparent vanishing of the asymmetry term in pre-fragments at high energy

Are the contributions of the asymmetry and pairing energy for the fragment formation energy dependent? This question has been raised by the FOPI Collaboration in [12]. There, the mean ^3He and ^4He multiplicities in central collisions of Au+Au are shown as a function of the beam energy, see Fig. 5. Whereas at low energy (around 100 A.MeV), the ^4He dominates the ^3He production by an order of magnitude, above the A.GeV, the contrary is the case. For IQMD-SACA, one obtains a very good agreement with the experimental data at low energy only if asymmetry and pairing energies are included. The domination of ^3He at higher energies, on the contrary, is not reproduced yet: only if one switches off in SACA the asymmetry and pairing terms, the high energy data can be reproduced. We are presently investigating the origin for this observation. .

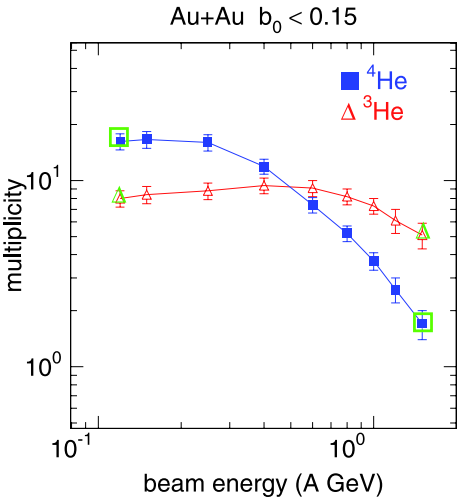

Figure 5: ^3He (triangles) and ^4He (squares) mean multiplicities as a function of the beam energy in central Au+Au collisions measured by FOPI (red and blue symbols) [12]. The green symbols correspond to the IQMD predictions, using SACA with (at low beam energy) or without (at high beam energy) asymmetry and pairing potentials in the pre-fragments formation.

Another application of SACA : hypernuclei production

A hypernucleus is a nucleus which contains at least one hyperon ($\Lambda(uds)$, ...) in addition to nucleons. Extending SACA to the strange sector requires the knowledge of the ΛN potentials. For a first study, we consider the strange quark as inert and use $V_{\Lambda N} = \frac{2}{3}V_{nN}$ for protons as well as for neutrons. Using this potential, SACA produces hypernuclei with the same algorithm as for non strange fragments. In the underlying IQMD program, which propagates the hadrons, Λ's are produced in different reactions: $K+N \rightarrow \Lambda+\pi, \pi+n \rightarrow \Lambda+K^+, \pi^-+p \rightarrow \Lambda+K_0, p+p \rightarrow \Lambda+X$. Their abundance, position and momentum distributions are strongly influenced by the reaction kinematics, the nuclear equation of state and the in-medium properties of the K^+ (kaon potential, etc.) which are implemented in the transport model.

To have a realistic description of the production of hypernuclei over the wide mass range which can be measured in relativistic heavy-ion collisions is a challenging task because it demands to reproduce correctly, within the present scope, all details which influence the creation of an hypernucleus. They can be subdivided into the three following steps : first, we have to know the yield, the positions and the momenta of the hyperons at the time of clusterisation, second, we have to know the hyperon-nucleon interaction potential which determines the probability that a hyper nucleus prefragment is formed and third we have to reproduce the properties of the hyperisotopes which are formed. Whereas the first step depends on the transport modelisation, the two others depend on the SACA parametrisation. As an illustration of this extension of SACA towards the hypernucleus production applied to IQMD simulations, fig. 6 shows the predicted yields of a wide variety of light hypernuclei in semi-central collisions of $^{58}Ni + ^{58}Ni$ at 1.91 A.GeV bombarding energy, for a clusterisation time $t = 20 fm/c$.

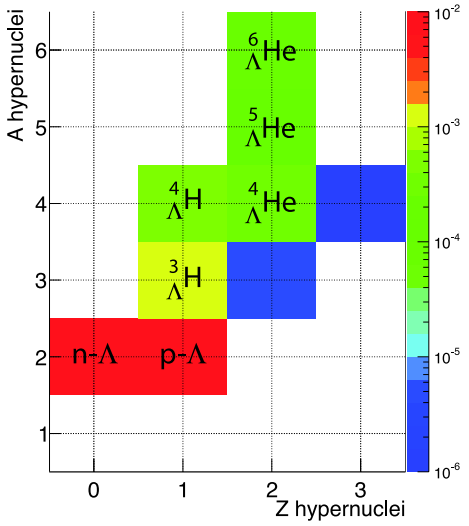

Figure 6: Yields of hypernuclei as predicted by IQMD+SACA for semi-central collisions (corresponding to the most central half of the total cross-section) of $^{58}Ni + ^{58}Ni$ at 1.91 $A.GeV$ incident energy. Here, SACA contains no asymmetry and pairing terms. The clusterisation is done at t=20 fm/c, and IQMD uses a soft equation of state, a momentum dependant interaction and a kaon potential of 20 MeV.

Fig. 7 shows the rapidity distributions of tritons, Λ's and hypertritons ($d+\Lambda \rightarrow_{\Lambda} t$), where we see that the hypertritons, though similar in mass and charge to the tritons, are produced in a very different phase space, mostly in the fireball - mid-rapidity region, like the Λ's, whereas the tritons are mainly following the spectator regions. In comparison with the Λ's, we observe that the hypertriton rapidity distribution is flatter, extending more towards the spectators, because this is where the yields of the deuterons are peaked, which are needed to create them.

Conclusions

We present here the first step towards an understanding of the production of isotopic yields and hypernuclei in heavy ion reactions. The production of these particles has up to now been beyond the scope of transport models. Improving SACA by including pairing and asymmetry energies and hence by a more precise description of the nucleus, allows for realistic predictions of absolute isotope yields, and of hypernuclei. We have seen that the asymmetry and pairing potentials can have a strong influence on the momentum anisotropies (i.e. apparent stopping power) for the isotopes (tritons, ^3He, ^4He, ...). According to this model the nucleons which form fragments have initially a low density. They contract and form finally slightly excited fragments. Therefore fragment formation is sensitive to the density dependence of the asymmetry energy and the pairing energy. However, fragments test this dependence only for densities below saturation density.

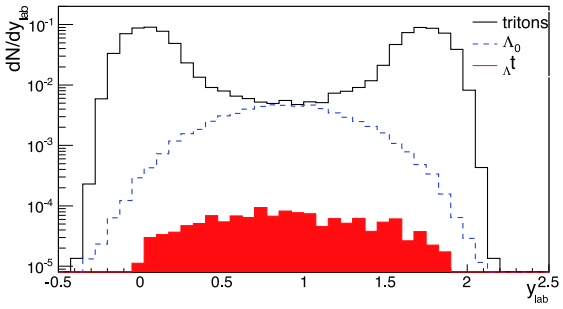

Figure 7: For the same system as in fig. 6, the predicted rapidity distributions of tritons (full black line), Λ's (dashed blue line) and hypertritons (red filled area).

For the dependence on densities higher than normal nuclear matter density, one has to focus on "elementary" particles which are produced in the most dense phases of the collisions, like Δs, kaons or pions. Still unclear is why SACA fails to describe the ^3He and ^4He yields at high beam energies when including pairing and asymmetry potentials.

Further developments in SACA are needed and on the way. We have to employ more realistic ΛN potentials, secondary decays have to be taken into account at low beam energies and the treatment of fragments with a short lifetime has to be improved.

References

[1] C. O. Dorso and J. Randrup, Phys. Lett. B **301**, 328 (1993).

[2] R. K. Puri and J. Aichelin, J. Comput. Phys. **162**, 245 (2000).

[3] J. Aichelin, et.al., Phys. Rev. **202** (1991).

[4] P.B. Gossiaux, R. Puri, Ch. Hartnack, J. Aichelin, Nucl. Phys. A **619** (1997) 379-390.

[5] Ch. Hartnack et al., Eur. Phys. J. A **1** (1998) 151.

[6] E. Khan, Nguyen Van Giai, N. Sandulescu, Nucl. Phys. A **789** (2007) 94.

[7] E. Khan, M. Grasso and J. Margueron, Phys. Rev. C **80** (2009) 044328.

[8] A. Le Fèvre et al., Nucl. Phys. A **735** (2004) 219-247.

[9] K. Zbiri, A. Le Fèvre, J. Aichelin et al., Phys. Rev. C **75** (2007) 034612.

[10] A. Le Fèvre et al., Phys. Rev. C **80** (2009) 044615.

[11] S. Hudan et al. (INDRA collaboration), Phys. Rev. C **67** (2003) 064613.

[12] W. Reisdorf and the FOPI Collaboration, Nucl. Phys. A **848** (2010) 366-427.

Pulse shape analysis for the KRATTA modules

J. Łukasik, P. Pawłowski, A. Budzanowski[*]*, B. Czech, I. Skwirczyńska*
Institute of Nuclear Physics, IFJ-PAN, 31-342 Kraków, Poland
J. Brzychczyk, M. Adamczyk, S. Kupny, P. Lasko, Z. Sosin, pA. Wieloch
Institute of Physics, Jagiellonian University, 30-059 Kraków, Poland
M. Kiš, Y. Leifels, and W. Trautmann
GSI Helmholtzzentrum für Schwerionenforschung GmbH, D-64291 Darmstadt, Germany

Abstract

The off-line pulse shape analysis applied to the data from the triple telescope KRATTA modules allowed to decompose the complex signals from the Single Chip Telescope segment into realistic ionization and scintillation components and to obtain a satisfactory isotopic resolution with a single readout channel. The obtained, ballistic-deficit free, amplitudes were constrained to follow the trends of the range-energy tables, which allowed for easy identification and energy calibration.

Introduction

The construction of KRATTA, Kraków Triple Telescope Array [1], has been motivated by the needs of the ASY-EOS experiment [2] [3], designed to study the density dependence of the nuclear symmetry energy. However, the modular design, portability, low thresholds (below 3 MeV/nucleon) and high maximum energy (~260 MeV/nucleon for p and α), allow the array to be used in various configurations and experiments.

The modules of KRATTA are composed of three photodiodes for direct detection [4] and of two CsI(Tl) crystals [5]. The layout and dimensions of these active elements are presented in Fig. 1. The first photodiode (PD0) serves as a Si ΔE detector providing the ionization signal alone. The second photodiode (PD1), works in a "Single Chip Telescope", SCT [6], configuration and provides a composite signal combined of a direct (ionization) component and of a scintillation component coming from the thin crystal (CsI1).

[*]Deceased.

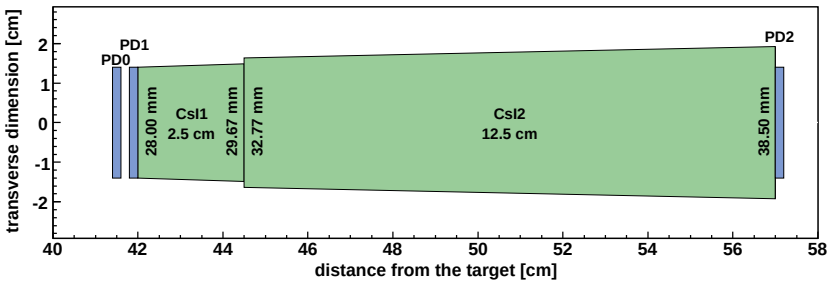

Figure 1: Schematic layout of the active elements.

The third photodiode (PD2) reads out the light from the thick crystal (CsI2) and, in addition, provides an ionization signal for particles that punch through the crystal within its active area.

Pulse shape analysis

The signals from the photodiodes have been digitized with the 100 MHz, 14 bits V1724 CAEN digitizers and stored for the off line analysis. The main purpose of the pulse shape analysis was to decompose the signals from the middle photodiode, PD1 (SCT), into the ionization and the fast and slow scintillation components. To accomplish this goal, the preamplifier response has been modeled using a simple parallel RC circuit approximation. It enabled the derivation of analytical forms for the measured waveforms under the assumption that the direct (ionization) and the two scintillation components of the induced current can be approximated with a difference of two exponential functions. Such a parametrization allowed for adjustment of both, the rise and fall times of the pulse. An overview of the fitting procedure can be found in [1], here, we present some more details.

Since the multi-parameter pulse shape parametrization and the preamplifier response used in the data analysis were only approximate, one could expect that the fit to the measured waveforms may not necessarily lead to physically correct decomposition into ionization and scintillation components. Indeed, one of the first attempts to fit the waveforms with all the amplitudes and time constant parameters treated as free fit parameters led to unphysical decompositions, despite perfect fits. The result of such a decomposition is presented in Fig. 2.

As can be seen, the reconstructed trends do not follow the predicted ATIMA [7] lines at higher energies, and artificially bend upwards, instead.

In order to superimpose on the ID map the predictions of the range-energy tables, the transformation from energies to FADC channels has been done using the

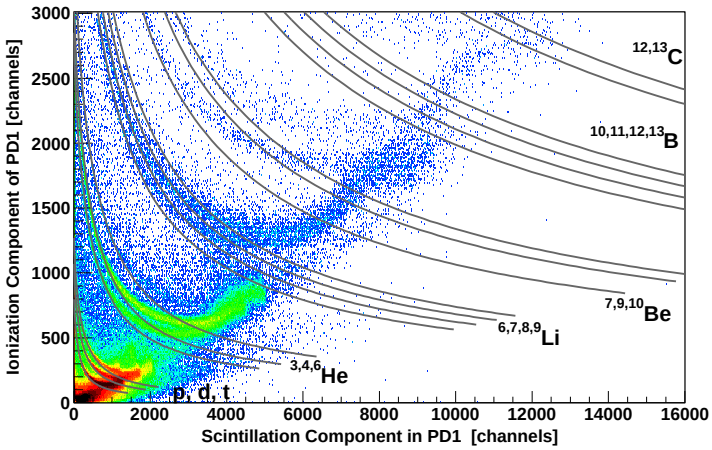

Figure 2: Ionization vs light component (2D histogram) for waveform fits leading to unphysical decomposition (dots). The lines represent predictions of the range-energy tables [7], and end at the punch through energy for the thin crystal.

(inverse) calibration parameters. The calibration parameters for the silicon photodiodes PD0 and PD1 and for the light from the CsI1 crystal [8], have been obtained from the matching of the ATIMA predictions to the ΔE-E ID map for the first two photodiodes (see Fig. 3).

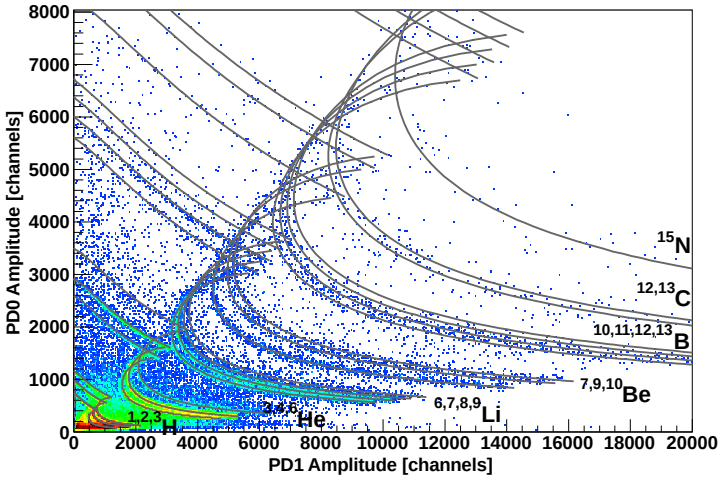

Figure 3: ΔE-E ID map for the first two photodiodes, PD0 vs PD1(SCT), for particles stopped in PD1 or in the thin crystal (CsI1). The lines are calculated with ATIMA.

This map is perfectly suited to perform the energy calibration, because it is much less sensitive to the actual decomposition (it uses the sum of all three components, which is approximately correct) and contains characteristic punch-through points and curvatures. The calculated ATIMA lines served here as a reference and allowed to impose some constraints on the waveform fits. These constraints were in fact limited to fixing some of the parameters, which led to a slight increase of the χ^2, but on the other hand, they allowed to obtain quite physical decompositions into ionization and scintillation components.

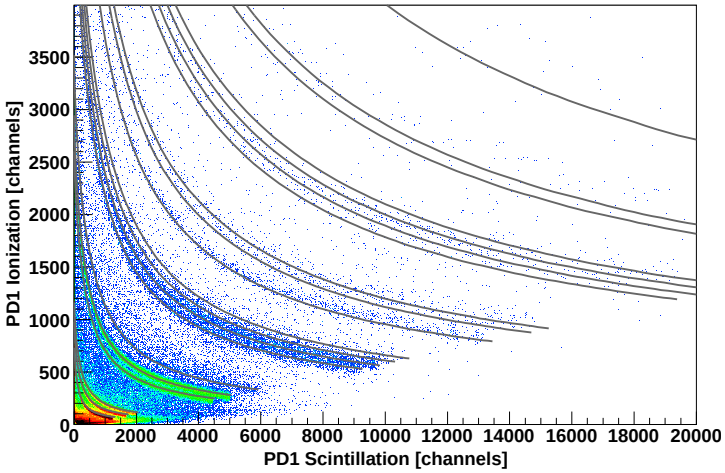

Figure 4: Decomposed SCT ΔE-E identification map (obtained with a single readout channel) with the superimposed ID lines calculated using the ATIMA tables. The sequence of lines is the same as in Fig. 3.

The final agreement between the decomposed ionization and scintillation components and the calculated ATIMA lines presented in Fig. 4, is a result of an iterative procedure of improving the calibration and searching for optimal values of the fixed parameters. This procedure finally converged providing quite reasonable trends of the isotopic lines.

Waveforms for particles stopped in the photodiode of the SCT segment and for those barely punching through it, turned out to be the most demanding and problematic ones in terms of the fitting. One of the time constants of the ionization component (the “rise time”) has been fixed using the above iterative procedure. In order to specify the “fall time” constant parameter for the ionization component, its initial value has been calculated using the first few truncated moments of the measured waveforms. For a single ionization component, the problem could be reduced to solving a quadratic equation. For particles punching through the middle

photodiode, and thus producing the light in the thin crystal, this calculated value has been kept fixed, whereas for particles with predominant ionization component, this value was allowed to be improved by the fitting routine. Distinction between these two cases was done by comparing the value of the exponential fit to the tail of the waveform, to the known RC value of the preamp. This criterion was found to be very simple and efficient.

Summary

Pulse shape analysis allowed for realistic decomposition of the complex SCT pulse shapes into individual ionization and scintillation components and eventually profit from the, otherwise harmful, nuclear counter effect. The isotopic resolution obtained using a single readout channel was found to compete very well with those obtained using the standard two channel readout.

The pulse shape analysis allows also to identify particles stopped in the first photodiode [1] and helps to isolate the secondary reactions and scatterings in the crystal as well as the punch-through hits, and thus to reduce the background, but this goes beyond the scope of this contribution.

Acknowledgments

Work made possible through funding by Polish Ministry of Science and Higher Education under grant No. DPN/N108/GSI/2009.

We (S.K.) acknowledge the support by the Foundation for Polish Science - MPD program, co-financed by the European Union within the European Regional Development Fund.

References

[1] J. Łukasik et al., arXiv:1301.2127 [physics.ins-det], to be published in Nucl. Instr. Meth. A (2013)
[2] P. Russotto et al., IWM 2011 Proc., Conf. Proc. Vol. 105, p. 91. P. Russotto et al., IWM 2009 Proc., Conf. Proc. Vol. 101, p. 22. http://www.irb.hr/users/mkis. http://www.ct.infn.it/asyeos2010.
[3] P. Russotto et al., Phys. Lett. B 697 (2011) 471.
[4] HAMAMATSU Si Photodiode for Direct Detection (S5377-0052(X)).
[5] Manufacturer: Institute of Modern Physics, Chinese Academy of Sciences, Lanzhou, China.
[6] G. Pasquali et al., Nucl. Instr. Meth. A 301 (1991) 101.
J. Friese et al., Conference Record of the 1992 IEEE, 1 (1992) 61.
[7] http://www-linux.gsi.de/~weick/atima
[8] D. Horn et al., Nucl. Instr. and Meth. A 320 (1992) 273.

Extracting information on the symmetry energy by coupling the VAMOS spectrometer and the 4π INDRA detector to reconstruct primary fragments

Paola Marini
GANIL, Caen, France

Abstract

The properties of nuclear matter in the nucleonic regime are determined by the nuclear interaction, which is, in turn, uniquely linked to the nuclear equation of state (EOS). In spite of its key role in determining important properties of exotic nuclei and astrophysical objects such as neutron stars, the equation of state for asymmetric nuclear matter has relatively few constraints. In particular, the density dependence of the potential part of the symmetry energy term of the EOS represents one of the main challenges for the research activities in nuclear physics. The isotopic distributions of complex fragments produced in reactions at intermediate energies are expected to be a good observable to extract information. However secondary decay is known to distort the signatures of the symmetry energy. We will present the first results in primary fragment reconstruction obtained exploiting the high mass resolution of the VAMOS spectrometer, coupled to the high granularity of the 4π charged particle array INDRA.

Breakup Reactions of Exotic Nuclei at the large acceptance spectrometer SAMURAI at RIBF

Takashi Nakamura
Tokyo Institute of Technology, Meguro, Tokyo, Japan

Abstract

SAMURAI (Superconducting Analyzer for MUlti-particle from RAdio-Isotope Beam) at RIBF, RIKEN, is a large acceptance spectrometer to measure neutron(s)/proton(s) and charged fragments in coincidence, which has just been commissioned early this year. The combination of such a spectrometer with the leading RI-beam facility in the world offers unique opportunities to study exotic nuclear structures and their related nuclear reactions. In this talk, I will introduce the SAMURAI facility, and present about the commissioning experiment as well as the day-one experiment, where the Coulomb and nuclear breakup reactions were applied to study the exotic structure of neutron drip line and even beyond. I will also show and discuss the planned experiments at SAMURAI in the near future.

Nuclear cluster formation in the participant zone of heavy-ion relativistic reactions

P. Pawłowski[1] *and Z. Sosin*[2] *for the ALADIN2000 Collaboration*
[1]*IFJ-PAN, Kraków, POLAND*
[2]*Jagiellonian University, Kraków, POLAND*

Abstract

A new approach to cluster formation, based on thermodynamic principles, is tested in the regime of relativistic heavy-ion reactions. The reaction is described with a simple participant-spectator mechanism, coupled to the clustering model, applied to the nucleons located in the participant zone. The results are confronted with the data obtained by the ALADIN group for the ^{124}Sn + ^{nat}Sn reaction at 600 AMeV incident energy. The general properties of the particles observed in the output channel are in quite good agreement with those observed in the experiment. Model predictions for the reaction scenario and primary fragment properties are presented.

The experiment

In the frame of the S254 experiment at GSI, the decay of hot quasi-projectiles from ^{124}Sn+^{nat}Sn reaction, at the incident energy of 600 AMeV, was studied. The charged products of quasi-projectile decay were analyzed using the ALADIN magnet and the TP chamber MUSIC IV coupled to the time-of-flight wall ToF. The LAND detector was located about 9 meters downstream from the target, perpendicularly to the beam axis, to register neutron tracks. In front of the LAND detector, a VETO wall was installed, to identify the light charged particles. The tracks of neutrons registered in LAND were analyzed off-line using the Shower Tracking Algorithm [1]. A detailed description of the experiment can be found elsewhere [2].

The model

In the model we assume that the particles and fragments observed in the experiment come mainly from the projectile. The projectile is considered as a system of nucleons interacting with their mean potential. Each nucleon is represented by a 3-dimensional Gaussian wave-packet. The wave-packet is considered as a nuclear

matter density distribution around the nucleon. The positions and momenta of the nucleons are drawn randomly in phase-space, but in a way conserving the total energy, momentum, spin and the Fermi statistics.

To determine the system energy, a special mean-field potential [3] was used, derived from the nuclear equation of state. Neglecting the nucleon spin asymmetry, one can expand the equation of state around normal density ρ_0 up to the quadratic term, obtaining:

$$e_{tot} = E + \frac{1}{18}K\frac{(\rho-\rho_0)^2}{\rho_0^2} + \delta^2 e_{sym} \tag{1}$$

where e_{sym} is the symmetry energy per baryon, expanded in the form:

$$e_{sym} = S + \frac{1}{3}L\frac{(\rho-\rho_0)}{\rho_0} + \frac{1}{18}K_{sym}\frac{(\rho-\rho_0)^2}{\rho_0^2}. \tag{2}$$

In the equations above the symbols $E = -15.85$ MeV, $K = 300$ MeV, $S = 30$ MeV, $L = 60$MeV, $K_{sym} = 50$ MeV, and $\rho_0 = 0.159$ fm$^{-3^-}$ are the parameters of the equation of state, and $\delta = \frac{\rho_n-\rho_p}{\rho}$ is the isospin asymmetry. The Fermi gas model provides the kinetic energy per particle for a two-component fermionic system:

$$e_{kin} = \frac{3}{20m}\hbar^2\left(\frac{3}{2}\pi^2\right)^{2/3}\rho^{2/3}\left[(1+\delta)^{5/3} + (1-\delta)^{5/3}\right] \tag{3}$$

Now, the potential energy per baryon can be expressed as:

$$u(\rho,\delta) = e_{tot}(\rho,\delta) - e_{kin}(\rho,\delta). \tag{4}$$

In this way a nuclear potential depending only on proton and neutron densities is obtained.

As the reaction time at relativistic energies is extremely short, the collision with the target is considered as a perturbation in momenta of a certain number of nucleons, while the positions remain approximately unchanged. Relying on this assumption, we first select a number of nucleons called "*participants*", and determine for them the effective momentum transfer. As participants we select all nucleons located in the geometrical overlap zone of the volume V, and some number of nucleons located outside this volume, in a maximal distance $\Delta x = 0.25V^{1/3}$.

The momentum transfer to a participant has two components: a stochastic component, drawn randomly from a 3-dimensional Gaussian distribution, and, in the beam direction, a diffusive component, drawn from an exponential distribution. Parameters of these distributions are free parameters of the model and were approximately fixed by observing rapidity plot of neutrons registered during the experiment.

Cluster formation

For the cluster definition we applied the idea presented in [4], and successfully tested in the low-energy domain [5]. The participants are considered as quasi-free particles, residing in a virtual (undetermined) quantum state. The new state for each particle is chosen from all possibilities: the particle can stay free, but it can also join any other participant (forming a cluster), or be absorbed either by the spectator or a previously-formed cluster. The probability of each scenario is assumed to be proportional to the density of states of the whole system in the final state. The code performs a series of test transfers and calculates the density of states for the whole system in each case. Then it chooses randomly one of the possible transfers according to the calculated probabilities.

The density of states of the whole system is given by:

$$\Omega = \Omega_{tr} \times \prod_i \omega_i \tag{5}$$

where Ω_{tr} is the density of states related to the translational motion of fragments, and ω_i is the internal density of states of the i-th fragment. For $A > 2$ fragments:

$$\omega_i = \begin{cases} 0, & E_i^* > -B_i \\ \sim \exp\left(2\sqrt{aE_i^*}\right), & -B_i > E_i^* > 0 \\ 0, & E_i^* < 0 \end{cases} \tag{6}$$

where E_i^* is the thermal component of the excitation energy, B_i is bounding energy of i-th fragment, and a is the level density parameter. For deuteron ($A = 2$), $\omega_i = 3$ is assumed, corresponding to spin degeneracy of the particle.

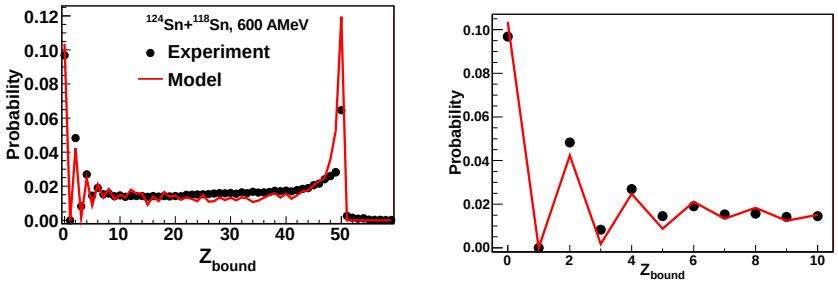

Figure 1: Z_{bound} distribution for the experimental data (dots) and the model result (lines). In the right panel a zoom of [0..10] Z_{bound} range is presented.

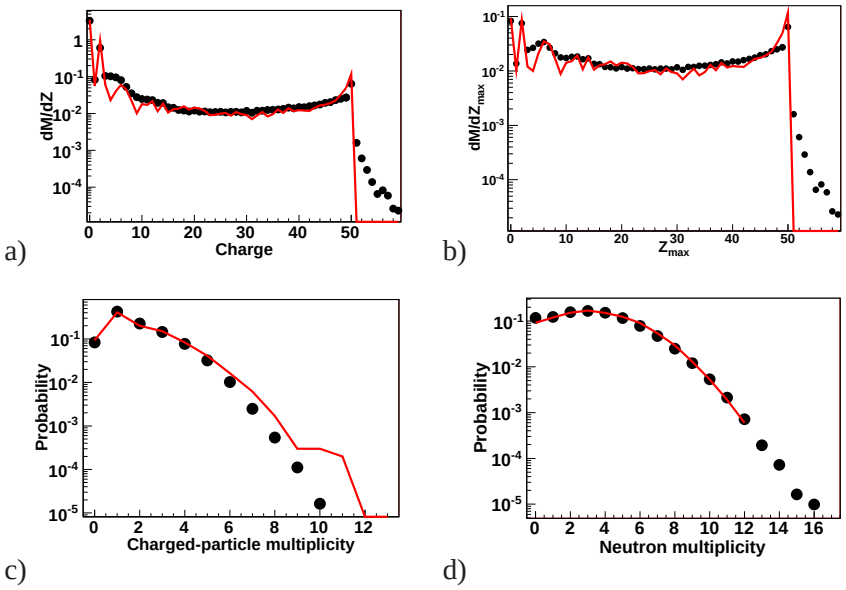

Figure 2: Comparison model (lines) - data (dots): a) charge distribution; b) heaviest fragment charge distribution; c) charged particle multiplicity distribution; d) neutron multiplicity distribution.

Comparison model-experiment

The simulation was performed in the whole impact parameter range. The resulting excited fragments were cooled-down with the use of the GEMINI code [6]. Afterwards, all the particles were processed by an experimental filter, taking into account geometrical acceptance, energy thresholds and detection efficiencies for each particle. Only the particles accepted by the filter were considered. Finally, the model results were confronted with the experimental data.

The reaction mechanism is generally characterized in Fig. 1 where the Z_{bound} distribution is presented. The plot shows the dominance of quasi-elastic (right-hand peak) and vaporization (left-hand peak) events. The model describes the data very well, especially in the range of lower Z_{bound} (see the right panel). Fig. 2 presents general properties of charged particles and nucleons, and their remarkable description by the model.

The model predictions for the properties of the primary fragments are presented in Fig. 3. In the left panel the correlation between the primary fragment mass and incident impact parameter is shown. One can observe here a transition from quasi-binary reaction scenario ($b > 4$ fm) to the multifragmentation ($b \approx 4$ fm) and

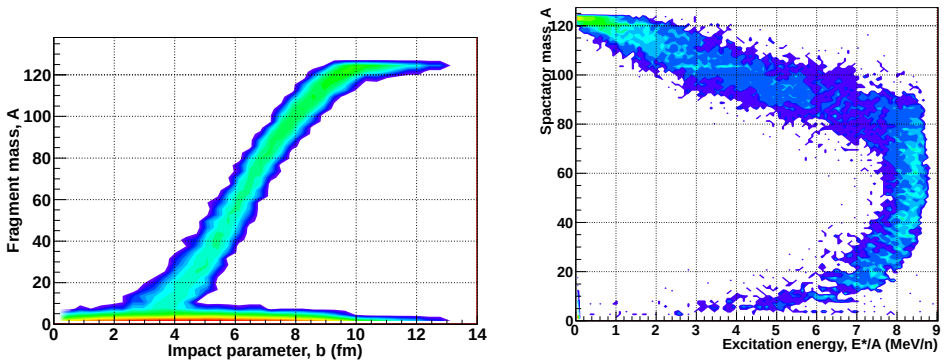

Figure 3: Model predictions for primary-fragment properties. Left panel: correlation between fragment mass and impact parameter; right panel: correlation between spectator mass and its excitation energy per nucleon.

vaporization ($b < 2$ fm) regimes. In the right panel, the correlation between the spectator mass and its excitation energy per nucleon is presented. The characteristic shape observed in this plot is different from the usually assumed monotonic dependence (see e.g. [2]). This is a consequence of the competition between the absorption of a participant by the spectator, and the cluster formation process.

Conclusions

The model applied in this work allowed to describe with satisfactory accuracy the general properties of the studied reaction. The stochastic clustering method used in the participant zone of the reaction allows to reproduce correctly the Z_{bound} distribution in the range of the most central collisions. The model predicts a smooth change of the reaction scenario from quasi-binary, through multifragmentation to vaporization, with decreasing impact parameter. The competition between spectator absorption and cluster formation processes leads to a characteristic drop of excitation energy per nucleon of the spectator in the range of more central collisions.

References

[1] P. Pawłowski, et al., Nucl. Instr. & Meth. A **694**, 47 (2012).

[2] see R. Ogul, at al., Phys. Rev. C **83**, 024608 (2011), and references therein.

[3] P. Pawłowski and Z. Sosin, in Proc. of the International Workshop on Multifragmentation and related topics IWM2009, 4-7 Nov. 2009, Catania, Italy, Conference Proceedings vol. **101**, p. 300 (2010).

[4] Z. Sosin, Eur. Phys. J. A **11**, 311 (2001).

[5] R. Płaneta, et al., Eur. Phys. J. A **11**, 297(2001); Z. Sosin, et al., Eur. Phys. J. A **11**, 305(2001).

[6] R.J. Charity et al., Nucl. Phys. A **483**, 391 (1988).

The CALIFA calorimeter in the versatile R^{3}B setup

H. Alvarez Pol for the R^{3}B collaboration
Dept. of Particle Physics, Universidade de Santiago de Compostela
15782, Santiago de Compostela, Spain

Abstract

The R^{3}B experiment will investigate relativistic exotic nuclei making use of many different direct reaction mechanisms. The present paper summarizes the status of the CALIFA (CALorimeter for the In Flight detection of γ-rays and light charged pArticles) calorimeter surrounding the R^{3}B reaction target, and its capabilities for the light charged particle identification.

Introduction

The forthcoming facilities for the study of exotic short lived nuclei using secondary beams of radioactive nuclei will present the means to investigate a vast area of the nuclear chart for which only the most general properties have so far been observed. One of the most advanced instrument for such research is the R^{3}B experiment [1], a versatile reaction setup proposed for direct reactions with high-energy radioactive beams, located at FAIR [2] (Facility for Antiproton and Ion Research), the next-generation international accelerator facility in Darmstadt, Germany.

R^{3}B is designed for experimental reaction studies with exotic nuclei far off stability, with emphasis on nuclear structure and dynamics. Some astrophysical questions and technical applications can also be studied. The reaction types include knockout reactions, quasi-free scattering, total absorption measurements, elastic proton scattering, heavy-ion induced electromagnetic excitation, charge-exchange reactions, fission, spallation and projectile multifragmentation. Such a broad and challenging physics programme requires kinematically complete measurements of the reaction products in inverse kinematics, with the greatest possible efficiency and full solid-angle coverage.

The proof of concept of the R^{3}B setup, using partially developments based on improvements from the previous existing ALADIN-LAND detectors, has been tested in a preliminary version in different experiments in the last years, demonstrating the advanced capabilities for the reconstruction of the direct reactions observables. With some modifications in the detectors and the setup configuration,

QFS [2], light ion direct (p,pn) and (p,2p) reactions [3] and different fission systems [4] has been analyzed and reconstructed. Additional tests and experiments are devised in the next months using an upgraded set of detectors which should demonstrate the improvement of the new developments.

CALIFA conceptual design and simulations

CALIFA is the calorimeter proposed for the detection of gamma-rays and light charged particles originating from nuclear reactions induced by relativistic exotic beam. The requirements imposed on the CALIFA calorimeter reflect the wide spectrum of experiments to be performed employing this versatile setup. In certain spectroscopical physics cases, a high gamma energy resolution (5% at 1 MeV) and multiplicity determination is requested. In others, the goal is to obtain a calorimetric response with high efficiency. Charged particles of moderate energy, as protons up to 300 MeV, should be identified with an energy resolution below 1%. Part of the complexity arises from the kinematics of the reactions, producing a large Lorentz boost and broadening, the correction of which should be accounted for by the detector. CALIFA features a high photon detection efficiency and good energy resolution even for beam energies approaching 1 AGeV. This is in addition to the required calorimetric properties for detection of multiple cascades, and high efficiency for proton detection [8].

CALIFA consists of two sections, a “Forward EndCap” and a cylindrical “Barrel” covering an angular range from 43.2 to 140.3 degrees. Figure 1 shows an engineering design of the whole CALIFA detector, including the mechanics solutions. The CALIFA Barrel is an integral part of the R3B experimental setup, meeting the challenging demands imposed by the wide-ranging R3B physics program; which requires both detection of low energy γ-rays from single-particle excitations and high-energy γ-rays associated with different collective modes, in addition to the detection of charged particles emitted from the reaction zone [5].

Several prototypes have been developed based on the solutions proposed for the scintillator material, light readout photodiodes, wrapping materials and with the adequate geometry corresponding to different kinematical regions of the CALIFA detector [6, 7]. A prototype consisting of fifteen CsI(Tl) truncated pyramidal scintilling crystals coupled to avalanche photodiodes contained inside an aluminum box for electric and external light isolation, has been tested at the GSI (Helmholtzzentrum fur Schwerionenforschung at Darmstadt, Germany). The prototype was part of a set of detectors installed in Cave C, to study the reactions produced when a pulsed $^{197}Au^{65+}$ beam of E = 400 AMeV impinge on a Pb target. The goals were to test the energy resolution and particle identification algorithms as well as test

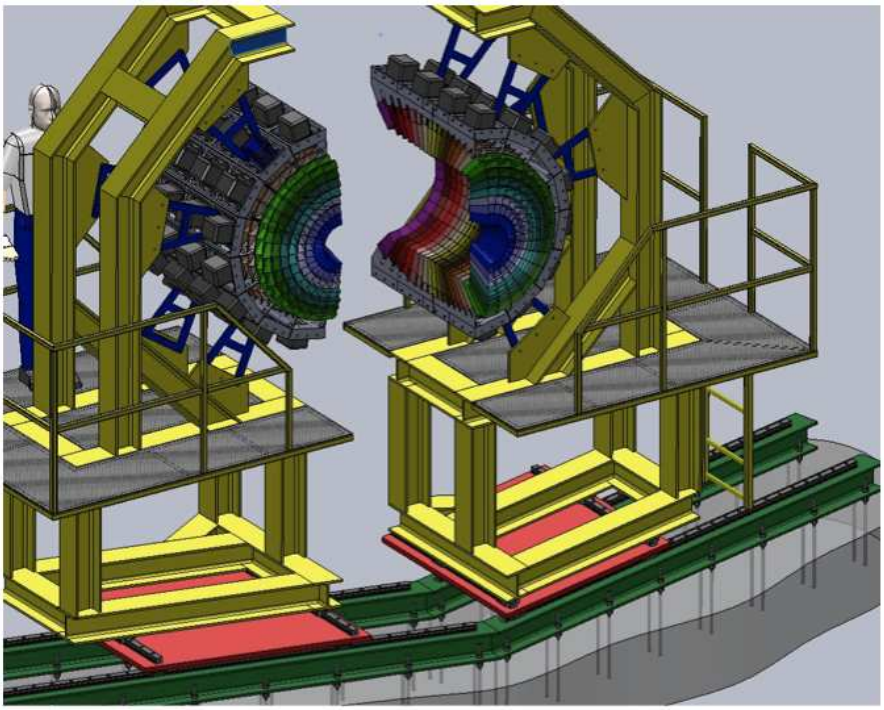

Figure 1: Artistic view of the complete CALIFA design, including the mechanical support structure.

the new data acquisition system, based on a new FPGA able to perform real-time data analysis [9].

Light charged particle ID capabilities

Two pulse shape analysis techniques were tested to achieve the light charged particle identification. The first one is based on the analysis of the signal rise time and the total deposited energy, while the second one is based on the derivation of two components, fast and slow, extracted by a combination of Moving Deconvolution Window (MDW) methods with variable gates over the digitized pulse and its derivative, both explained in detail in the reference [9]. This second method delivers a better identification; the figure 2 shows the results obtained with the CALIFA prototype crystals.

The algorithm allows the unambiguous and complete separation of the light ions reaching the detector, practically free of contamination. In this way protons,

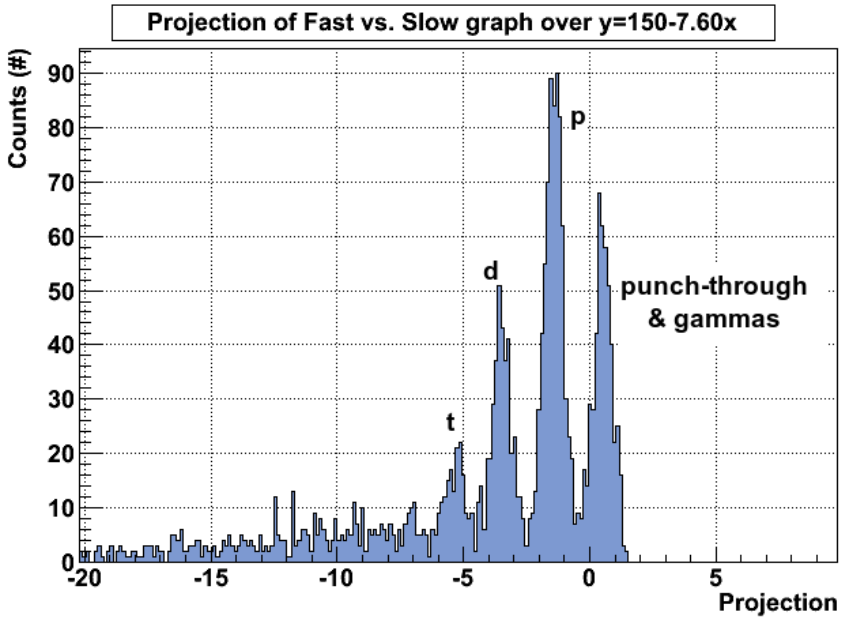

Figure 2: Particle identification plot (arbitrary units) obtained from the fast vs. slow identification method. Protons (p), deuterons (d) and tritium (t) ions are clearly separated.

deuterons and tritium could be identified and tagged online, implementing the algorithm directly in the FPGA electronics. The lack of energetic heavier ions such as alpha particles could be explained by the large angle between the beam line axis and the detector position, reducing the probability of being detected by our prototype.

References

[1] Technical Proposal for the Design, Construction, Commissioning and Operation of R3B, universal setup for kinematical complete measurements of Reactions with Relativistic Radioactive Beams. FAIR-PAR/ NUSTAR/R3B, December 2005. Available in http://www-land.gsi.de/r3b/docu/R3B-TP-Dec05.pdf

[2] F. Wamers, “Quasi-Free-Scattering and One-Proton-Removal Reactions with the Proton-Dripline Nucleus ^{17}Ne at relativistic Beam Energies”, PhD Thesis,

IK-TUD, Darmstadt 2011.

[3] P. Díaz Fernández, “An investigation into quasifree scattering of neutron-rich carbon and nitrogen nuclei around N=14” in this proceedings.

[4] A. Bail *et al*, “Next generation Fission experiments at GSI: short and long term perspectives” in Proceedings of Seminar on Fission, Het Pand, Ghent, Belgium, 17-20 May 2010.

[5] H. Alvarez-Pol *et al*, Nucl. Instr. and Meth. Phys. Res. B **266** (2008) 4616 - 4620.

[6] M. Gascón *et al*, IEEE Trans. on Nucl. Sci **56**, N. 3, June 2009.

[7] M. Gascón *et al*, IEEE Trans. on Nucl. Sci **57**, N. 3, June 2010.

[8] Technical Report for the Design, Construction and Commissioning of The CALIFA Barrel: The R3B CALorimeter for In Flight detection of γ-rays and high energy charged particles.

[9] D. Ramos Doval, Master Thesis: ”Pulse-shape analysis of signals from a CALIFA scintillator prototype fired by photons and light charged particles and its application to PID”. University of Santiago de Compostela, June 2012. http://igfae.usc.es/~genp/academic/mastertesis/MasterTesis_Ramos.pdf

Heavy ion collisions in the 1A GeV regime: how well can we join up to astrophysics?

W. Reisdorf for the FOPI collaboration
GSI, Planckstr,, Darmstadt, Germany

Abstract

The derivation of information useful for understanding the physics inside compact stars from HIC observations is a difficult task. Complications due to finite size, different chemistry, non-adiabatic compression, incomplete stopping and structural effects must be overcome. Using now available systematic FOPI data in the SIS energy range we try to trace the path to take.

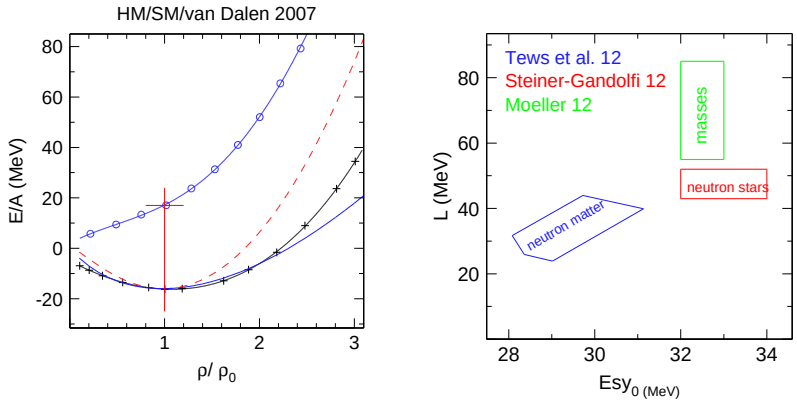

Figure 1: Various nuclear matter EoS (left) and constraints (right)

There now exists an extensive set of data on heavy ion reactions in the 1*A* GeV range [1]. In the sequel we confront the data with IQMD [2] simulations. The two options of purely phenomenological *cold* nuclear EoS that we use are plotted in Fig.1 and confronted with a 'microscopic' (Dirac-Brueckner-Hartree-Fock, DBHF) calculation [3] for symmetric matter. It is seen that in the density range relevant for SIS energies (up to $\rho/\rho_0 = 2.5$) our 'soft' version, SM, is rather close to the theoretical calculation. We will see in the sequel that FOPI data are strongly favouring the SM version (full blue) over the stiff, HM, version (dashed).

Also included from the same theoretical work is the cold EoS for pure neutron matter. It is not possible in the laboratory to determine directly the neutron matter EoS. We have to rely on theoretical help. The adequacy of the theory, in turn, can be tested by confrontation with high quality experimental data constraining the symmetric matter EoS. Recent constraints on the EoS parameters L and Esy_0 from theoretical efforts [4], nuclear masses [5] and neutron star data [6] reflect incompatibilties associated with different physics sensitivities, see Fig.1 right.

In Fig.2 we show a sample of proton yield and flow data from our Collaboration (black dots with error bars) together with simulations using IQMD with the stiff version of the EOS (HM, red dashed) and the soft version (SM, blue full).

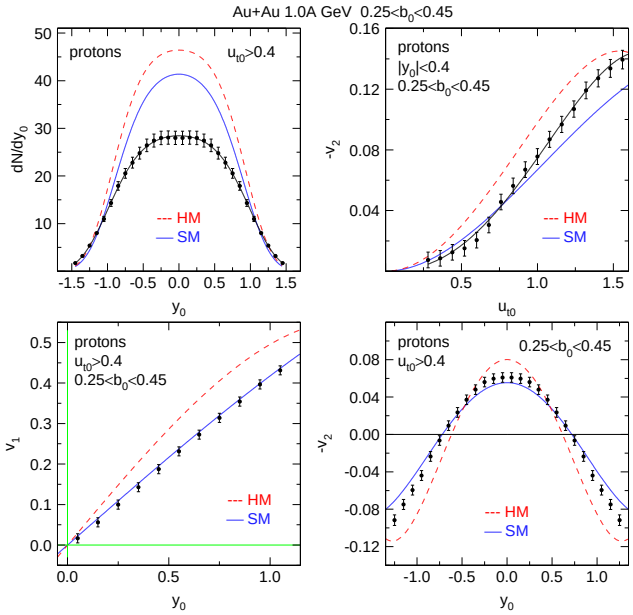

Figure 2: Proton rapidity and flow data and IQMD-SM/HM simulations

It can be seen that the three projections shown are best described by the SM version: see the rapidity (y) dependences of the directed, $v1$, and the elliptic ($-v_2$) flow in the two lower panels and the $p_t/m = u_t$ dependence of the elliptic flow in the upper right panel. As IQMD underestimates clusterization it overpredicts single nucleon (proton) yields (upper left panel). Notice a moderate, but still remarkable dependence on the EoS, however.

Taking a closer look at $-v_2(y_0)$ (we use the index 0 to indicate scaling with the beam parameters [1]) we see that the predicted shape is sensitive to the EoS *in the full rapidity range*. To take advantage of this feature we introduce a quantity

dubbed v_{2n} defined by $v_2 n = -v_{20} + |v_{22}|$ where the parameters are fixed by a fit to the flow data using $v_2(y_0) = v_{20} + v_{22} \cdot y_0^2$ in the scaled rapidity range $|y_0| < 0.8$.

The result for Au+Au between 0.4A and 1.5A GeV is shown in Fig.3 for protons (left) and deuterons (right).

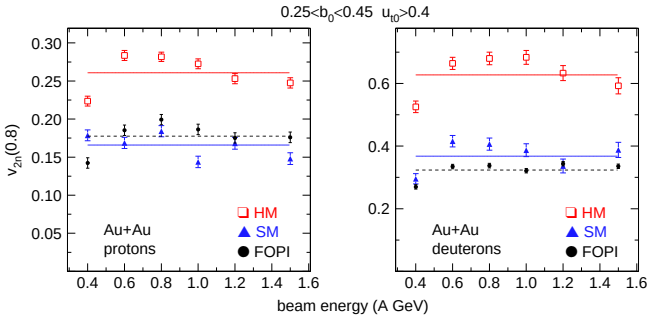

Figure 3: Elliptic flow v_{2n} for protons (left) and deuterons

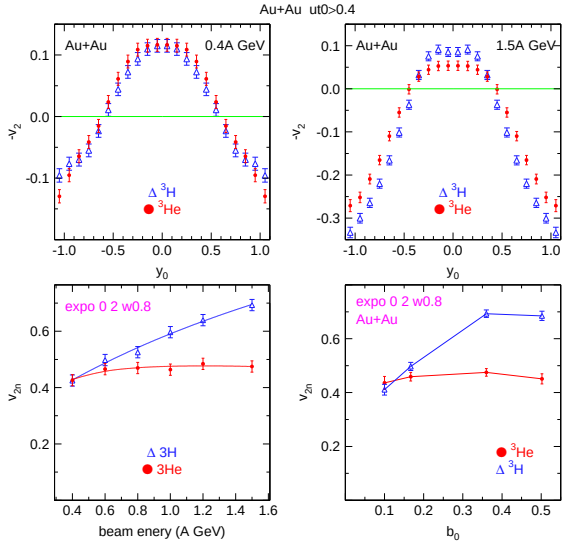

Figure 4: Studies of v_2 and v_{2n} for the two mass three isotopes

As the beam energy dependences are rather weak, we indicate the average behaviour by straight lines. The comparison of the data for v_{2n} with the calculations shows a rather convincing preference for SM! The sensitivity is large: there is a factor 1.6 between HM and SM, a difference exceeding significantly the indicated

experimental error bars. This strongly supports the Tübingen calculation (Fig.1).

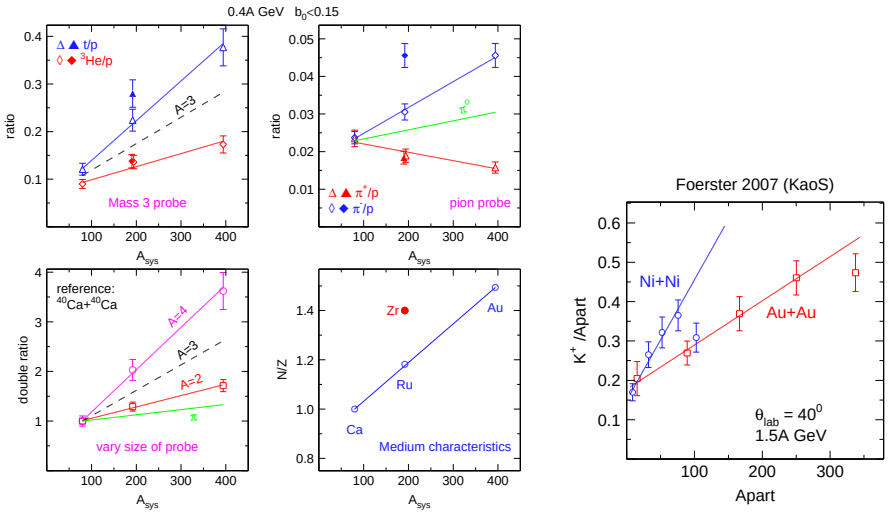

Figure 5: System size dependences of various indicated ejectiles

Including mass three clusters (besides protons and deuterons) leads to the same conclusions. In view of high interests in isospin dependences it is worth looking in more detail at elliptic flow data of ^{3}H and ^{3}He: see the two upper panels in Fig.4 for Au+Au at $E/A = 0.4A$ (left) and $1.5A$ GeV (right). While there is no significant (within error bars) difference at the lower beam energy we see a remarkable effect at $1.5A$ GeV: the shape difference in $-v_2(y_0)$ is reminiscent of the SM/HM shape difference seen in Fig.2. We therefore use again v_{2n} to systematize this isotopic difference in terms of a single parameter: see the two lower panels showing the energy dependence for both isotopes (left) and, for the $1.5A$ GeV data, the centrality dependence in terms of the scaled impact parameter b_0 [1].

These observations, so far, are not reproduced by our IQMD version. Considering the limitation of the isotopic split to larger b_0 and higher E/A, we suggest unaccounted for momentum dependences and connection to Δ formation in an asymmetric medium. For future clarification of the latter we expect our pion yield and flow data [1] to be helpful.

Our conclusions concerning preference, in the SIS energy range, of a 'soft' EoS (see Fig.1) are in line with earlier findings using the comparison of K^+ yield data varying system size or centrality. A sample of such data [7] is shown in the right panel of Fig.5. Once cluster formation is better understood, there is some chance, that conclusions on the EoS can also be derived from system dependences (size and isospin) of various clusters, see the various panels in Fig.5. There is evidence

for more efficient cooling (condensation) if the achieved density was higher, i.e. for more massive systems. For pions the increased production in softer, denser systems, is compensated out by the final cooling before freezeout. There is a loss of memory for the high density phase here.

To conclude, heavy ion data obtained at SIS, represent by now rather convincing constraints for the EoS of nuclear matter in the density range up to $\rho = 2.5\rho_0$.

References

[1] W. Reisdorf et al. (FOPI Collaboration), Nucl. Phys. A **781**, 459 (2007), **848**, 366 (2010), **876**, 1 (2012).

[2] C. Hartnack, et al., Eur. Phys. J. A **1**, 151 (1998).

[3] E.N.E. van Dalen, C. Fuchs, A. Faessler, Eur. Phys. J. A Lett. **31**, 29 (2007).

[4] I. Tews, T. Krüger, K. Hebeler and A. Schwenk, Phys. Rev. Lett. **108**, (2012).

[5] P. Möller, W.D.Myers, H. Sagawa and S. Yoshida, Phys. Rev. Lett. **108**, 05201 (2012).

[6] A.W. Steiner and S. Gandolfi, Phys. Rev. Lett. **108**, 081102 (2012).

[7] A. Förster et al.(KaoS Collaboration), Phys. Rev. C **75**, 024906 (2007).

Scattering of ^{8}He on ^{208}Pb at energies around the Coulomb barrier

A. M. Sánchez-Benítez[1], G. Marquínez-Durán[1], I. Martel[1], K. Rusek[2], L. Acosta[1,3] for the E578S collaboration
[1] Dpto. de Física Aplicada, Universidad de Huelva, 21071 Huelva, Spain
[2] Heavy Ion Laboratory, University of Warsaw
[3] Laboratori Nazionali del Sud-INFN, via S. Sofia 62, 95123 Cat. Italy

Abstract

Preliminary results on elastic scattering of ^{8}He on a ^{208}Pb target at *Elab* = 22 MeV are presented in this work. The experiment was performed at SPIRAL/GANIL facility in Caen (France). Experimental elastic cross sections follows the trend of ^{6}He up to the scattering angles around 80°. For larger angles the absorption becomes even greater which can be due to 1n transfer reactions.

Introduction

^{8}He is the lightest skin nucleus and it has the largest neutron to proton ratio of the particle-stable nucleus. Only a few scattering data sets at barrier energies are presently available [1, 2] and there is still a lack of information concerning collective aspects as characteristic nuclear excitations, coupling between different reaction channels and neutron-core correlations.

As compared with ^{6}He, previously studied by the collaboration [3–5], ^{8}He has more neutrons of valence but more tightly bound and its binding energies for 1n ans 2n systems are similar whereas in the ^{6}He the breakup of 2n is energetically favored.

Experimental setup

The experiment was performed at the SPIRAL-GANIL facility at Caen, France. The produced ^{8}He beam was driven through various collimators and beam diagnostics into the reaction chamber. A ^{208}Pb self-supported target with a thickness of 1 mg/cm^{2} was placed inside GLORIA (GLObal ReactIon Array) silicon array

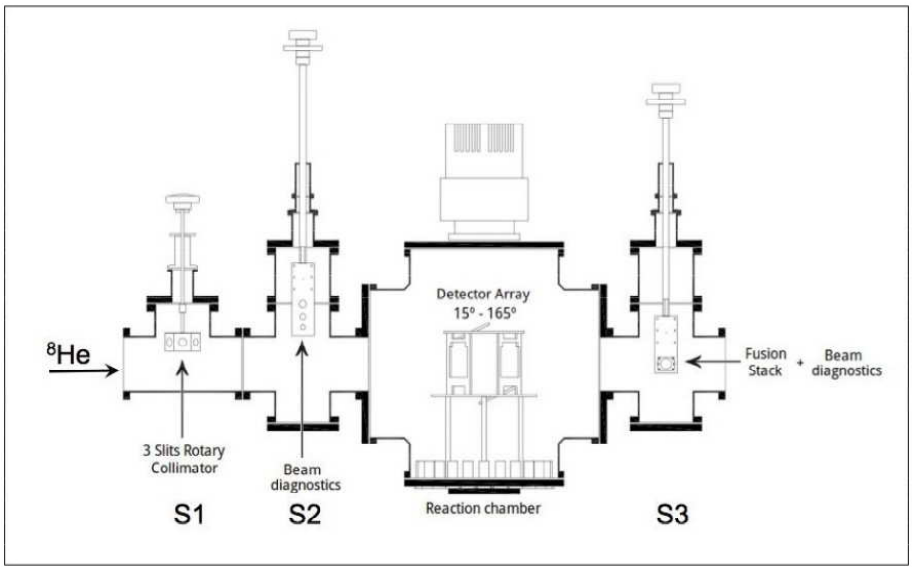

Figure 1: Sketch of the experimental setup.

developed at the University of Huelva. The experimental setup is schematically shown in Fig. 1.

The detector array GLORIA consists on twelve DSSSD detectors arranged in six particle detector telescopes. Each telescope is made of a 40 μm ΔE-detector of 50 mm x 50 mm, segmented in 16 strips on each side, and by a 1 mm E-detector of the same size and segmentation; the strip pitch all detectors of the array is 3 mm. The relative position of these telescopes with respect to the reaction target was optimized considering the following parameters: (i) a maximum angular range coverage, (ii) a good angular resolution (less than 5°), (iii) an angular range overlap between telescopes and (iv) a symmetric position of detectors. The array was design in such a way that it covers a continuous angular range between 15° and 165°, with no gaps and with a high granularity. The ^{208}Pb target is tilted 30° with respect to the vertical direction avoiding the shadowing of detectors and ensuring the detection of particles around 90°.

A set of collimators (S1, S2 and S3) was used for driving and focusing the radioactive beam on the scattering target. The S1 system consists of a rotary frame with 2 cm, 1 cm and 8 mm diameter collimators. The S2 system is made of a metal frame (inox) with 1 mm, 5 mm, 1 cm and 3 cm diameter collimators; a standard transmission PIP silicon detector 500 μm thick from ORTEC was placed at the same frame. The system could be rotated so that the full detector area (2 cm diameter) could be directly exposed to the radioactive beam. The S3 system

consisted on a metal frame with a 1 mm diameter collimator and a PIP detector. All systems could be rotated and push-pull in/out of the beam axis. The beam was driven trough the centre of the chamber by alternative focusing at the 1 mm collimators of the S2 and S3 systems.

On the other hand, the beam operator could reduce the beam intensity at S2 (at the 1 mm collimator) down to about 10 pps using a set of pepperpots, so that S2 and S3 could be rotated with the PIP detector facing the beam with no risk of damaging the detectors. In this configuration, the transmission and alignment of the beam was optimized. Furthermore, by measuring the yield at S3 for each of the three collimators placed at S1 and S2, the beam size at target position could be deduced to be <4 mm diameter on the target position.

Preliminary results

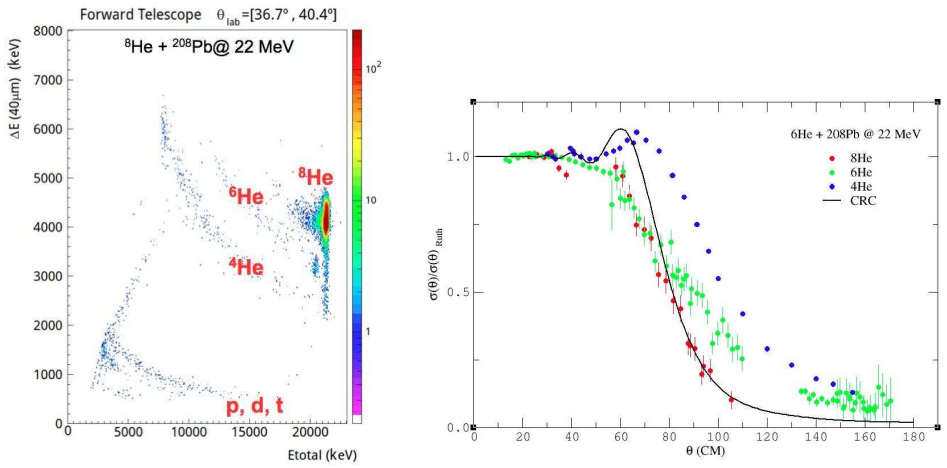

(*a*) (*b*)

Figure 2: *(a) Typical ΔE-E spectrum obtained at forward angles. (b) Obtained angular distribution of the elastic scattering. See text for discussion.*

A typical particle ΔE/E spectrum obtained at forward angles with beam energy E_{lab} = 22 MeV is shown in Fig. 2(a). The elastic as well as the ^{6,4}He production channels are clearly separated, and even a small fraction of contaminants of ^{6}He ions, estimated below 0.0001 %, was observed during the experiment. The energy resolution achieved in our experiment was around 150 keV. In Fig. 2(b) we show preliminary results obtained for the elastic channel of ^{8}He+^{208}Pb system at 22 MeV (red dots). The data are normalized to the corresponding Rutherford cross sections

and compared with ^{6}He+^{208}Pb [3] and ^{4}He+^{208}Pb [6] scattering systems at similar collision energies. The ^{4}He data is plotted with blue dots and was measured at Elab = 23.5 MeV; it exhibits a strong rainbow pattern around the grazing angle (around 75° Lab) characteristic of light stable nuclei. The angular distribution for ^{6}He (green dots) shows the usual strong absorption pattern down to 50° Lab, where the Coulomb-nuclear rainbow has disappeared. The angular distribution of the elastic scattering of ^{8}He follows the trend of the ^{6}He data up to about the grazing angle, where the absorption becomes even stronger.

Conclusions

We have measured the elastic scattering and reaction channels for the system ^{8}He + ^{208}Pb at 18 MeV and 22 MeV using the novel charged particle detector array GLORIA. The experiment was performed at the SPIRAL radioactive beam facility at GANIL (Caen, France). The elastic and ^{6,4}He reaction channels have been properly separated by means of GLORIA detector array. The preliminary angular distribution of elastic channel at 22 MeV exhibits an absorption pattern similar to the one found for the ^{6}He system, becoming even larger as the scattering angle increases beyond the grazing angle. The data analysis is still in progress.

Acknowledgments

This work was supported by the Grant from the Spanish Research Council FPA-2010-22131-C02-01 and the Grant from the Ministry of Science and Higher Education of Poland No. N202 033637.

References

[1] A. Lemasson *et al.*, *Phys. Rev.* **C82**, 044617 (2010).

[2] A. Lemasson *et al.*, *Phys. Lett.* **B697**, 454 (2011).

[3] A.M. Sánchez-Benítez *et al.*, *Nucl. Phys.* **A803**, 30 (2008).

[4] L. Acosta *et al.*, *Phys. Rev.* **C84**, 044604 (2011).

[5] D. Escrig *et al.*, *Nucl. Phys.* **A792**, 2 (2007).

[6] J. S. Lilley *et al.*, *Nucl. Phys.* **A342**, 165 (1980).

GASPHYDE particle detectors

A. M. Sánchez-Benítez, J. A. Dueñas, I. Martel
Dpto. de Física Aplicada, Universidad de Huelva, 21071 Huelva, Spain

Abstract

The scientific community, specially from Europe, is nowadays deeply involved in R&D projects on new instrumentation to be operated in the future european RIB facilities FAIR (GSI, Darmstadt) and SPIRAL2 (GANIL,Caen). The silicon detector arrays HYDE and GASPARD represent an example of a fruitful sinergy between such R&D projects. Technical issues concerning particle identification and detector design which have been addresed by the two collaborations will be described.

Context of HYDE & GASPARD highly segmented compact detectors

Nuclear reactions involving unstable nuclei with low breakup thresholds and exotic structures display features remarkably different from those of well-bound stable nuclei. With the advent of recent radioactive ion beam (RIB) facilities, new nuclei far from the line of stability have been available for study. The construction of the new facilities FAIR (GSI, Germany) [1] and SPIRAL2 (GANIL, France) [2], and the SPES project (LNL, Italy) [3] already funded, has generated good perspectives in the experimental nuclear physics community.

The new exotic nuclear species are of great importance for nuclear structure studies as well as for providing a deeper microscopic picture of nuclear physics in a wide scope: isospin-symmetry breaking effects in heavy nuclei, proton-neutron pairing phase or for the study of rare decay modes, such as the recently observed two-proton radioactivity. On the other hand, the weaker binding may lead to a more diffuse mean field and a modified spin-orbit interaction, all of which lead to a modification of the shell gaps. Such modifications of shell structure have an influence on the evolution of nuclear shapes and collective modes that should be investigated in detail. The possibility to produce of the most exotic isotopes offer direct access to the relevant astrophysics paths, leading to a fruitful synergy of nuclear structure and nuclear astrophysics.

The FAIR (Facility for Antiproton and Ion Research) is an extension of the existing RIB facility GSI in Darmstadt (Germany). It will allow for the production

of radioactive nuclei of very short life, down to a few microseconds, with enough intensity to perform nuclear spectroscopy studies. At the Low Energy Branch of FAIR, the ions will be slowed down to energies of a few MeV/u, where direct nuclear reaction studies can be performed. This is the objective of the experiments foreseen for HISPEC collaboration at FAIR. The main instrument for such studies will be the HYDE (Hybrid Detector) array, which should be able to perform measurements of reaction cross sections induce by these very short-lived nuclei.

The development and construction of HYDE is made in collaboration with the research groups of GASPARD and TRACE detectors for the SPIRAL2 and SPES facilities, allowing for the exploitation of the existing synergies and providing common working groups for R&D activities.

Tackling particle identification under extreme experimental conditions

Charged particle identification has been normally achieved in the past by time of flight (TOF) and energy loss techniques with particle telescopes (PT). The former requires long flight paths, which translate into large, expensive and somewhat cumbersome arrays. The latter implies relatively high thresholds, which preclude the identification of low energy particles with large Z, and very fast particles leaving too low energy in the first stage detector. Digital Pulse Shape Analysis (DPSA) of both current and charge signals produced by charged particles impinging on silicon detectors has been proposed as a particle identification tool [4]. Preliminary results were very promising and therefore DPSA studies play an important role among the various R&D activities performed by our collaboration in the last few years. This technique is an important challenge from both experimental and instrumental points of view, with applications in many other fields. At present it appears that a suitable combination of these three techniques (TOF, PT and DPSA) should be implemented for the design and construction of the new generation of particle detectors. The basic DPSA method consists in the digitalization of the signals produced in the silicon detectors using a large bandwidth preamplifier (300 MHz typical), together with a fast digitizer having a high sampling rate (1GS/s). The digitalized pulses can be offline analyzed and classified according to the mass and charge of the impinging particles. The R&D activity must also cover a convenient design and implementation of the FEE electronics in the proximity of detector cells. Various parameters concerning the quality of the silicon wafers play an important role in this technique, like crystallographic orientation [5] and non-uniformity in thickness and resistivity [6].

An important issue is to determine the limits of DPSA technique: range of

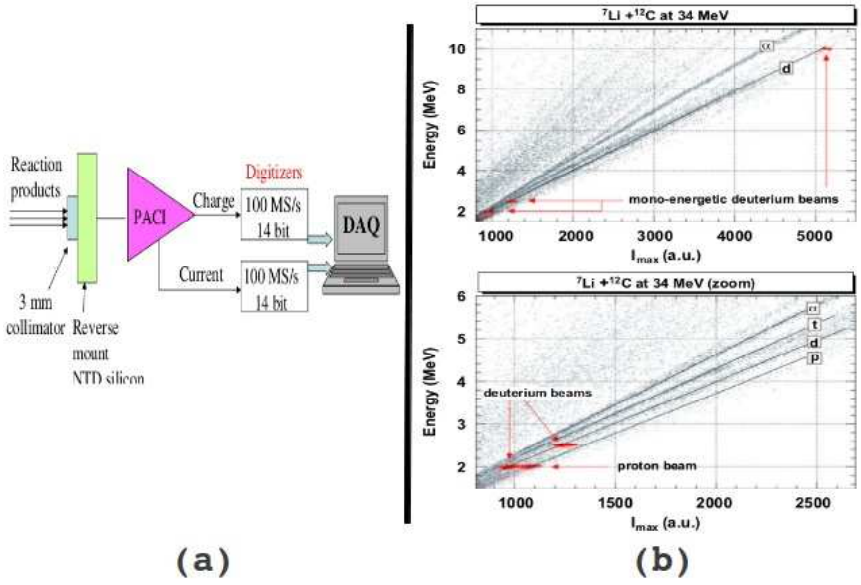

Figure 1: (a) Sketch of the experimental setup; (b) Energy vs I_{max} correlation plots (see text for details)

energies, masses and charges, optimal silicon thickness, strip effects and radiation degradation. For this purpose a database of digital pulses is being built using nuclear reactions with stable beams. In Fig. 1 (a) we show the experimental setup for DPSA studies prepared for a recent experiment carried out at TANDEM/ALTO facility (Orsay, France) [7]. A high uniformity NTD (Neutron Transient Doped) silicon detector was bombarded by low energy, low intensity light ions after scattering on ^{12}C and gold targets. The signals were collected by using a 300 MHz bandwidth preamplifier (PACI) [8] and driven to a four channels NIM-based card (N1728B from CAEN) with a 100 MS/s sampling rate. The obtained Energy vs I_{max} plot for the ^{7}Li+^{12}C reaction products and for mono-energetic proton (2 MeV) and deuterium (2, 2.5 and 10 MeV) beams is shown in Fig. 1 (b).

Conclusions

The new generation of radioactive beam facilities being built is demanding large particle detector arrays using the last advances in particle detection technology. The collaborations for construction of the detectors HYDE, GASPARD and TRACE are leading important developments on digital pulse shape analysis, silicon produc-

tion, front end electronics and data acquisition systems that will be used to build a new generation of particle detectors.

Acknowledgments

This work was supported by the Grant from the Spanish Research Council FPA-2010-22131-C02-01.

References

[1] www.gsi.de/en/research/fair.htm

[2] www.ganil-spiral2.eu/

[3] http://web.infn.it/spes/

[4] M. Mutterer et al., IEEE Trans. Nucl. Sci. **47**, 3 (2000).

[5] L. Bardelli et al., NIM A **605**, 353 (2009).

[6] L. Bardelli et al., NIM A **602**, 501 (2009).

[7] J. A. Dueñas et al., NIM A **676**, 70 (2012).

[8] H. Hamrita et al., NIM A **531**, 607 (2004).

[9] B.A. Li, L.W. Chen and C.M. Ko, Phys. Rep. **464**, 113 (2008).

Elastic scattering and reaction mechanisms induced by light halo nuclei at the barrier

Valentina Scuderi
INFN-LNS, Catania, Italy

Abstract

Elastic scattering and reaction mechanisms around the Coulomb barrier, in collisions induced by halo nuclei, has been the object of many publications in the last years. Elastic scattering, being a peripheral process, can in fact be an ideal tool to investigate the surface properties of the halo nuclei. In collisions induced by halo nuclei, direct reactions, as for instance transfer or break-up, are expected to be favored owing to the low binding energy, the extended tail of valence nucleons and the large Q-value for selected transfer channels. Moreover, the fusion cross sections may be affected by dynamic effects, due to coupling not only to bound states but also to the continuum, and by static effects due to the diffuse surface of these nuclei that can affect the shape of the projectile-target potential reducing the Coulomb barrier. In this contribution an overview of the recent experimental results obtained at the LNS concerning the study of the collisions around the barrier induced by the 2n-halo nucleus ^{6}He and by the 1n-halo ^{11}Be will be presented. These studies have shown that coupling to the continuum strongly affects the elastic cross-section, with dramatic changes in the elastic cross section from the expected behavior and with an overall increase in the total reaction cross section in favor of direct reaction channels. However, almost all the results obtained so far for collisions induced by halo nuclei have been obtained with ^{6}He beams, only few experiments have been performed with ^{11}Be beams and additional data with different halo nuclei would be necessary. At the same time, new fusion cross section measurements with halo nuclei, better exploring the sub barrier region, are still needed in order to disentangle between static and dynamic effects. Perspectives and possible future experiments with different radioactive beams will be also discussed.

Reaction programs beyond NSCL

M. Betty Tsang
NSCL, Michigan State University, East Lansing, MI, USA

Symmetry energy and nucleon-nucleon cross sections

Martin Veselsky
Institute of Physics, Slovak Academy of Sciences, Bratislava, Slovakia

Abstract

The extension of the Boltzmann-Uhling-Uhlenbeck model of nucleus-nucleus collision using the isospin-dependent nucleon-nucleon cross sections, extracted from the equation of state of nucleonic matter using transformation into the van der Waals-like form, demonstrates sensitivity of the results to this effect. Dependence of results of such simulations on symmetry energy typically varies strongly from the results obtained using only the isospin-dependent mean-field. The evolution of the n/p multiplicity ratio with angle and kinetic energy, in combination with the elliptic flow of neutrons and protons, provides a suitable set of observables for determination of the density dependence of the symmetry energy. The model thus provides a suitable platform for testing of equations of state, used for various applications in nuclear physics and astrophysics.

Symmetry energy and maximum rotation of neutron stars

Isaac Vidaña
Centro de Física Computacional, Department of Physis,
University of Coimbra, PT-3004-516 Coimbra (Portugal)

Abstract

We analyze the role of the symmetry energy slope parameter L on the r-mode instability of neutron stars. Our study is performed using both microscopic and phenomenological approaches of the nuclear equation of state.

Talk's Summary

In this work [1], we have studied the role of the symmetry energy slope parameter L on the r-mode instability of neutron stars. A similar study has been recently done by Wen, Newton and Li [2] using a simple model for the nuclear equation of state (EoS) that consistently describes the crust-core transition density. Assuming that the main dissipation mechanism of the r-modes is due to electron-electron scattering at the crust-core boundary and using the estimated core temperature of several low-mass x-ray binaries (LMXBs), these authors conclude that neutron stars are stabilized againts r-mode oscillations if L is smaller than ~ 65 MeV. In our work we use different models for the nuclear EoS that include the microscopic Brueckner–Hartree–Fock (BHF) approach [3], the variational Akmal–Pandharipande–Ravenhall (APR) EoS [4], a parametrization of recent Auxiliary Field Diffusion Monte Carlo (AFDMC) calculations [5], and several phenomenological Skyrme forces and relativistic mean field models. We consider both bulk (ξ) and shear (η) viscosities as the main dissipative mechanism of r-modes, including in the calculation of ξ the contribution of the modified and direct electron and muon Urca processes and, in that of η, the contribution of neutron and electron scattering.

Conclusions

We have found that the r-mode instability region is smaller for those models which give larger values of L. We have shown that this is due to the fact that both bulk

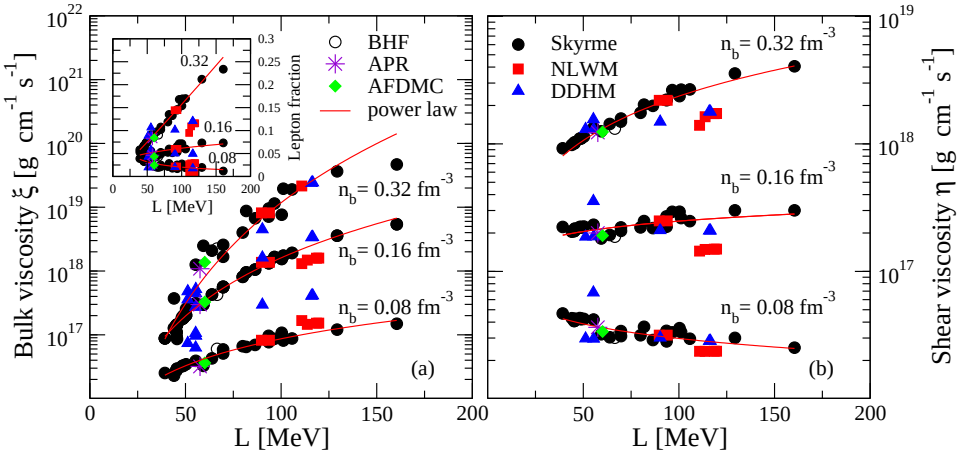

Figure 1: Bulk (a) and shear (b) viscosities as a function of the symmetry energy slope parameter L for several densities and different models. Solid lines show the power laws $\xi = A_\xi L^{B_\xi}$ and $\eta = A_\eta L^{B_\eta}$. The frequency of the mode and the temperature are taken as 10^4 s^{-1} and 10^9 K, respectively. In the inset is shown the lepton fraction as a function of L for the same densities and models.

and shear viscosities increase with L (see Fig. 1) and, therefore, make the damping of the mode more efficient for the models with larger L. We have shown also that the dependence of both viscosities on L can be described at each density by simple power-laws of the type $\xi = A_\xi L^{B_\xi}$ and $\eta = A_\eta L^{B_\eta}$. Finally, we have tried to constrain the value of L using the measured spin frequency and the estimated core temperature of the pulsar in the low-mass X-ray binary 4U 1608-52 (see Fig. 2). We have concluded that observational data seem to favor values of L larger than ~ 50 MeV if this object is assumed to be outside the instability region, its radius is in the range $11.5-12(11.5-13)$ km, and its mass $1.4M_\odot(2M_\odot)$. Outside this range it is not possible to draw any conclusion on L from this pulsar. These results are in contrast with the recent work of Wen, Newton and Li [2], where these authors show that observation seems to be more compatible with smaller values of L. We should mention, however, that these authors assume that the main dissipation mechanism of the r-mode is due to the viscous boundary layer at the crust-core interface where densities are smaller than the saturation density ($\rho_0 \sim 0.16$ fm^{-3}). Therefore, their calculation of the shear viscosity is done in a region of densities for which, as it can be seen in Fig. 1, η decreases with L. Finally, we note that the inclusion of other sources of dissipation, such as *e.g.*, hyperon or quark bulk viscosities, is not expected to change the qualitative conclusions of this work.

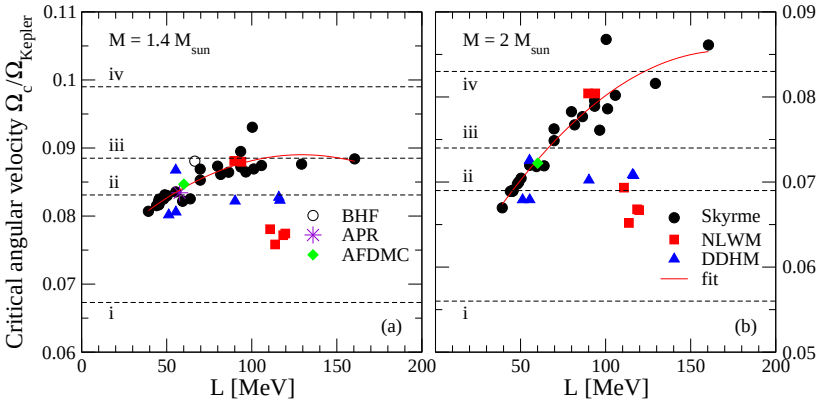

Figure 2: Critical angular velocity as a function of the symmetry slope parameter for a $1.4M_{\odot}$ (a) and $2M_{\odot}$ (b) neutron star at the estimated core temperature of 4U 1608-52, $T \sim 4.55 \times 10^8$ K, and different models. The frequency of the mode is taken at $\omega = 10^4$ s^{-1}. Solid lines show the result of a quadratic fit. The horizontal dashed-lines show the observational spin frequency of 4U 608-52 in units of Ω_{Kepler} assuming that the radius of this object is (i) 10, (ii) 11.5, (iii) 12, or (iv) 13 km.

Acknowledgments

This work is partly supported by COMPSTAR, and ESF (European Science Foundation) Research Networking Programme, and by the initiative QREN financed by the UE/FEDER through the programme COMPETE under the projects, PTDC/FIS/113292/2009, CERN/FP/109316/2009, CERN/FP/ 116366/2010 and CERN/FP/123608/2011.

References

[1] I. Vidaña, Phys. Rev.C **85**, 045808 (2012).

[2] D. H. Wen, W. G. Newton, and B. A. Li, Phys. Rev. C **85**, 025801 (2012).

[3] I. Vidaña, C. Providência, A. Polls and A. Rios, Phys. Rev. C **80**, 045806 (2009).

[4] A. Akmal, V. R. Pandharipande, and D. G. Ravenhall, Phys. Rev. C **58**, 1804 (1998).

[5] S. Gandolfi, A. Yu. Illarionov, S. Fantoni, J. C. Miller, F. Pederiva, and K. E. Schmidt, Mon. Not. R. Astron. Soc. **404**, L35 (2010).

Precision Measurement of Isospin Diffusion in Sn+Sn Collisions

Jack Winkelbauer
NSCL, Michigan State University, East Lansing, MI, USA

Abstract

In heavy-ion collisions, the tendency for isospin to drift from a neutron (proton) rich region to a neutron (proton) deficient region is sensitive to the density dependence of the symmetry energy. Until recently, most of the isospin diffusion results have been obtained with mid-central to central collisions and different isospin observables have been used in experiment and in model simulations. To provide more accurate understanding of the dependence of isospin diffusion on impact parameters and different isospin observables, we have measured isotopic fragment and residue yields for ^{112,118,124}Sn + ^{112,118,124}Sn collisions at E/A=70 MeV. The measurements were carried out at the Coupled Cyclotron Facility at Michigan State University. Fragment yields were measured using the Large Area Silicon Strip Array (LASSA) and heavy residue yields emitting at the forward angles were measured using the S800 Spectrograph. Impact parameter was selected on an event-by-event basis using the MSU Miniball-WU Miniwall array. Preliminary heavy residue cross sections will be presented and compared with previous results with these reaction systems.

This work is supported by the National Science Foundation under Grant PHY-0606007.

Tandem session on Status of transport models in the search for the symmetry energy (at sub- and supra-saturation densities)

Joerg Aichelin[1] *and Hermann Wolter*[2]
[1] *SUBATECH Nantes, France*
[2] *University of Munich, Garching, Germany*

Asymmetry Dependence of the Nuclear Caloric Curve

Sherry Yennello
Texas A&M University, College Station, TX, USA

Abstract

Quasi-projectile sources produced in collisions of ^{70}Zn+^{70}Zn, ^{64}Zn+^{64}Zn and ^{64}Ni+^{64}Ni at E/A=35 MeV have been reconstructed using the charged particles and free neutrons measured in the NIMROD-ISiS detector. Equilibrated sources were selected which have a mass A=48-52 and which are on average spherical. Caloric curves for these quasi-projectiles have been extracted with the quadrupole momentum fluctuation thermometer. The caloric curves for the different light charged particle probes show a clear ordering which is consistent with a scenario in which the "expensive" particles are emitted preferentially at early times, when the source is hottest. For all light charged particle probes, the caloric curves show a clear dependence on the composition, (N-Z)/A, of the source. For a given excitation (E*/A), the neutron-poor sources exhibit higher temperatures. A consistent but smaller dependence is observed by selecting on the composition of the initial system rather than the composition of the source. The dependence on source composition is also observed in caloric curves extracted with the Albergo yield-ratio thermometer.

Measurement of emitted tritons and ^{3}He from ^{112,124}Sn+ ^{112,124}Sn collisions at E_{beam}=50 and 120 MeV/nucleon

Mike Youngs
NSCL, Michigan State University, East Lansing, MI, USA

Abstract

The nuclear symmetry energy affects many aspects of nuclear structure, nuclear astrophysics, and nuclear reactions. The spectral ratio of neutrons to protons from central heavy ion collisions is sensitive to the symmetry energy below saturation density, but is difficult to measure experimentally. t/^{3}He ratios, however, provide an easier measurement, since neutron detection efficiency is not an issue. A recent experiment at NSCL/MSU has measured n/p ratios from collisions of ^{112,124}Sn+^{112,124}Sn at E_{beam}=50 and 120 MeV/nucleon. In addition, t/^{3}He ratios were also measured. Results of the t/^{3}He double ratios as well as systematic studies of theoretical calculations of t/^{3}He single and double ratios will be discussed.

2 Acknowledgements